



## Master Thesis

submitted within the UNIGIS MSc programme  
Interfaculty Department of Geoinformatics - Z\_GIS  
University of Salzburg

# Re-Engineering the Past: Countrywide Geo-referencing of Archival Aerial Imagery

by

Dipl. Geoökol. Holger Heisig  
105152

A thesis submitted in partial fulfilment of the requirements of  
the degree of  
Master of Science (Geographical Information Science & Systems) – MSc (GIS)

Advisor:

Prof. Dr.-Ing. habil. Christian Heipke

Bern, 10 December 2020

# Science Pledge

I hereby declare that the thesis is entirely the result of my own work. I have cited all sources I have used in my thesis I have always indicated their origin. This thesis was not previously presented to another examination board and has not been published.

# Acknowledgements

First, I would like to thank my employer, the Swiss Federal Office for Topography swisstopo, for the general endorsement of my post-graduate studies and this Master Thesis. In particular, I would like to thank my superiors Jean-Luc Simmen, Dr. Philip Jörg und Dr. André Streilein for their support in all aspects. Furthermore, I am grateful to my colleagues that have contributed through their knowledge and helpfulness to this work: To Simon Hagmayer and Théo Gaillet for realization of the accuracy assessment and their contributions in the production process, Florian Gandor for support with FME and Python, Christian Loup for development of PhotoShop macros, Elias Raymann for LUBIS management, Handy Rusli for general application development, Alicia Windler for preceding conceptual works and Liam O'Sullivan for the English language revision. It is an enormous privilege to work in a real competence center with people willing to share their knowledge!

Next, I would like to thank Jean-Sébastien Bouffard and Stewart Wyseman from PCI Geomatics for reviewing the manuscript and the general excellent support with the HAP system.

I owe particular thanks to Prof. Dr.-Ing. Christian Heipke for his supervision of this Thesis, his encouragement, his critical reviews and his most constructive feedbacks.

Furthermore, I would like to thank the entire University of Salzburg UNIGIS team for their support throughout this master's program.

Finally, I would like to thank my partner Elke and our wonderful children: Without their patience, the conduct of these studies would not have been possible for me.

# Preface

This framework describes work undertaken to fulfil the requirements of the degree of Master of Science (Geographical Information Science & Systems) – MSc (GISc). It consists of two main parts: first, a manuscript to be publishable in a peer reviewed, ISI-indexed, international journal, and second, a report that documents the methodological steps of the technical implementation.

Holger Heisig (first and corresponding author) and Jean-Luc Simmen (second author) have read and agreed to the published version of the manuscript. The first author carried out conceptualization, methodology and the writing-original draft preparation of the manuscript. The second author supervised the conceptualization and contributed in reviewing and editing the manuscript. The manuscript was written to be submitted to either *Remote Sensing* (Impact Factor 2019: 4.51) or *ISPRS International Journal of Geo-Information* (Impact Factor 2019: 2.24).

# Table of Contents

<b>SCIENCE PLEDGE .....</b>	<b>II</b>
<b>ACKNOWLEDGEMENTS .....</b>	<b>III</b>
<b>PREFACE .....</b>	<b>IV</b>
<b>TABLE OF CONTENTS.....</b>	<b>V</b>
<b>MANUSCRIPT.....</b>	<b>VII</b>
<b>1. Introduction .....</b>	<b>1</b>
<b>2. Materials and Methods .....</b>	<b>3</b>
2.0 Study area.....	3
2.1 Data .....	3
2.1.1 Aerial image data .....	3
2.1.2 Aerial image metadata .....	4
2.1.3 Reference and auxiliary data.....	5
2.2 Orientation of image data .....	5
2.2.1 The HAP core process .....	5
2.2.2 Workflow adaptation and process parametrization .....	7
2.3 Generation of image products and accuracy assessment .....	8
2.3.1 Orthophoto generation and mosaicking.....	8
2.3.2 Generation of DSMs .....	8
<b>3. Results.....</b>	<b>9</b>
3.1 Results of the automated processing chain.....	9
3.2 Final QA .....	9
3.3 Orthophotos and mosaics .....	13
3.4 Digital Surface Models .....	14
<b>4. Discussion .....</b>	<b>15</b>
<b>References.....</b>	<b>17</b>
<b>REPORT.....</b>	<b>VIII</b>
<b>1 General remarks.....</b>	<b>1</b>
1.1 Scope and aim of this report .....	1
1.2 Motivation .....	1
<b>2 Image orientation process .....</b>	<b>2</b>
2.1 Workflow progress table.....	2
2.2 Block definition and additional lines.....	3
2.2.1 General considerations .....	3
2.2.2 Definition of aerial triangulation blocks .....	3
2.2.3 Additional lines.....	4
2.3 Automated processing.....	5
2.3.1 Introduction.....	5

2.3.2	Parameter assignment.....	5
2.3.3	Image data and metadata preparation.....	6
2.3.4	Reference data preparation.....	8
2.3.5	HAP Ingest process .....	9
2.3.6	Python API scripts.....	10
2.3.7	HAP coarse alignment.....	13
2.3.8	HAP fine alignment run .....	15
2.4	Quality Assurance process.....	16
2.4.1	Check jpegs.....	16
2.4.2	OrthoEngine.....	17
2.4.3	Digitize missing TPs.....	19
2.4.4	Running bundle block adjustment.....	21
2.4.5	Check orthoimages .....	24
2.4.6	Report statistics.....	26
2.5	HAP_PostAT .....	26
<b>3</b>	<b>DSM generation process.....</b>	<b>27</b>
3.1	Epipolar pairs .....	28
3.2	Generate DSMs.....	29
3.3	Quality assessment: Hillshading and difference building .....	29
<b>4</b>	<b>Orthoimage generation process.....</b>	<b>30</b>
4.1	Create list.....	30
4.2	Calculate Orthos.....	31
4.3	Post-treatment: Radiometric optimization.....	34
4.4	Identify incomplete orthoimages .....	36
4.5	Build Mosaic Dataset.....	36
4.6	Quality Assurance Mosaic Dataset.....	37
4.7	Archive orthoimages .....	39
<b>5</b>	<b>Ortho mosaic generation process .....</b>	<b>39</b>
5.1	General remarks .....	39
5.2	Build image list .....	41
5.3	Retrive orthoimages .....	41
5.4	Run auto-mosaic .....	41
5.5	Edit seam lines .....	42
5.6	Seam applicator.....	43
5.7	Final quality assurance of produced mosaic tiles.....	44
5.8	Metadata base.....	44
5.9	Integration of mosaic tiles for long-term storage .....	45

# Manuscript

# Re-Engineering the Past: Countrywide Geo-referencing of Archival Aerial Imagery

Holger Heisig\* and Jean-Luc Simmen

Federal Office for Topography swisstopo, Seftigenstrass 264, CH-3084 Wabern, Switzerland;  
holger.heisig@swisstopo.ch

\* Correspondence: holger.heisig@swisstopo.ch; Tel.: +41-58-469-0280

Received: date; Accepted: date; Published: date

**Abstract:** Archival Aerial Imagery (AAI) represents a unique and relatively unexploited resource for assessing long-term environmental changes at a very high spatial resolution. A major constraint for the wider use of AAI often lies in the difficulties of establishing precise geo-referencing, namely in the difficult and time-consuming task of assigning ground reference through manual digitization of Ground Control Points (GCPs). We present a highly automated photogrammetric workflow for orientation of AAI. The workflow substitutes manual GCP measurements by generating image matches to a digital reference. The resulting abundant observations are algorithmically filtered and used in a bundle block adjustment (BBA) to obtain final image orientations. The proposed workflow has successfully been employed to process a complete coverage of AAI over the territory of Switzerland. The obtained accuracies from the orientation process allow for generating meaningful 2D and 3D products. The absolute accuracy for derived orthophotos and their mosaics is around 1 m. The relative accuracies are in subpixel range and allow for generation of countrywide Digital Surface Models (DSMs) through dense-image matching. The obtained accuracies are comparable to those obtained at the authors' affiliation using classical workflows that involve manual GCP identification from a digital reference data. In our case, the workflow has proven to be at least five times more efficient than classical workflows while the required computational resources are very moderate.

**Keywords:** photogrammetry; orientation; co-registration; geo-referencing; analog; aerial; matching; automation; Switzerland

## 1. Introduction

Aerial photos can literally be seen as one of the most important immediate visual testimonies of the Earth's surface. Aerial imagery with country-wide coverage has systematically been acquired since the 1930's by National Mapping and Cadastral Agencies (NMCAs) or military cartographic sections [1]. A time series of archival aerial imagery (AAI) can today reveal a huge but yet vastly unexploited potential for retrospectively assessing long-term environmental changes [2,3]. A rapidly growing interest in the use of historical aerial photos and their derivatives was observed over recent years. The interest comes from domains of application as diverse as archaeology [4,5], forest sciences [6,7], historic landscape and settlement analysis [8–11], glaciology [9,12–14] or geomorphology [15–17]. Due to recent developments in dense image matching [18], special interest is often given to the multi-temporal analysis of Digital Elevation Models (DEMs) derived from historical aerial photos.

The challenges in fully exploiting the potential of AAI for environmental studies include their exposure to physical and chemical deterioration, the multitude of applied acquisition systems, missing or incomplete metadata, the heterogeneous radiometric properties of corresponding image scans and the problems encountered in establishing precise geo-referencing [3].

Precise geo-referencing is a mandatory pre-requisite for relating aerial images to other geodata, e.g. by use of Geographic Information Systems (GIS). Photogrammetric approaches are the most established means to perform geo-referencing of aerial images. These approaches aim at modelling the



internal and external orientation elements of a number of overlapping images defined as an aerial triangulation (AT) block. Classical photogrammetric workflows for orientation of AAI typically encompass the following steps:

Measurement of fiducial marks: Provided sufficient image scan quality is available, the detection of fiducial marks on the image scan files can be carried out in fully-automated mode.

Measurement of Tie Points (TP): Tie points identify common features on overlapping images. Detection of TP is nowadays typically carried out in a fully-automated mode [6,19–21].

Measurement of Ground Control Points (GCPs): Coordinates from a reference are assigned to manually identified objects or points in the images. The reference coordinates may either come from field measurements [15] or are extracted from digital reference data like road vectors or orthophotos [9,12]. The task of manual GCP digitization on AAI is often referred to be difficult, error-prone and time consuming. Most authors explicitly mention the difficulty of identifying well defined points that are stable over time on both, reference and historic aerial photo.

Bundle block adjustment (BBA): The modelling of accurate viewing geometries is commonly achieved through bundle block adjustment. In bundle block adjustment, which is based on the collinearity equations, the TP and GCP observations together with the camera’s interior orientation are used to estimate the unknowns: the elements of exterior orientation and the 3D coordinates of the tie points. In this way, photogrammetric approaches “re-engineer” the original pose of the camera at acquisition time.

Once established, precise orientation elements allow for (1) extraction of 3D geo-information by visual stereoscopic interpretation; (2) automated extraction of Digital Surface Models (DSMs) and (3) production of orthophotos and ortho mosaics-

Like other NMCA, the Swiss Federal Office of Topography swisstopo, holds a large collection of historic aerial imagery. The systematic acquisition of aerial photographs in Switzerland began in 1926. National aerial photography campaigns, organized in constant cycles, allowed for continuous updates of the national topographic maps. swisstopo's archive image collection contains around 400,000 aerial photographs. Only a small portion of these have so far been oriented. Important country-wide uses of swisstopo’s oriented archival aerial images have been established, though. This concerns stereoscopic visual analysis for assessing land use statistics [22], historical DSM generation [23,24] and ortho mosaic generation [25]. Growing physical and chemical deterioration of the image collection has led to LSA. The measures on swisstopo’s aerial image collection include: Conservation measures on the originals, long-term storage of originals in climatized rooms, photogrammetric scanning of originals, metadata collection and its management. Customers can purchase digital copies of all scanned archival aerial imagery. Alternatively, full resolution image files, together with basic metadata, can freely be consulted through a webservice [26].

For ease of public access to the image information, precise geo-referencing of all scanned aerial images as well as production and publication of ortho mosaics is highly desirable. Figure 1 displays the general workflow from the original analogue images to ortho mosaics. Due to limited resources for establishing precise geo-referencing in a classical photogrammetric workflow, a need for a highly automated photogrammetric workflow capable of efficiently orienting thousands of aerial photos with high accuracy was identified at swisstopo.

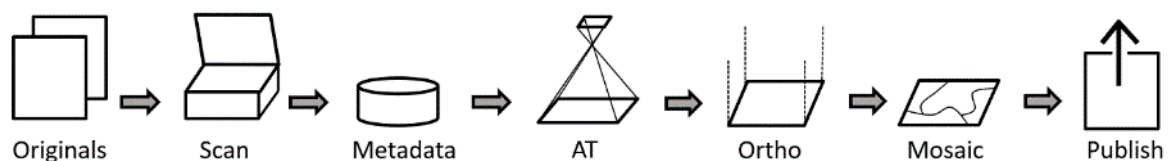


**Figure 1.** General workflow from aerial image originals to published digital ortho mosaics.

In classical photogrammetric workflows, the establishment of exterior image orientation was identified as being the most time-consuming step in the image orientation process. Despite early attempts [27], surprisingly few methods have been proposed to overcome this issue [3]:

Minimization of the number of GCPs by geostatistical methods has been proposed by [28]. Co-registration on the basis of stable linear features is presented by [29,30]. Manual digitization of these linear features in archival imagery and ground reference are still required in [29]. [30] proposes matching of extracted lines in archival images to a vector reference of linear features. A method for automatic detection of GCPs was presented by [3]. The GCPs are detected in recent orthophotos and then transferred to archival imagery. The method relies on the detection of keypoints between images of different times.

Despite the encouraging results reported from the different authors, none of the proposed methods was reported to be implemented on a production scale.

Note: The use of the notion *Ground Control Points* in the context of automated collection is not unproblematic, since the points are not (user-) *controlled*. Since these reference points fulfill the same function in BBA as user controlled points, we will stick to the notion of *GCPs* for automatically collected points in this article.

In this study, we applied an extended workflow based on the commercial software package HAP (*Historical Air Photo*) from software provider *PCI Geomatics*.

The main objectives of the present study are: (1) to demonstrate the highly automated workflow to achieve precise geo-referencing of a national coverage of AAI; (2) to evaluate accuracies and efficiency obtained on orientations and derived products; and (3) to present the potential and limitations of the workflow by discussing its transferability into time and space.

## 2. Materials and Methods

### 2.0 Study area

The study area comprises the entire Swiss territory that covers 41,285 km<sup>2</sup>. The Swiss Alps constitute about 60% of the country's total area. According to federal land use statistics from 2013 [31], the predominant types of land use in Switzerland are agriculture and farming (36.9%) forests and woodlands (30.8%) and unproductive areas (25.5%). Unproductive areas comprise lakes, rocks, glaciers and perpetual snow. Settlements account for 6.8% of the national territory. With its high altitudinal range (200 to 4600 m a.s.l.) and its big variety of land use and cover, the study region represents a most challenging test ground for a highly automated photogrammetric workflow.

Orientation and product creation in this study is carried out in the reference system of the Swiss national survey 1903 (EPSG:21781). The reference system bases on the Mercator projection and the Bessel ellipsoid.

### 2.1 Data

#### 2.1.1 Aerial image data

The aerial images processed in the scope of this article were captured by swisstopo between 1985 and 1991. The set consists of 8'507 aerial images covering the complete Swiss territory in full stereo mode. According to flight reports, the average image scale is around 1:25'600, the minimum image scale is around 1:35'300. The annual acquisition zone was divided into an alpine sub region and a sub region in the lowlands. The regions in the lowlands were acquired under snow free and cloud free conditions with leaves off during springtime (March to June). The alpine regions were acquired between July and September in order to assure equally snow free images. The regions of Zürich and Geneva have been covered twice in the given period. The flying height varied in function of topography between 4000 m and 7000 m a.s.l. The overlap in flight direction varies, again depending on the topography, between 60 and 80%. The lateral overlap is around 20 - 25 %.

In general, all flight lines are oriented East-West or vice versa. Exception to this rule occurs in larger alpine valleys where supplementary flight lines have been flown at lower altitude. The azimuthal orientation of these valley lines follows the topography of the valley. Figure 2 gives an overview of flight line geometries.

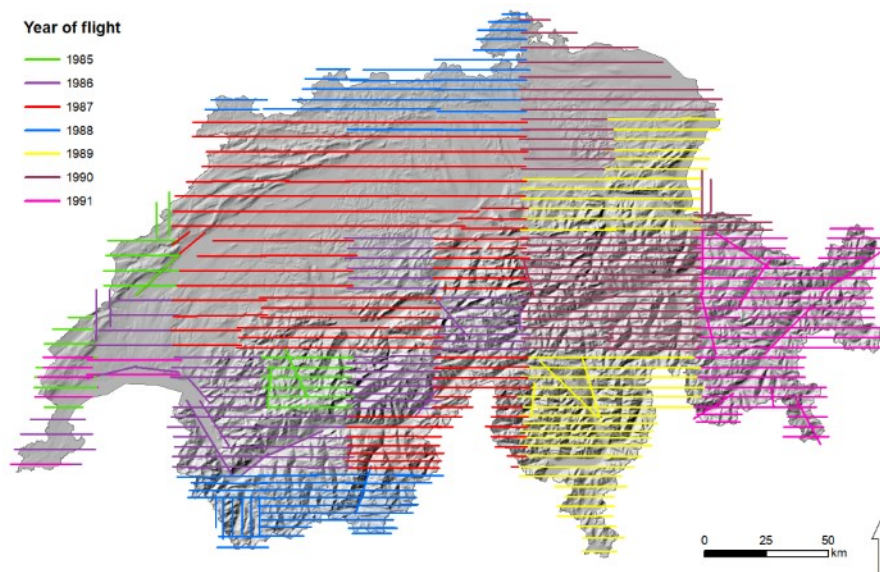


**Figure 2.** Geometry and flight year of flight lines. Initial geo-referencing results in straight lines.

All images of this data set were digitized at swisstopo during the past years using the Leica DSW 700 photogrammetric scanner. The original image negatives were scanned with a geometric resolution of 14 micrometers per pixel and a radiometric resolution of 8 bit. The average ground sampling distance (GSD) resulting from image scale and scan resolution is 35 cm, the maximum GSD is 49 cm.

### 2.1.2 Aerial image metadata

With the conservation and digitization measures taken in recent years, a most complete set of metadata was collected. Primary sources of metadata included information from flight plans, flight reports, calibration protocols, etc. The collected metadata are managed in an Aerial Image Information System (*Luftbildinformationssystem LUBIS*). The LUBIS metadata system consists of a geo-relational DBMS running on ArcSDE/Oracle.

Initial geo-referencing for the archived images are obtained as follows: The first and the last image of each flight line is manually located in X and Y in the 3D coordinate space. The accuracy for these values is estimated to be 100-300 m. The flying height is derived from flight report. All image projection centers belonging to the same flight line are derived through interpolation following the order of image acquisition. Each flight line's projection centers thus lie on a straight line. The accuracy of the interpolated projection centers vary with the length of the flight line and the corresponding flight conditions (e.g. accuracy of navigation, wind) between 100 m and around 4000 m.

A camera of the type Wild RC10 with a Leica 15/4 UAG lens was used for the acquisition campaigns processed in this study. The image format is 23 cm \* 23 cm. The calibration protocol that was assumed valid for the entire acquisition cycle has been digitized into the LUBIS system. The calibrated focal length is given with 153.37 mm.

The 8'507 images to be processed were grouped into 36 blocks for aerial triangulation. The repartition is displayed in figure 3. For each image, a block identifier was added to LUBIS. Blocks were primarily defined by spatial coherence. Temporal coherence was a criterion to be neglected due to the short time span (6 years) of image acquisition. The size of the blocks varied between 70 and 700 images.

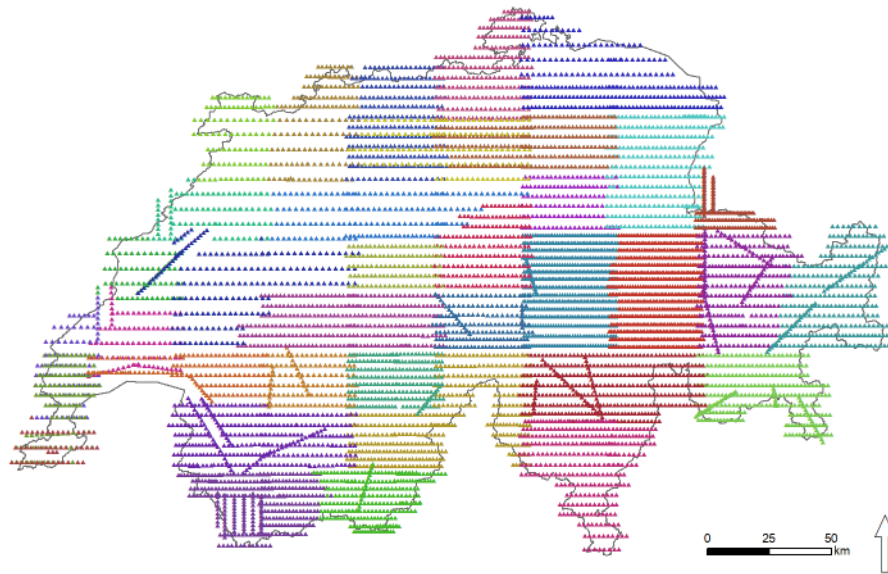


**Figure 3.** Repartition of aerial images into 36 contiguous blocks.

### 2.1.3 Reference and auxiliary data

The external orientation in our proposed workflow is determined by the use of GCPs that are automatically collected from reference data sets. The planimetric reference coordinates of the GCPs are derived from an ortho reference, the height information from a DEM.

Our ortho reference is the Swiss national ortho mosaic SWISSIMAGE [32]. The reference year of the utilized ortho mosaic version is 2016. The SWISSIMAGE product consists of a complete and cloud-free coverage of seamlessly mosaicked orthorectified aerial images acquired between 2014 and 2016. The absolute planimetric accuracy of these data is defined with a standard deviation of 25 cm. The original RGB product with a pixel size of 25 cm has been resampled to 3 m for the coarse alignment run for and to 1 m for the fine alignment run. The resampling is carried out to account for the geometric resolution of the corresponding image pyramid layers used in the alignment process. As we matched panchromatic images only, a panchromatic derivative from SWISSIMAGE was produced.

The national orthophoto mosaic SWISSIMAGE is furtherly used in its full resolution to measure the accuracy of the obtained orthorectified image products.

For assigning height information to GCPs we used the Swiss national height model product *swissALTI3D* [33] from the reference year 2016. This Lidar-based Digital Terrain Model (DTM) with countrywide coverage has a vertical accuracy with a defined standard deviation of 50 cm. The utilized height model has 2 m pixel size. The height model is also used in the later orthorectification process.

For the GCP collection process, the derived ortho reference has been masked by *NoData* values for land cover classes which are highly likely to produce erroneous matches. These land cover classes comprise water surfaces, glacier surfaces and forested surfaces. Data from the Swiss Topographic Landscape Model (*swissTLM3D*) [34] were used to define the masks.

## 2.2 Orientation of image data

### 2.2.1 The HAP core process

The developed workflow is based on the commercial software package *HAP* (Historical Air Photo) from the remote sensing software provider *PCI Geomatics*. *HAP* itself uses the functionality defined within *PCI's* photogrammetric software product *OrthoEngine*. The orientation process was performed with version 2018 SP1. *HAP* is composed of a fully featured photogrammetric workflow. Its components can either be executed through a graphical user interface (GUI) or, with advanced

capabilities, by calling associated Python routines through scripting applications. Apart from a White Paper [35], no public technical documentations about HAP are available. Therefore, its core functionality needs to be briefly summarized here. The traceability of the process is given through the human readable Python scripts, through which HAP is executed. Figure 4 (a) summarizes the workflow recommended by the software provider. It consists of following steps:

**Data preparation process:** In the data preparation, a metadata file in text format is manually prepared. The file contains metadata for each image of the aerial triangulation block. Required metadata include the image file name, its approximate external orientation (projective center coordinates in X, Y and Z), the image size and the focal length of the camera.

**Ingest process:** The so-called ingest process creates an ASCII-based photogrammetric project file based on the metadata text file. The process imports the image scan files into PCI's intrinsic PIX format and links these to the project file. The project file is stepwise updated during the further processes. Internally, the orientation angles  $\omega$  and  $\phi$  angles are set to zero in the initial state whereas the  $\kappa$  corresponds to the azimuth of the flight line.

**Interior orientation:** After running the ingest process, automated fiducial mark detection is carried in order to establish the interior orientations of the images. For a given project, the user is required to digitize fiducials on a template image. A routine is then launched to auto-detect fiducials on all other images belonging to the same project. Details about the utilized algorithm are not available within the software documentation.

**Alignment process:** The following (so-called) alignment process identifies automatically GCPs and TPs and filters these to user-defined error thresholds. The process requires as input the photogrammetric project file, the reference orthophoto file and the DEM file. Parameters for the collection of points, like intended point density, search radius, the image pyramid level, the point matching method and the minimum correlation score can either be provided through the GUI or a parameter file. The GCP Collection is conducted using phase matching that identifies corresponding keypoints between images in the frequency domain. Further details about the utilized algorithm are not available within the software documentation. GCP collection and filtering is carried out independently for each image. Therefore, no stereo measurements of GCPs are established. After successful GCP candidate detection, a RANSAC based algorithm [36] is employed for removal of GCP candidates until the user defined error threshold for each image is met. Once the GCP collection is completed, the TP collection and filtering process are run. Based on image footprints from the initial geo-referencing and the search radius, image tuples are identified for the TP collection. After completing the TP detection, the automatic TP refinement is carried out. The refinement step identifies TPs with higher residuals after running BBA. These TPs are then removed from subsequent processing. The TP refinement step is implemented as an iterative process. The result of the alignment process is a potentially large number of collected and filtered GCPs and TPs that are saved to the photogrammetric project file. Details about the utilized algorithm for GCP and TP detection are not available within the software documentation.

**Quality Assurance (QA):** This step corresponds to the validation and improvement of the results of the automated processing in an interactive process. First, good connectivity of all images of the block should be assured. In case of missing measures, GCPs/TPs may need to be added by either manual digitization or by re-running automated GCP/TP collection locally from within the OrthoEngine project. Persisting blunders are identified and eliminated in an iterative procedure of evaluating BBA results, performing edits to TPs and GCPs and re-running BBA again. The result of the QA process following the first alignment process is presumably a substantial improvement of exterior orientation (EO) parameters compared to the initial geo-referencing.

The software provider recommends executing alignment runs and interactive QA steps in an iterative procedure. Improved image orientation after the first QA work serve as input to the next alignment run. In this second run, parameters adapted to the improved EO can be used. In a second alignment run, e.g. the search radius or the image pyramid level may be lowered to account for the

improvement of EO. Therefore, the first alignment run is referred to as *coarse alignment* whereas consecutive alignment runs are referred to as *fine alignment*. The orientation process ends, when the user is satisfied with the results from his/her last QA step.

In summary, the HAP system can be described as a highly automated photogrammetric workflow tailored for bulk orientation of AAI. One of its principal advantages consists of relieving the user from the potentially time-consuming step of manual GCP detection. HAP is tailored for processing imagery with sparse metadata.

Limitations in the performance of the system or to the quality of the output may, for example, originate from insufficient image or scan quality, cloud cover, insufficient quality of reference files, or initial geo-referencing being too imprecise.

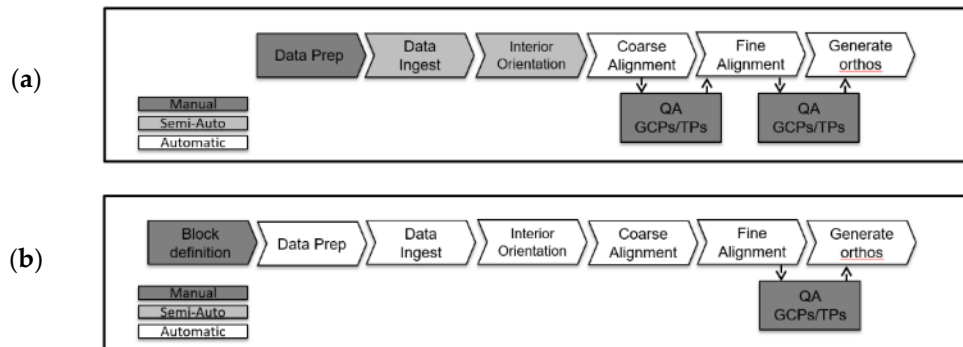


**Figure 4.** Schematic of the HAP workflow. (a) original workflow; (b) our adapted workflow.

### 2.2.2 Workflow adaptation and process parametrization

Following a close examination of the HAP original workflow, it was found that the workflow proposed by the software provider exhibited further potential for automation. The following adaptations to the workflow have been implemented:

**Automated data preparation:** A data preparation routine has been developed and implemented into *Feature Manipulation Engine* (FME) software. The routine prepares all required image data, metadata and reference data for the HAP processing on a per-block base. The reference orthophoto and DEM files are clipped to the buffered geographic extent of footprints from initial georeferencing of the current aerial triangulation block. Land cover classes not suited for GCP detection (water surfaces, forests, glaciers) are masked out from the reference orthophoto. The OrthoEngine Python API is employed to automatically import precise calibration information and setting the project file projection system to the Swiss national reference system with geoidal heights.

**Interior orientation:** Fiducial mark detection is carried out on a sample template image located physically in a (so-called) chip database. This omits the process of having to interactively digitize fiducials on a per-project base.

**Omitting QA step after first alignment and archival of orientation elements:** It was found that the first alignment process improves the image orientations sufficiently well so that its output can directly be used as input to the second alignment step without any interactive QA work. The final QA step figures thus as the only manual step in the processing chain. Its importance is high, though, as it defines the final accuracy of the orientations. After acceptance of the results of BBA in the final QA process, resulting internal and external orientation parameters are written to the meta-database LUBIS using an application developed in-house.

Our adapted workflow applied in this study thus automates the image orientation process starting after block definition in LUBIS to the final (and only) manual QA step into one single fully automated computational process. The processing of each of the 36 aerial triangulation blocks was controlled

through a single batch file. From this file, the corresponding Python scripts for data preparation and HAP processing are called and executed. Figure 4 (b) summarizes the adapted workflow.

The processing was run on a standard PC in a Virtual Desktop Environment. The PC configuration was as follows: Intel(R) Xeon(R) CPU E5-2667 v4 @ 2\*3.20 GHz processors, 24 GB installed memory (RAM). Either three or four AT projects were run in parallel.

### 2.3 Generation of image products and accuracy assessment

#### 2.3.1 Orthophoto generation and mosaicking

The retrieved orientation parameters allow for straightforward generation of the principal image products. Hence, orthophotos for each of the 8'507 input images have been calculated after completion of the orientation process.

The swissALTI3D [33] DTM product with 2 m pixel size was used as an elevation source to calculate orthophotos with 50 cm pixel size in the Swiss national reference system (EPSG:21781). For maximum consistency, it would have been preferable to use an elevation model that represents the topography at the time of image acquisition. A historic height model with sufficient geometric resolution is not available at the author's affiliation. The option of producing a countrywide DSM from the oriented historic images themselves for the use in the orthorectification process was discarded due to the significant effort involved. By using the recent swissALTI3D height model, a time difference of around 35 years between acquisition of images and acquisition of elevation data is thus taken into account. In areas with substantial changes in terrain height such as, for example glaciers, this results in planimetric inaccuracies in the orthorectified images.

Since an orthoimage bulk production workflow existed already, the orthoimage calculation and mosaicking was not carried out with functionality provided by OrthoEngine. Instead, an in-house built application based on *OrthoMaster* from *TRIMBLE ApplicationsMaster 10.1* was used. In order to radiometrically harmonize and sharpen resulting orthophotos, an in-house built PhotoShop macro was run on the orthoimages. After this, single orthophotos are written to the image archive.

From the orthophotos, homogeneous and cloud-free mosaics are produced into year-wise contiguous blocks. The software used in this process is *TRIMBLE ApplicationsMaster*. An automated process generates a first mosaic version using automatic color adaptation and seam line generation. The automated mosaic output is visually checked for remaining artefacts such as remaining cloud patches. The operator evaluates alternative orthoimages covering the detected problematic regions and edits manually the corresponding seam lines. No manual geometric corrections, e.g. for bridges, were carried out on orthoimages or mosaics.

The absolute geometric accuracy of the obtained ortho mosaic has been assessed by comparison with the most current version of *SWISSIMAGE*. A set of around 300 samples has been defined by overlaying a regular grid. Within a given radius around each intersection the planimetric distance of an object identifiable in reference and on the generated mosaic has been measured.

#### 2.3.2 Generation of DSMs

DSMs can be derived from overlapping and accurately oriented aerial imagery through highly automated processing routines based on dense image matching algorithms. In our case, no systematic DSM extraction over the whole study area was carried out due to limited resources. In order to demonstrate the potential, though, we generated DSMs over a number of 10 arbitrary samples of 6 km by 9 km. The samples cover a wide range of diverse landscapes and associated land cover types in Switzerland. The subsequent subtraction of the correlated DSM from a reference DEM allows for straightforward quantification of topographic changes such as changes in glacier volume. With the orientation parameters stored in a database, complete DSM extraction may still be performed at a later time.

In our case, the OrthoEngine DEM extraction module has been used to calculate DEMs directly from the OrthoEngine project file. The module uses a semi-global matching (SGM) based algorithm [37]. The extraction has been run on the images' full resolution.

### 3. Results

#### 3.1 Results of the automated processing chain

For all 36 aerial triangulation blocks the automated processing chain delivered: (1) complete and reliable measures of fiducial marks for establishing the IO; (2) consistently high numbers and good general distribution of both GCPs and TPs; (3) high shares of multi-ray TPs, important to ensure a robust model and (4) generally high reliability of automatically detected points.

Results of IO: The automated fiducial detection collected four corner fiducial marks on each of the 8'507 images without failing once. The mean value for all residuals from automated fiducial detection amounts to 0.51 pixels with a standard deviation of 0.28 pixels and a maximum value of 1.6 pixels

Results of TP & GCP detection: An exemplary block configuration figuring automatically detected TPs and GCPs is depicted in figure 5 and figure 6. The block is numbered *AT\_22*. It contains 136 images and is geographically located in the *Emmental* region. The landscape of the region is characterized by meadows and pastures and its altitudinal range stretches from 400 to 1400 m a.s.l.. Table 1 summarizes the number of extracted GCPs and TPs for all of the 36 AT blocks.

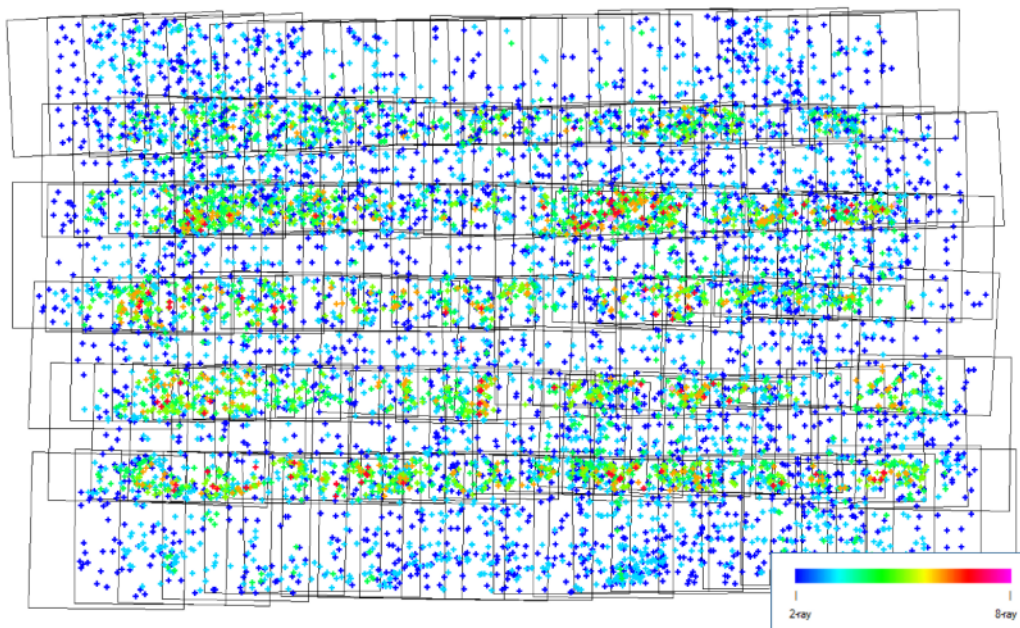


**Figure 5.** Result of automated TP detection on an exemplary block. Dark blue corresponds to TPs with two rays, TPs with multiple rays are depicted in green and reddish colors.

Performance: The average processing time per image was around 5-8 minutes, comprising all steps of the automated workflow. It is calculated by dividing the block processing time by the number of images.

#### 3.2 Final QA

The results of the automated processing chain laid the base for conducting the final QA step in a straightforward manner for most of the defined AT projects. The final QA was carried out in two steps: (1) Running BBA by use of TPs only; and (2) establishing exterior orientation on the result of step 1 by running BBA with TPs and GCPs combined.



Step 1 was carried out when each image had a minimum of 4-6 well distributed TPs and showed an RMS not (much) higher than one pixel. Step 2 was achieved when the overall statistics from BBA figured acceptable residuals on well distributed GCPs. The a priori accuracies for GCP coordinates during BBA were defined with 0.5 m in X, Y and Z. No self-calibration was used in BBA.

The most important techniques for iteratively arriving at the final orientations during QA work showed to be: (1) Manually adding TP measures in order to ensure good linking and a stable configuration of all images within the block; and (2) semi-automatic selection and subsequent elimination of GCP and/or TP coordinates based on their residuals after running BBA.

On archival aerial images, manual TP digitization showed to be a fast and relative convenient technique compared to manual GCP identification and digitization.

In order to obtain final orientations on the *Emmental* sample block (see figure 5), no manual TPs nor GCPs needed to be added to the block. QA work was limited to semi-automatically filtering and de-activating or eliminating TPs and GCPs through iterative BBA calculations. The total amount of human operation time spent to arrive at the final orientations was around 20 minutes for the whole block. Figure 6 depicts a display of GCP residuals for this sample block. The azimuthal orientation of the residuals appears to be non-systematic.

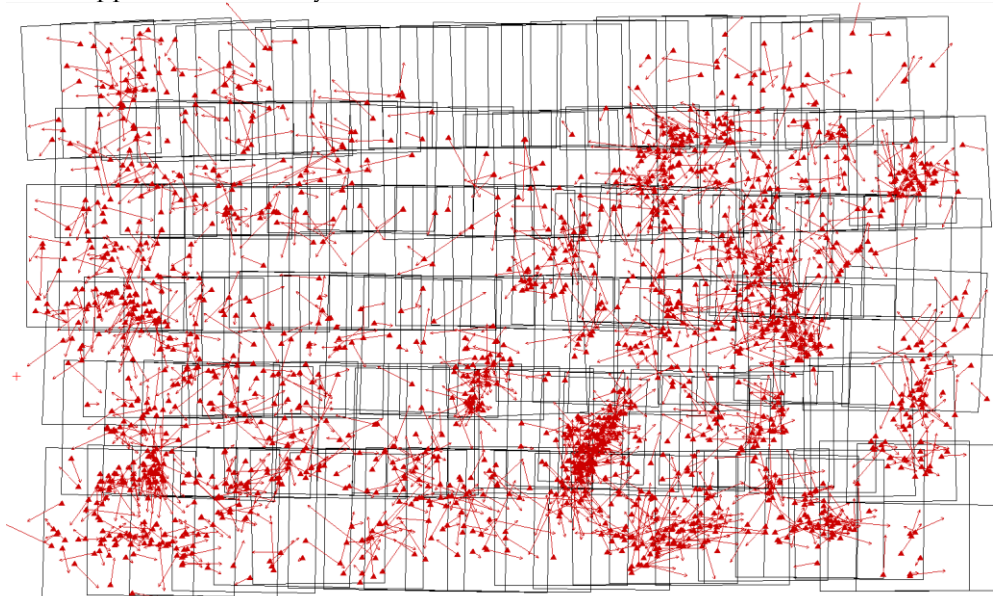


**Figure 6.** Depiction of GCP distribution and residuals for the exemplary *Emmental* block. Unfortunately, OrthoEngine does not display a legend for the magnitude of GCP residuals.

In general, about 5 % of detected TPs and around 25 % of detected GCPs were removed during QA work to arrive at the final orientations. The required amount of manual work (time) for establishing the final orientations was found to vary significantly between the different blocks. The manual time for QA work largely depended on the number of manual TPs that needed to be added. A number of reasons are found to contribute to incomplete or erroneous point detection. The most important ones are assumed to be input data inconsistencies, land cover, flight block configuration and the parametrization of the alignment process.

In some cases, inconsistencies in data input caused, as can be expected, erroneous or no matches for TPs and GCPs. These inconsistencies included e.g. mismatches between documented and real scan orientation or wrong naming of scan file. The extent of these data input inconsistencies caused problems of local magnitude only, resulting e.g. in no tie point matches for the concerned image. These cases were solved by manually correcting for the base problem. Then, the corrected image was connected to the block again through manual TP measurements. Thanks to a good consistency in data and metadata, the number of such cases was low.

Some of the problems encountered in establishing final orientations were related to land cover. Erroneous matches (blunders) for TPs were, e.g., detected over lake surfaces or surfaces covered by snow or ice. These erroneous matches had to be identified and removed. For the GCP detection these regions were simply masked out from the reference data and presented no problems. For the TP detection, masking out problematic land cover cannot be done directly from, e.g., an existing vector dataset because of the lack of precise orientation data.

A further potential to yield more complete image matching results is believed to lie in optimizing parametrization of the alignment process.

Table 1 summarizes the statistics for the orientations of all 36 blocks achieved after final QA work. In classical photogrammetric workflows, the quality of orientations is typically assessed by analyzing residuals on independent Check Points (CPs). In our case, it may appear tempting to simply declare a subset of the abundant amount of GCPs as CPs. This approach was discarded because of the unknown accuracy of the automatically collected reference points. By doing so, a systematic shift among automatically collected reference points would, e.g., remain undetected.

**Table 1.** Summary of statistics of the orientation process. *Extracted* Auto-TPs/AutoGCPs refers to the number of TPs/GCPs extracted by the data processing routine, *retained* Auto-TPs/AutoGCPs refers to the number of TPs/GCPs active in the last BBA run.

Block Name	Number images	Auto-TPs - extracted - retained	AutoGCPs - extracted - retained	TPs manual	Max. Res. GCP X/Y [m]	Max. Res. GCP Z [m]	RMS GCP X/Y [m]	RMS GCP Z [m]
AT_01	625	74683 73174	20846 18066	69	3.44	1.73	0.76	0.39
AT_02	649	88751 86646	28442 24990	43	3.92	2.38	0.79	0.42
AT_03	126	16439 15947	5615 4996	33	3.25	2.05	0.86	0.45
AT_04	73	17296 16201	2518 1943	0	3.46	4.81	0.92	1.22
AT_05	132	35082 32305	4762 3382	0	4.38	2.17	0.84	0.39
AT_06	86	11134 10249	3151 2549	8	4.50	2.30	1.20	0.55
AT_07	252	33177 31248	8303 7240	1	3.69	3.90	0.71	0.97
AT_08	199	27191 24332	3330 2568	0	3.35	1.65	1.07	0.46
AT_09	260	35914 34836	10429 5492	56	1.56	0.90	0.43	0.19
AT_10	128	22706 20428	5918 4647	4	2.48	1.17	0.69	0.30
AT_11	298	22616 21014	11773 10024	15	3.82	1.80	0.84	0.41
AT_12	292	28358 26870	9915 6450	0	3.70	1.90	0.81	0.37
AT_13	72	5212 4667	1948 1398	12	2.90	1.39	0.86	0.40

AT_14	97	6857 6486	4069 3059	11	3.70	1.60	0.82	0.37
AT_15	123	10698 9929	4050 2997	9	1.96	1.11	0.65	0.28
AT_16	129	6932 6548	6527 4564	33	3.17	1.54	0.74	0.36
AT_17	62	4224 4062	2782 1729	11	1.51	0.68	0.57	0.25
AT_18	189	17767 16701	5696 4462	4	2.62	1.36	0.68	0.31
AT_19	185	16891 15734	3923 2879	52	2.84	3.03	0.82	0.45
AT_20	310	25932 24956	5425 4139	64	2.76	1.40	0.71	0.33
AT_21	210	26980 25629	3860 3124	7	3.61	1.85	0.68	0.36
AT_22	136	11323 10782	3119 2219	2	2.18	1.01	0.58	0.28
AT_23	183	13947 13282	5967 4915	66	2.81	1.31	0.67	0.35
AT_24	392	42207 40685	16699 14969	43	3.76	2.19	0.77	0.44
AT_25	231	12691 12310	4446 3913	275	4.00	1.98	0.74	0.39
AT_26	361	18389 17959	5936 5376	179	3.82	1.70	0.77	0.42
AT_27	141	13553 13157	5424 4675	16	3.62	1.95	0.80	0.43
AT_28	154	13457 12923	4300 3927	105	3.96	1.83	0.80	0.42
AT_29	269	17742 15904	5489 4437	286	3.09	1.40	0.64	0.33
AT_30	356	37133 36514	8291 7266	117	4.01	1.91	0.80	0.42
AT_31	136	16844 16366	5021 4521	16	3.19	1.86	0.88	0.47
AT_32	307	23586 23323	14053 12453	72	3.37	1.92	0.85	0.46
AT_33	329	30595 29569	13949 12731	104	4.17	2.00	0.80	0.43
AT_34	295	25694 25282	15387 13817	91	3.81	2.04	0.80	0.46
AT_35	407	38123 37500	15247 13497	51	3.52	1.81	0.78	0.43
AT_36	312	20623 20394	3094 2742	139	3.02	1.77	0.80	0.38

The obtained image orientations allow assessing the accuracies of the initial geo-referencing that was used as input. This information may be used to retrospectively evaluate the plausibility of the defined parameter settings, such as the search radius. Figure 7 displays for each image the planimetric

difference in meters between input coordinates and final position of the projection centers. Figure 8 (a) displays the corresponding histogram.

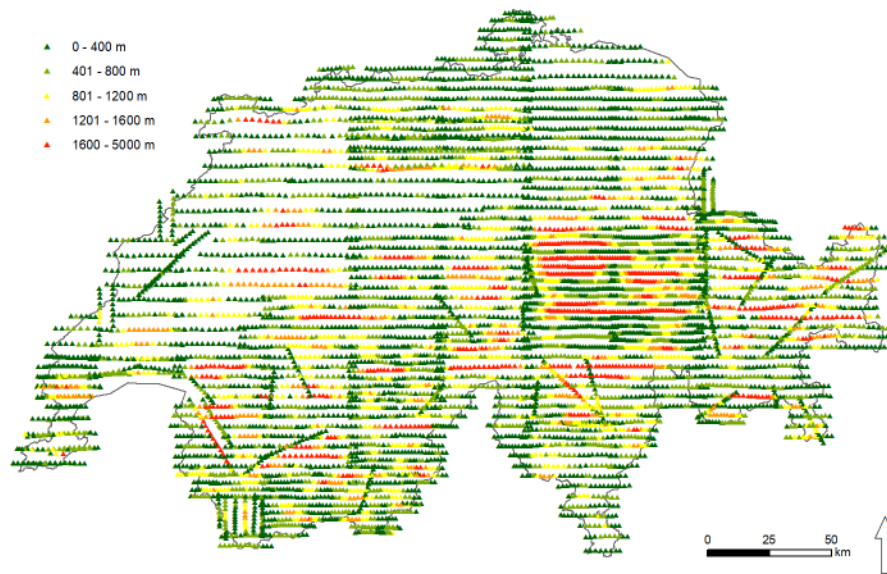


**Figure 7.** Planimetric distances in meter between input geo-referencing and final projection centers of images. The mean value amounts to 603.4 m.

At the authors' affiliation, large experiences in the conduct of orienting AAI using classical photogrammetric workflows exist. A classical photogrammetric workflow in this context involves automated fiducial detection, automated TP matching but manual GCP digitization from a digital reference source. Due to the heterogenic nature of AT blocks and the parallel QA conduct of several blocks, comparing the efficiency of the workflow on a per-block base is not an appropriate approach. Efficiency is therefore assessed based on the summative time spent for orientation of a country-wide coverage only: In our case, one person, working around 20 hours on this project per week, carried out the whole orientation process within 10 weeks. This includes the automatic processing and all manual QA steps for obtaining the final orientations. In consequence, we found that the proposed orientation workflow reduces massively the human working time compared to classical workflows. In our case, we estimate the workflow to be minimum five times more efficient than classical workflows.

### 3.3 Orthophotos and mosaics

The geometric accuracy of the final orthophoto mosaic is derived by comparison with the reference ortho mosaic. Figure 9 displays the generated countrywide orthophoto mosaic and the geographic distribution of measured differences on the sample grid. Figure 8 (b) shows the histogram of the error distribution. No systematic effects on the error distribution were found. Some of the outliers were identified to lay in (potentially) unstable alpine terrain. It is likely that in these cases physical displacement through geomorphological processes between reference and historical air photos has taken place.

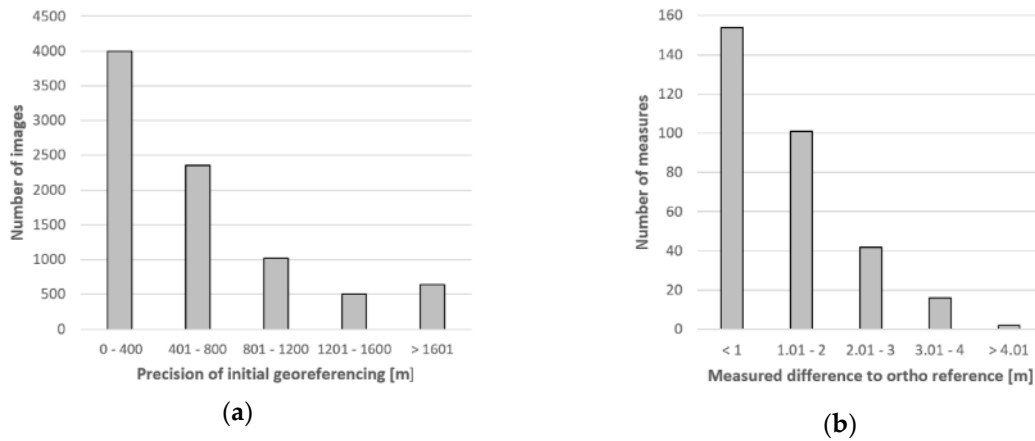


**Figure 8.** (a) The histogram evaluates the accuracy of input coarse geo-referencing. The mean value is 603.4 m. (b) The histogram depicts the positional accuracy of the derived ortho mosaic relative to the ortho reference image. The mean value including the outliers amounts to 1.26 m.

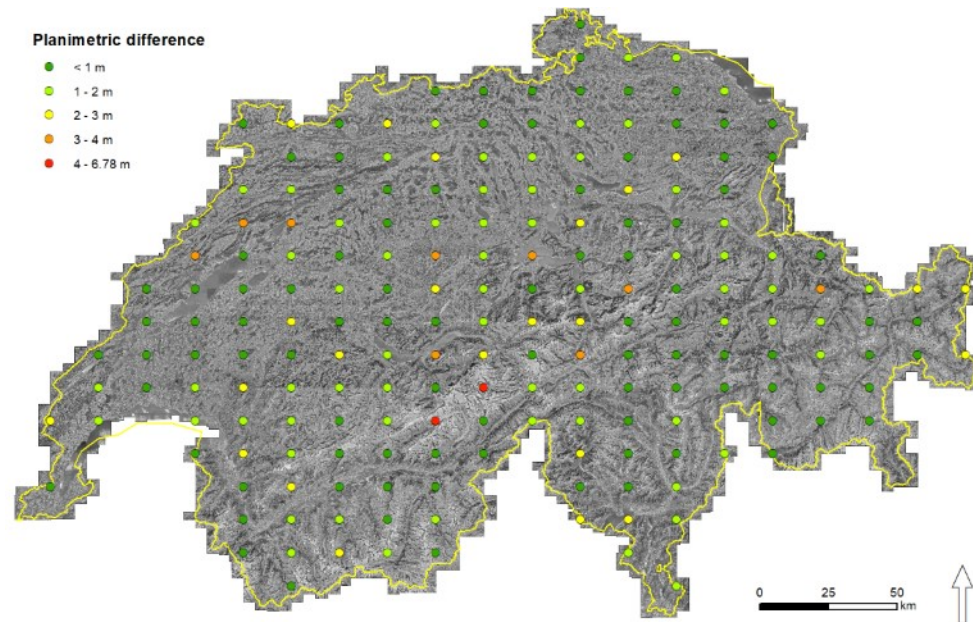


**Figure 9.** Results of accuracy assessment from comparing the generated country-wide ortho mosaic with the ortho reference. The two red dots were identified to lay on unstable terrain.

### 3.4 Digital Surface Models

The obtained DSMs showed practically complete coverage. *NoData* values appeared in areas occluded by viewing geometry only. Hillshades of obtained DSMs display vast details and allow to track topographic changes when comparing to a reference DEM hillshade. The difference of the calculated DSM to the reference DEM is estimated to be better than +/- 1 m for around 90 % on well-defined surfaces. Well-defined surfaces include, e.g., bare rock, paved surfaces and grasslands. Similar accuracies were found on all zones independent from their landscape type. Figure 10 displays examples of the derived DSMs and the orthomosaic.

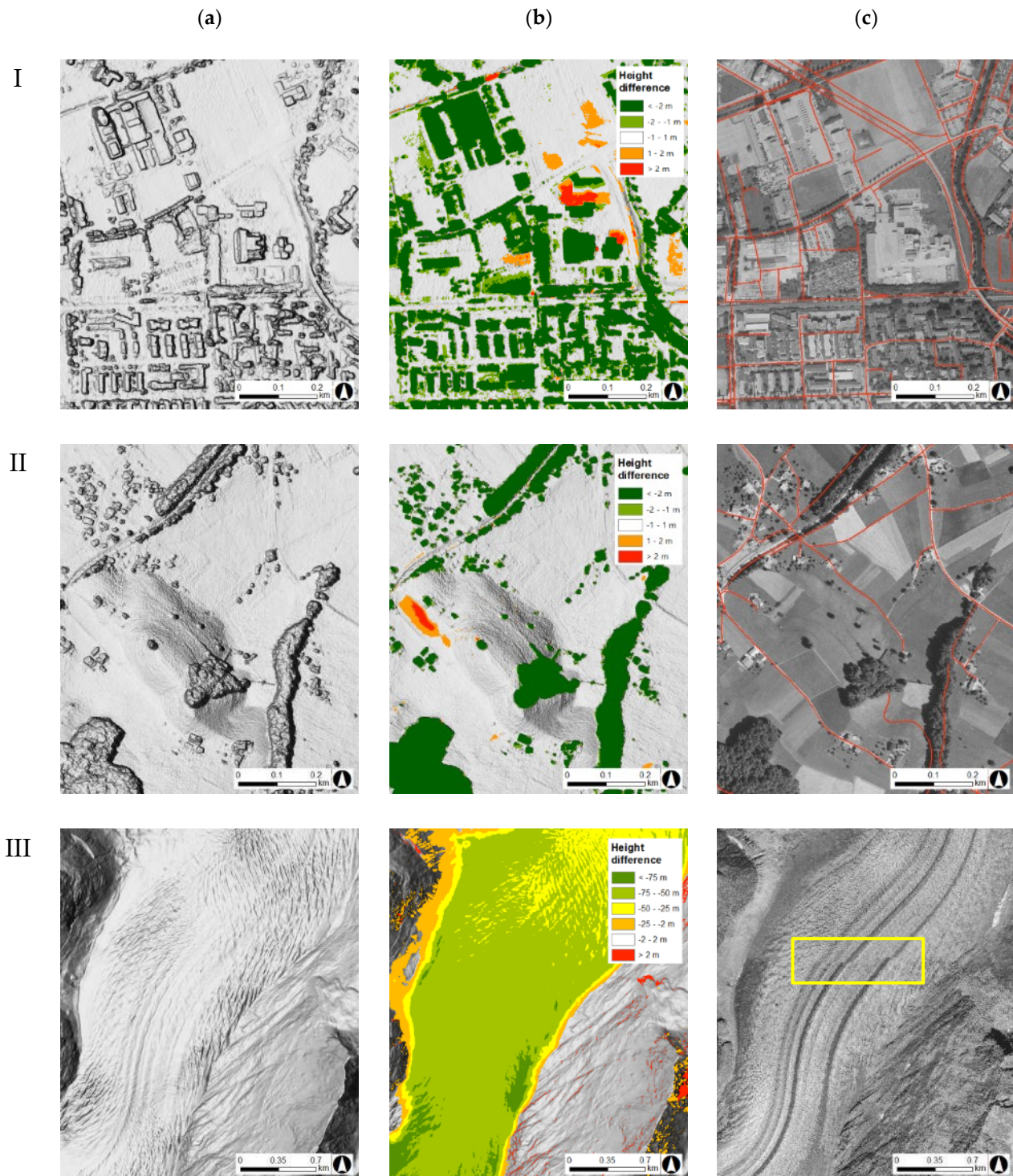


**Figure 10.** Examples to illustrate the quality of produced DSM and orthomosaic for (I) an urban zone (city of Zuerich), (II) a rural pre-alpine zone near the lake Thun, (III) an alpine zone figuring the Aletsch glacier. (a) Shaded relief on generated DSM. (b) Absolute height difference between the reference DTM and the generated DSM. Since the derived DSM is subtracted from a DTM, buildings and vegetation stick out in greenish colors. (c) Orthomosaic overlaid with precise road reference vectors. The planimetric mismatch in (III) (yellow box) is due to the use of a recent DTM in the orthorectification process.

#### 4. Discussion

The highlight of the country-wide geo-referencing approach presented here is the complete substitution for manual GCP measurements. Automated reference image matching in conjunction with BBA and algorithmic filtering have proven to be efficient substitutes in establishing absolute orientation.

One key factor for successfully employing the proposed workflow to yield precise geo-referencing relates to the quality of input data, corresponding metadata and reference data. Digital image scans should be geometrically precise and radiometrically balanced. Flight geometry needs to assure sufficient lateral and in-flight overlap. Fiducial marks need to be identifiable for successful automated establishment of the interior orientation. Metadata relevant for the processing should be complete and reliable. Accuracy and consistency of reference data directly relate to the accuracy of the absolute image orientation that can be obtained.

These findings lead to the question of transferability of the proposed workflow. Transferability in time looks at the adaptability of the workflow to process other generations of archival aerial imagery over the same area of interest (AOI) revealing different characteristics. Aerial images with differing camera formats, focal lengths, support material (glass plates) etc. are available at the authors' affiliation. Extensive tests have been carried out on these. The results indicate that specific adaptation of processing parameters suffices to successfully process most of the different aerial image types with similar efficiency. The accuracies that can be achieved are a function of the data input quality. An example for another country-wide geo-referencing of aerial images acquired in 1946 (Operation Casey Jones) is given in [38]. The processing has been performed at swisstopo using the HAP GUI workflow. The input imagery are copies of low quality and no calibration information was available. Despite these unfavorable preconditions, it was possible to produce a country-wide ortho mosaic with an absolute accuracy of about 5 m. swisstopo has committed itself to continue processing and publishing further series of archival aerial imagery [39].

Transferability in space looks at the possibility of employing the workflow over a different AOI. Our current AOI (Switzerland) covers among the most complex topography in Europe. It contains large lake surfaces and is home to the largest glaciers of the Alps. The authors therefore believe that, provided the data input quality is adequate, the workflow is likely to perform well on other AOIs. Adaptations to the processing parameters in function of the input data may be required, though.

However, there is also potential to improve the current workflow. This encompasses the use of further auxiliary data. If available, a mask of unstable terrain for GCP detection might, e.g., be easily integrated. Furthermore, parameter optimization in the alignment process is expected to lead to further reducing manual QA work by providing even more complete TP patterns. The HAP and OrthoEngine software is actively developed. Most recent releases contain new functionality such as feature-based matching, enhanced accuracy assessment and automated refinement methods.

One major motivation for the processing of AAI is to ease the access to the information contained for the general public and expert applications alike. Currently, the general public can freely consult the produced year-wise orthophoto mosaics through the national Swiss web mapping portal at its full resolution [25]. Other countries' NMCAs chose similar ways to make historic ortho images accessible [40]. In our case, expert users can order aerial image scans provided together with the obtained orientation parameters which allow, e.g., generation of DSMs in a straight-forward manner [24]. At the current state, a fee-based license must be obtained to use the images. The license primarily is restricted to the use for internal purposes, excluding publication or redistribution of the derived data. The Swiss confederation has recently adopted the Open Government Data (OGD) principles for distribution of its national geodata [41]. OGD-based distribution principles together with eased technical access, like online selection and download, and an active communication about the potential of these images, are likely to increase the use of AAI. This may especially hold true for climate change related research activities in alpine environments [12,15].

The centralized fine geo-referencing follows a *once-only* principle. This approach is economically sound because (1) redundancies of multiply orienting images at different customers are avoided and

(2) the establishment of an economic production scale at the data provider is fostered. If, however, higher accuracies are required by the user, he/she can further refine the orientations to his/her needs.

Apart from optimizing geometry, radiometric processing holds further potential in making information in AAI more accessible. Colorization of pan-chromatic aerial images, e.g., through means of artificial intelligence is a promising and interesting technique to help color up our views into the past [42].

**Author Contributions:** Conceptualization, Methodology, Writing-Original Draft Preparation: Holger Heisig, Writing-Review & Editing, Supervision: Jean-Luc Simmen. All authors have read and agreed to the published version of the manuscript.

**Funding:** This research received no external funding

**Acknowledgments:** Internally, we are grateful to S. Hagmayer for realization of the accuracy assessment and his contributions in the production process, F. Gandor for support with FME and Python, C. Loup for development of PhotoShop macros, E. Raymann for LUBIS management, H. Rusli for general application development, A. Windler for preceding conceptual works and L. O'Sullivan for the English language revision. Externally, we like to thank J.-S. Bouffard and S. Wyseman from PCI Geomatics for reviewing and general support and to Prof. C. Heipke for reviewing and his constructive and helpful comments.

**Conflicts of Interest:** The authors declare no conflict of interest.

## References

1. Redweik, P.; Roque, D.; Marques, A.; Matildes, R.; Marques, F. Triangulating the past—recovering Portugal's aerial images repository. *Photogrammetric Engineering & Remote Sensing* **2010**, *76*, 1007–1018.
2. Pinto, A.T.; Gonçalves, J.A.; Beja, P.; Pradinho Honrado, J. From archived historical aerial imagery to informative orthophotos: A framework for retrieving the past in long-term socioecological research. *Remote Sensing* **2019**, *11*, 1388.
3. Giordano, S.; Le Bris, A.; Mallet, C. Toward automatic georeferencing of archival aerial photogrammetric surveys **2018**.
4. Verhoeven, G.; Sevara, C.; Karel, W.; Ressel, C.; Doneus, M.; Briese, C. Undistorting the past: New techniques for orthorectification of archaeological aerial frame imagery. *Good practice in archaeological diagnostics*; Springer, Cham, 2013; pp 31–67.
5. Cowley, D.C.; Stichelbaut, B.B. Historic aerial photographic archives for European archaeology. *European Journal of Archaeology* **2012**, *15*, 217–236.
6. Božek, P.; Janus, J.; Mitka, B. Analysis of Changes in Forest Structure using Point Clouds from Historical Aerial Photographs. *Remote Sensing* **2019**, *11*, 2259.
7. Nurminen, K.; Litkey, P.; Honkavaara, E.; Vastaranta, M.; Holopainen, M.; Lyytikäinen-Saarenmaa, P.; Kantola, T.; Lyytikäinen, M. Automation aspects for the georeferencing of photogrammetric aerial image archives in forested scenes. *Remote Sensing* **2015**, *7*, 1565–1593.
8. Nebiker, S.; Lack, N.; Deuber, M. Building change detection from historical aerial photographs using dense image matching and object-based image analysis. *Remote Sensing* **2014**, *6*, 8310–8336.
9. Mertes, J.R.; Gulley, J.D.; Benn, D.I.; Thompson, S.S.; Nicholson, L.I. Using structure - from - motion to create glacier DEMs and orthoimagery from historical terrestrial and oblique aerial imagery. *Earth Surface Processes and Landforms* **2017**, *42*, 2350–2364.
10. Sevara, C.; Verhoeven, G.; Doneus, M.; Draganits, E. Surfaces from the visual past: Recovering high-resolution terrain data from historic aerial imagery for multitemporal landscape analysis. *Journal of archaeological method and theory* **2018**, *25*, 611–642.
11. Gomez, C.; Hayakawa, Y.; Obanawa, H. A study of Japanese landscapes using structure from motion derived DSMs and DEMs based on historical aerial photographs: New opportunities for vegetation monitoring and diachronic geomorphology. *Geomorphology* **2015**, *242*, 11–20.
12. Mölg, N.; Bolch, T. Structure-from-motion using historical aerial images to analyse changes in glacier surface elevation. *Remote Sensing* **2017**, *9*, 1021.



13. Vargo, L.J.; Anderson, B.M.; Horgan, H.J.; Mackintosh, A.N.; Lorrey, A.M.; Thornton, M. Using structure from motion photogrammetry to measure past glacier changes from historic aerial photographs. *Journal of Glaciology* **2017**, *63*, 1105–1118.
14. Fischer, L.; Eisenbeiss, H.; Käab, A.; Huggel, C.; Haeberli, W. Monitoring topographic changes in a periglacial high - mountain face using high - resolution DTMs, Monte Rosa East Face, Italian Alps. *Permafrost and Periglacial Processes* **2011**, *22*, 140–152.
15. Micheletti, N.; Lane, S.N.; Chandler, J.H. Application of archival aerial photogrammetry to quantify climate forcing of alpine landscapes. *The Photogrammetric Record* **2015**, *30*, 143–165.
16. Ford, M. Shoreline changes interpreted from multi-temporal aerial photographs and high resolution satellite images: Wotje Atoll, Marshall Islands. *Remote Sensing of Environment* **2013**, *135*, 130–140.
17. Strozzi, T.; Ambrosi, C.; Raetzo, H. Interpretation of aerial photographs and satellite SAR interferometry for the inventory of landslides. *Remote Sensing* **2013**, *5*, 2554–2570.
18. Remondino, F.; Spera, M.G.; Nocerino, E.; Menna, F.; Nex, F. State of the art in high density image matching. *The Photogrammetric Record* **2014**, *29*, 144–166.
19. Bakker, M.; Lane, S.N. Archival photogrammetric analysis of river–floodplain systems using Structure from Motion (SfM) methods. *Earth Surface Processes and Landforms* **2017**, *42*, 1274–1286.
20. Feurer, D.; Vinatier, F. Joining multi-epoch archival aerial images in a single SfM block allows 3-D change detection with almost exclusively image information. *ISPRS journal of photogrammetry and remote sensing* **2018**, *146*, 495–506.
21. Fischer, M.; Huss, M.; Hölzle, M. Surface elevation and mass changes of all Swiss glaciers 1980–2010. *The Cryosphere* **2015**, *9*, 525–540.
22. Beyeler, A. Arealstatistik der Schweiz–Methodik und aktuelle Ergebnisse. *Flächennutzungsmonitoring II. Konzepte–Indikatoren–Statistik. IÖR Schriften* **2010**, *52*, 111–126.
23. Ginzler, C.; Hobi, M.L. Countrywide stereo-image matching for updating digital surface models in the framework of the Swiss National Forest Inventory. *Remote Sensing* **2015**, *7*, 4343–4370.
24. Ginzler, C.; MARTY, M.; WASER, L.T. Landesweite digitale Vegetationshöhenmodelle aus historischen SW-Stereoluftbildern.
25. swisstopo. A journey through time – aerial images. <https://www.swisstopo.admin.ch/en/maps-data-online/maps-geodata-online/journey-through-time-images.html> (accessed on 31 August 2020).
26. swisstopo. Information system for aerial photographs / LUBIS viewer. <https://www.swisstopo.admin.ch/en/maps-data-online/maps-geodata-online/lubis.html> (accessed on 31 August 2020).
27. Heipke, C. Automation of interior, relative, and absolute orientation. *ISPRS journal of photogrammetry and remote sensing* **1997**, *52*, 1–19.
28. Persia, M.; Barca, E.; Greco, R.; Marzulli, M.; Tartarino, P. Archival Aerial Images Georeferencing: A Geostatistically-Based Approach for Improving Orthophoto Accuracy with Minimal Number of Ground Control Points. *Remote Sensing* **2020**, *12*, 2232.
29. Nagarajan, S.; Schenk, T. Feature-based registration of historical aerial images by area minimization. *ISPRS journal of photogrammetry and remote sensing* **2016**, *116*, 15–23.
30. Cléry, I.; Pierrot-Deseilligny, M.; Vallet, B. Automatic georeferencing of a heritage of old analog aerial photographs. *ISPRS Annals of Photogrammetry, Remote Sensing & Spatial Information Sciences* **2014**, *2*.
31. Swiss Federal Statistical Office. *Land Use in Switzerland-Results of the Swiss Land Use Statistics*, 2013.
32. swisstopo. swissimage - The Digital Color Orthophotomosaic of Switzerland. <https://www.swisstopo.admin.ch/en/home/products/images/ortho/swissimage.html> (accessed on 24 August 2020).
33. swisstopo. swissALTI3D - The high precision digital elevation model of Switzerland. [https://shop.swisstopo.admin.ch/en/products/height\\_models/alti3D](https://shop.swisstopo.admin.ch/en/products/height_models/alti3D) (accessed on 24 August 2020).
34. swisstopo. swissTLM3D - The large-scale topographic landscape model of Switzerland. <https://shop.swisstopo.admin.ch/en/products/landscape/tlm3D> (accessed on 24 August 2020).
35. Shawn Melamed. Semi-Automated Historical Airphoto Processing. [https://www.pcigeomatics.com/pdf/HAP\\_WhitePaper.pdf](https://www.pcigeomatics.com/pdf/HAP_WhitePaper.pdf).

36. Fischler, M.A.; Bolles, R.C. Random sample consensus: a paradigm for model fitting with applications to image analysis and automated cartography. *Communications of the ACM* **1981**, *24*, 381–395.
37. Hirschmuller, H. Stereo processing by semiglobal matching and mutual information. *IEEE Transactions on pattern analysis and machine intelligence* **2007**, *30*, 328–341.
38. Heisig, H.; Simmen, J.L.; Zesiger, M. Die Amerikanerbefliegung von 1946 - von selbstentzündlichen Duplikatnegativen zum landesweiten Orthofotomosaik. *Geomatik Schweiz* **2019**, 268–271.
39. swisstopo. Prises de vue terrestres et orthophotos historiques sur map.geo.admin.ch. *Geomatik Schweiz* **9**, 2018, 274–275.
40. IGN. Remonter le temps. <https://remonterletemps.ign.fr/>.
41. swisstopo. Open Government Data (OGD). <https://www.isb.admin.ch/isb/en/home/themen/e-government/open-government-data-ogd.html> (accessed on 16 November 2020).
42. *Toward an Unsupervised Colorization Framework for Historical Land Use Classification*. IGARSS 2019-2019 IEEE International Geoscience and Remote Sensing Symposium; IEEE, 2019.

# Report

# 1 General remarks

## 1.1 Scope and aim of this report

This report is part of the manuscript-style based Master Thesis. It is complementary to the first part, the manuscript elaborated to be publishable in a peer reviewed, ISI-indexed, international journal.

This report intends to document the methodological steps to allow a clear and precise judgment to be made of the presented research. The report focuses on the technical implementation and operational application of the developed production workflow for orientation, orthorectification and ortho mosaic generation of different sets of archival aerial imagery (AAI). It is complementary to the manuscript in a sense that it avoids redundant information already given in the manuscript. It is also complementary in the sense that this report will not fully be comprehensible without thorough reading of the manuscript part.

Whereas the journal paper from the first part is strictly limited to the processing of a defined set of 8'507 images acquired between 1985 and 1991, this report discusses the workflow in a larger sense. At the time of writing, around another 15'000 images from the 1970's have yet been oriented with the presented workflow. This report therefore includes the reflection of workflow adaptations gained during these further processing.

## 1.2 Motivation

Figure 1 displays a simplified schematic cost-benefit analysis for the steps that process original historic air photos into a format that the information contained within are easily accessible and relatable to other geodata. The *cost* of each process roughly relates to the required human labour whereas the benefit consists in the *ease of access* to the information. Whereas the steps of physical image preservation, metadata collection and scanning require substantial human resources, the photogrammetric processing steps of orthoimage generation, surface model generation and ortho mosaic generation can, typically, be largely automated. In conventional workflows, image orientation of AAI requires substantial human resources as well. The motivation of this work consists in automating image orientation to a degree that its costs are no more prohibitive for the processing of large aerial image archives.

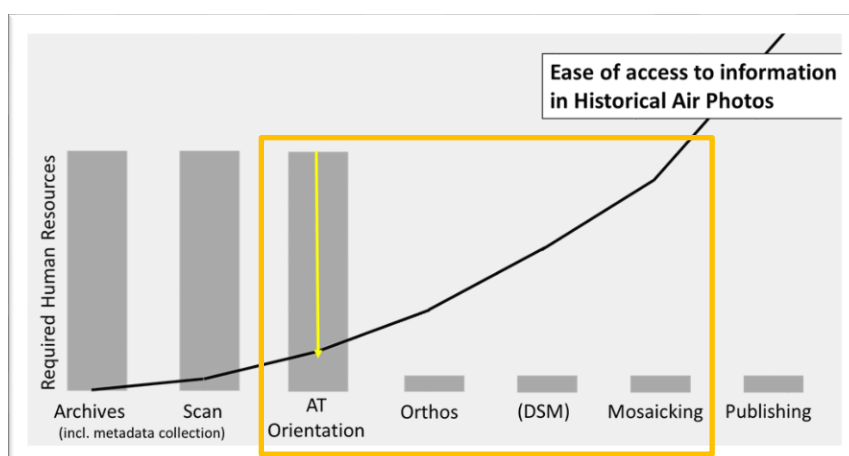


Figure 1: Schematic cost-benefit comparison for turning AAI into published ortho mosaics. The contents of this report is limited to the photogrammetric processing steps (orange box) with a strong focus on image orientation.

The workflow aims at balancing maximum efficiency while ensuring maximum data consistency. The described workflow has evolved over a period of around two years. It is not static but rather organic in nature and is intended to remain subject to a process of permanent improvement. The workflow encompasses the use of a number of different software. We are committed to migrating towards newest stable software versions. For these reasons, the workflow has undergone some minor changes since the processing of the 8'507 images which took place in 2019. This report represents the current state of the workflow (October 2020) and may therefore deviate in details. It contains, e.g., screenshots of software versions that were not used in the processing of the first part. However, the principal ideas remained unchanged.

The principal achievement of this work consists of a pragmatic but efficient implementation of a highly productive photogrammetric workflow. The theoretical photogrammetric background of certain elements of the workflow are therefore discussed rather from a practitioner's point of view. Even though, the complete workflow may, at times, appear to be (overly) complex, it follows an inherent logical structure. Although the author has designed and implemented, tested and operated the complete workflow, he has integrated existing internal and external applications and delegated part of the required application development. Wherever this was the case, it is indicated in this report.

## 2 Image orientation process

### 2.1 Workflow progress table

The image orientation and orthorectification processes are conducted block-wise, i.e. by grouping aerial images into aerial triangulation (AT) blocks. For each AT block, a number of consecutive processing steps is executed. For to keep track of the progress of processing the AT blocks, a spreadsheet table is established (see Figure 2). The table is constantly updated throughout the production process. In the following, these different processes will be described.

AT_project_ID	STATUS	Operator	nb AT images	Flight Year	Ref	abID: additional files	nb additional images	Total images	Check logs	start time	Data Preparation (prevAT)	Fix 3 fiducial problem (RCDB)	Point pattern	Assign/Refidist & correct Calibrations	Check ID residuals	Digitize missing TPs
RCH_C02_AT01	finished	hsl	439	1978	DOP25_1n	none	0	439	228458; 197; default	25.03.2020		N/A	default			
RCH_C02_AT02	finished	luk	437	1978	DOP25_1n	none	0	437		25.03.2020		N/A	default		correct 1 TPs	
RCH_C02_AT03	finished	luk	582	1978 & 1979	DOP25_1n	B30A743D-8885-4410-AEBC-A3FA20EAF093FD3596-2C68-48FD-3D4F-A99BDC0C40	46	630	238803 & 238804	03.04.2020		N/A	default			
RCH_C02_AT04	finished	luk	443	1978 & 1979	DOP25_1n	F0E0C26-9FCF-4F89-33FD-F77AEB1C7D4B	25	468		03.04.2020		N/A	default			
RCH_C02_AT05	finished	hsl	340	1978	DOP25_1n	6FAEB83D-BA7F-4753-B610-831TC3A02641	29	369		03.04.2020		N/A	default			
RCH_C02_AT06	finished	hsl	107	1977	DOP25_1n	none	0	107		25.03.2020		N/A	default			
RCH_C02_AT07	finished		336	1977	DOP25_1n	none	0	336		31.03.2020		N/A	default			
RCH_C02_AT08	finished	luk	608	1978	DOP25_1n	none	0	608		31.03.2020		N/A	default			
RCH_C02_AT09	finished		462	1978	DOP25_1n	00DB930D-9035-444A-8683-3036DFAE103	36	436	237871 - 90'	03.04.2020		N/A	default			
RCH_C02_AT10	created		434	1978	DOP25_1n	734FF28C-4F93-4662-AB43-AEF93784AE43	38	432		06.04.2020	corr. control ?	N/A	default		S_233-714	
RCH_C02_AT11	finished	hsl	356	1978	DOP25_1n	6E544D7E-9D7F-42FE-3014-7698F8251AE	35	331	S_240993 vs. S_240977 & S_240973	06.04.2020		N/A	default			
RCH_C02_AT12	created	luk	437	1978 & 1979	DOP25_1n	22E0CF39-496C-4758-88CB-6819714104	47	524		08.04.2020		N/A	default			
RCH_C02_AT13	finished		706	1977	DOP25_1n	C13F7489-846E-4816-8E4A-7888C0703E4E30FF7D8-30CC-43E1-83C8-F1AC322C-A04A24D91D76-92C1-454A-8DCA-E93E377F36313C633FEF73E14C4D-363D-34E2A056416	123	835	Tux 232508	04.04.2020		N/A	default			
RCH_C02_AT14	finished	hsl	822	1977 & 1978	DOP25_1n	none	0	822		04.04.2020		N/A	default		S_233-618	
RCH_C02_AT15	created	luk	712	1977 & 1978	DOP25_1n	1DB00E8E-5E0A-4CAB-9FD0-BCFD43328D1323CDD7F-CF63-4E5A-8C41-98182E844110	37	743	234708 & 234703 Review 234708 Tux 231801	10.04.2020		N/A	default			
RCH_C02_AT16	finished	hsl	626	1977	DOP25_1n	88590400-5D7E-4B18-9623-38F3908F7C277EFC4C76-44DD-4D4E-A531762328E20E8E	42	668	233771 & 234823; Knutwurf?	10.04.2020		N/A	default			



metadata base. The selection can either be done interactively or by using Standard Query Language (SQL) statements on the attribute table. Next, the user defines a name for the AT block. When executed, the tool creates a new entry into the LUBIS table *AT\_Projects* containing the name of the project as well as a new *AT\_BLOCK\_UUID*. All images selected obtain the new *AT\_BLOCK\_UUID* into the attribute field that relates the *Images* table with the *AT\_Projects* table.

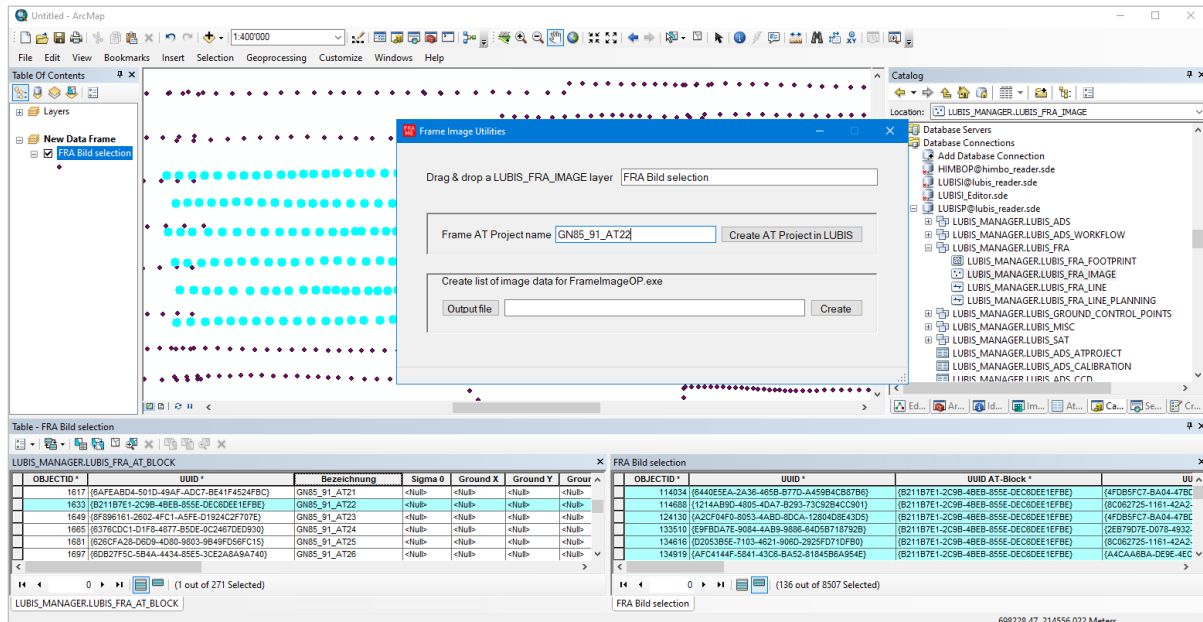


Figure 3: Definition of an AT block in LUBIS using the *FrameImageUtilities* tool.

Block definition can be undone only by manually editing the LUBIS database. Due to the incremental approach from defining and processing “small and easy” AT projects towards definition of bigger and more difficult AT projects, blocks had only to be re-defined in very exceptional cases.

### 2.2.3 Additional lines

Across the project perimeter, larger residuals, and thus a less favourable orientation, is often observed along the edges of the block<sup>1</sup>. This effect can, in practice, partly be mitigated through the use of *additional images*. Additional images are used in the orientation process to form a “buffer zone” around the images of the AT block. Images from flight lines surrounding the actual AT block images are treated throughout the orientation process as if belonging to the actual AT block. However, their orientations are not archived along with the AT block’s orientations. In our block definition process, additional lines were defined wherever appropriate. The very most number of the flight lines to be oriented is flown either East-West or West-East. Typically, the next line to the North and to the South were defined as additional lines. The implemented automated data preparation routines identify additional *images* by passing the UUIDs of the manually defined additional *lines* based on geographic buffering of existing coarse-georeferenced footprints (see 2.3.3). Figure 4 depicts an AT block together with the additional images used on it.

<sup>1</sup> K. Kraus. Lehrbuch Photogrammetrie. Band 1. De Gruyter. 7th Edition. 2004

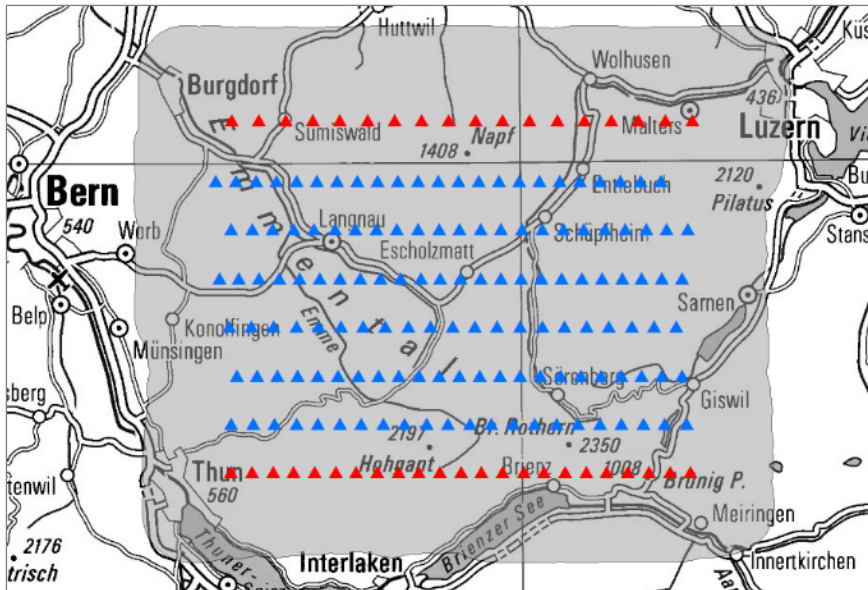


Figure 4: Configuration of an AT block with additional images in the *Emmental* region. Core images are depicted in blue, additional images are depicted in red. The extent of the reference files are depicted in grey.

Minor disadvantages in the use of additional images consist in increasing the processing time and a potential increase of the complexity of the block. The utilization of additional lines in the image orientation process is common practice at the author's affiliation within the orientation process of most recent digital imagery acquired with GPS/INS.

## 2.3 Automated processing

### 2.3.1 Introduction

All automated processing steps are executed through a single batch file per AT block. The file contains the calls for all involved routines, which are executed consecutively. The workflow is designed such that it allows for processing a number of series of different aerial image types, depending on camera type and calibration protocol.

In the following, an example of the batch file is given and explained in the order of its execution. The black-framed text boxes in the next sections form together the contents of the batch file.

### 2.3.2 Parameter assignment

In the first line of the batch file, the name of the AT block is defined:

```
REM set the block name
set block_name=RC08_GAM_AT08
```

The value of the block name variable is changed manually for each batch file. The naming of the block follows a convention that allows for deducing the camera type and the calibration protocol. The current implementation allows for to process images from 1946 to 1991. In this period, the WILD camera types RC05, RC08 and RC10 were operated by swisstopo.

Next, the definition of generic metadata path and output data path is followed by the definition of camera type and calibration protocol as deduced from the name of the AT block:



```

REM set metadata path
set q_path='\\v0t0020a.adr.admin.ch\topo\tbk\tbkb\frame\HAP\530_GN79_46'
REM set data path
set i_path='\\v0t0020a.adr.admin.ch\topo\tbk\imageprod\HISTORY-OP\AT'
REM camera is set
set cam=%block_name:~0,4%
REM calibration is set
set cam_calib=%block_name:~0,8%

```

In function of the camera type, the parameters file for the *Historic Air Photo (HAP)* processing module are assigned for the first and the second alignment run:

```

REM parameter file for coarse alignment is assigned in function of
camera/calibration
if %cam%==RC05 set coarseAlign='%q_path%\5_HAP\_coarseAlignDefaults_RC05.py'
if %cam%==RC08 set coarseAlign='%q_path%\5_HAP\_coarseAlignDefaults_RC08.py'
if %cam%==RC10 set coarseAlign='%q_path%\5_HAP\_coarseAlignDefaults_RC10.py'

if %cam%==RC05 set fineAlign='%q_path%\5_HAP\_fineAlignDefaults_RC05.py'
if %cam%==RC08 set fineAlign='%q_path%\5_HAP\_fineAlignDefaults_RC08.py'
if %cam%==RC10 set fineAlign='%q_path%\5_HAP\_fineAlignDefaults_RC10.py'

```

### 2.3.3 Image data and metadata preparation

The next line of the script calls the (first) data preparation routine that was implemented into a *Feature Manipulation Engine (FME)* workbench:

```

REM run first FME routine: folder structure, local copy of image files, prepare
metadata
'C:\Program Files\FME\fme.exe' '%q_path%\4_Pre-
AT\2_FME\PreAT_GN79_46_FME2019.fmw' --additional_lines '47F38830-8324-4252-A7F4-
4FF926E06BB1' --FRA_AT_BLOCK '%block_name%'

```

FME provides a graphical interface allowing for elaboration of geoprocessing scripts. The available geoprocessing functions, called *Transformers*, can be connected such that the output of one tool is direct input to another tool. This way, complex geoprocessing workflows can be implemented in a form of graphical programming. Figure 5 depicts a subset of the implemented FME workbench.

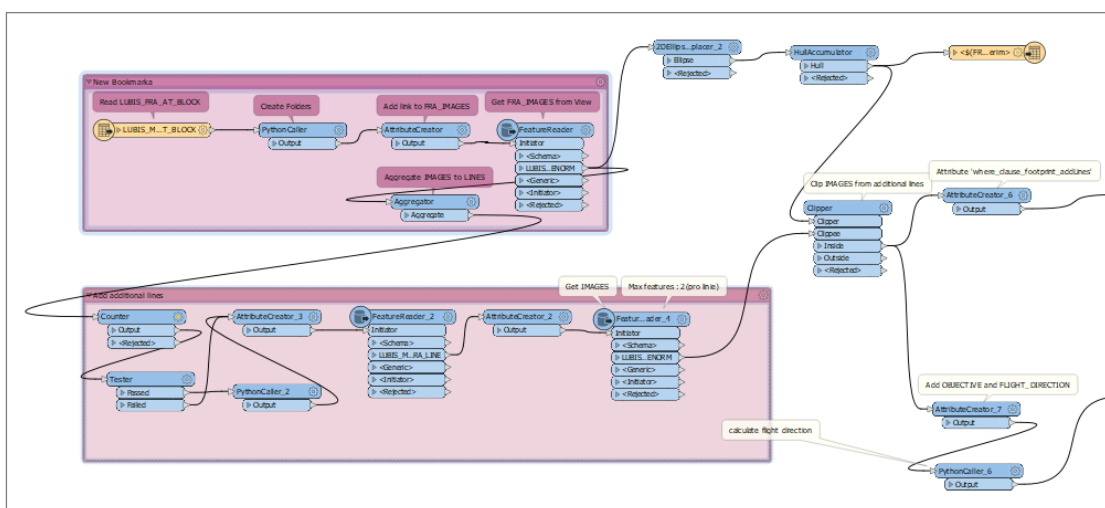


Figure 5: Graphical subset of the FME-based data preparation routine

The required parameters for to run the FME workbench are the AT block name, the UUID(s) of defined additional lines and the workspace (ending \*.fmw) itself.

The developed workbench executes following tasks:

- Building a pre-defined folder structure for the orientation process on the data work drive.
- Reading geometries of (coarsely georeferenced) images and their corresponding footprints from the Oracle/ArcSDE-based LUBIS metadata base.
- Reading and exporting associated calibration information from LUBIS into the pre-defined folder structure. Calibration information are written to an XML file (see Figure 6) that is later imported into the photogrammetric project file.
- Identification of additional images based on the provided UUIDs for additional lines and their geometric relation to the images of the defined AT block.
- Determination of the extent for the reference data (ortho reference and Digital Elevation Model (DEM) reference files) based on the image footprints, including a buffer that accounts for the inaccuracy of the coarse georeferencing. The extent is written as a polygon feature class into an ESRI file geodatabase.
- Copying the full resolution image scans (TIF format) from the image archives to the data work drive. Alongside with the full resolution images, compressed quick views in low resolution (JPEG format) are kept in the image archives. These quick views are copied as well to the data work drive.
- Preparation and export of the text file for the *HAP Ingest* process. The text file contains scan file name, latitude and longitude (WGS84) of initial georeferencing information, approximate flying height and image size.
- Based on the azimuth of the flight line, each image file is assigned a prefix (e.g. 'E\_' for a flight azimuth bigger than 45° and smaller or equal to 135°).

The scan image file dimensions are around 17'000 pixels by 17'000 pixels. The scan image file size amounts to around 300 MB per image. A block of 500 images thus involves the copy process of around 150 GB of scan image files. The execution of the workbench takes between 1 – 3 hours for execution depending on the number of images involved.

```
<?xml version="1.0" encoding="ISO-8859-1" standalone="no"?>
<!DOCTYPE CAMERA SYSTEM "FB9.dtd">
<CAMERA NAME="">
  <LENS_SERIAL/>
  <CALIB_SOURCE/>
  <CALIB_DATE/>
  <FL>153.02</FL>
  <StdDevFL>0.01</StdDevFL>
  <SYMMETRY PPX="0.004" PPY="-0.006"/>
  <STDDEV PPX="0.0114" PPY="0.0114"/>
  <RLDC name="R0">0</RLDC>
  <RLDC name="R1">0</RLDC>
  <RLDC name="R2">0</RLDC>
  <RLDC name="R3">0</RLDC>
  <RLDC name="R4">0</RLDC>
  <RLDC name="R5">0</RLDC>
  <RLDC name="R6">0</RLDC>
  <RLDC name="R7">0</RLDC>
  <DDC name="P1">0</DDC>
  <DDC name="P2">0</DDC>
  <DDC name="P3">0</DDC>
  <DDC name="P4">0</DDC>
</CAMERA>
<FILM>
  <CORNER/>
  <FID_COORD name="TopLeft" FID_X="-105.997" FID_Y="106.003"/>
  <FID_COORD name="TopRight" FID_X="106.003" FID_Y="105.998"/>
  <FID_COORD name="BottomRight" FID_X="106.005" FID_Y="-106.003"/>
  <FID_COORD name="BottomLeft" FID_X="-105.993" FID_Y="-106.004"/>
</FILM>
</CAMERA>
```

Figure 6: Calibration information XML file exported by the FME data preparation routine

### 2.3.4 Reference data preparation

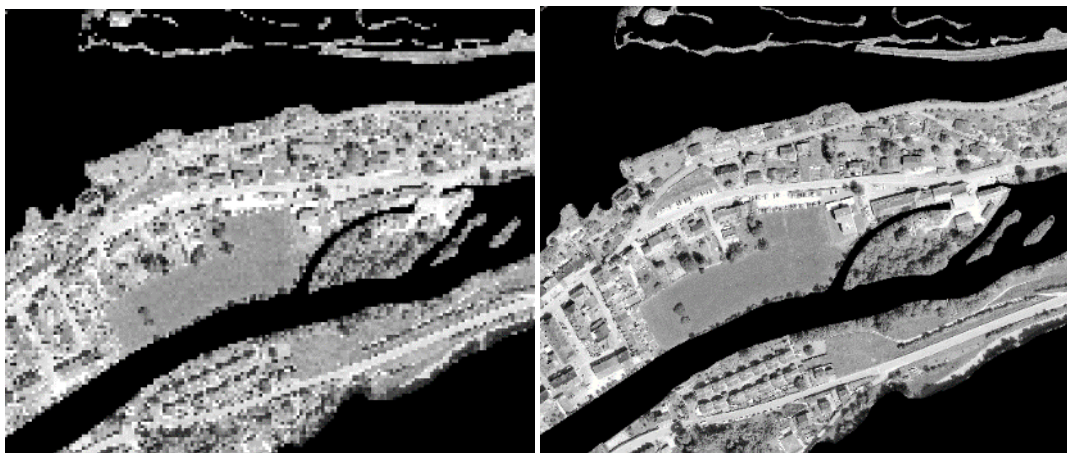
The next line in the batch files calls and executes a second FME data preparation routine. This FME routine prepares the reference files (ortho reference and DEM files) for the automated HAP processing:

```
REM run second FME routine preparing reference data sets
'C:\Program Files\FME\fme.exe' '%q_path%\4_Pre-
AT\2_FME\PreAT_GN79_46_ref_FME2019.fmw' --gsd_si_fine-align '1' --FRA_AT_BLOCK
'%block_name%'
```

The required arguments consist of the AT block name and the desired resolution of the reference ortho mosaic (*gsd\_si\_fine-align*).

The developed workbench executes following tasks:

- Clipping and exporting the reference DEM to the extent of the block as defined by FME routine 1. The reference DEM is exported with 2 m cell size from national height model SWISSALTI3D<sup>2</sup>.
- Clipping and exporting the reference ortho mosaic to the extent of the block as defined by FME routine 1. The input reference is a 1 m resolution panchromatic ortho mosaic. This country-wide ortho mosaic was derived from the 25 cm RGB SWISSIMAGE product<sup>3</sup> from the reference year 2016. Due to data handling and performance issues, it was decided not to use the full 25 cm resolution. Within the FME routine, the ortho mosaic reference is exported into two different resolutions: 3 m and 1 m. The 3 m reference is used in the first (*coarse*) HAP alignment run whereas the 1 m reference is used in the second (*fine*) HAP alignment run.
- Masking the ortho mosaic reference files for land cover classes that are susceptible to produce erroneous matches in the later GCP detection process. These land cover classes are water surfaces, forests and glaciers. The FME routine reads land cover information from the national landscape model (*Topographisches Landschafts Modell - TLM*)<sup>4</sup>.



<sup>2</sup> swisstopo. swissALTI3D - The high precision digital elevation model of Switzerland.

[https://shop.swisstopo.admin.ch/en/products/height\\_models/alti3d](https://shop.swisstopo.admin.ch/en/products/height_models/alti3d) (accessed on 24 November 2020)

<sup>3</sup> swisstopo. swissimage - The Digital Color Orthophotomosaic of Switzerland.

<https://www.swisstopo.admin.ch/en/home/products/images/ortho/swissimage.html> (accessed on 24 November 2020)

<sup>4</sup> swisstopo. swissTLM3D - The large-scale topographic landscape model of Switzerland.

<https://shop.swisstopo.admin.ch/en/products/landscape/tlm3d> (accessed on 24 November 2020).



- The input metadata text file
- The output folder

The routine executes following tasks:

- Import of scan image files into PCI's intrinsic PIX format
- Creation of a photogrammetric project file for *OrthoEngine*. *OrthoEngine* is the photogrammetric core module from *PCI Geomatics*. The created project file incorporates all information from the ingested metadata file and establishes the links to the imported scan image files. The *Ingest* process automatically defines the projection of the *OrthoEngine* project file. The projection is set to the appropriate UTM zone based on the initial input image georeferencing provided in the metadata file.

### 2.3.6 Python API scripts

#### 2.3.6.1 General functionality

The next line in the batch file calls a Python script that executes a number of operations using the *OrthoEngine* Python Application Programming Interface (API):

```
REM run Python scripts for reference file projection, calibration import, eo
import & prj creation (and autofid) --> folders must exist
'C:\Python27\ArcGISx6410.6\python.exe' '%q_path%\4_Pre-
AT\3_Python\530_python_PreAT_params.py' --ref_dir
'%i_path%\%block_name%\2_metadata_reference' --change_dir
'%i_path%\%block_name%\4_alignment\Ingest' --cal_id %cam%
```

This self-developed Python script executes following tasks:

- Assign the Swiss national projection (EPSG:21781) to the reference files.
- Re-project the photogrammetric project file to Swiss national projection (EPSG:21781). The workflow is designed to work within the same projection system. The idea is to reach maximum efficiency and consistency of results through avoiding on-the-fly projections during processing.
- Import of detailed calibration information. The HAP workflow does only require the focal length to be defined. However, if complete camera calibration information are available, these can be imported into the photogrammetric project file. In our case, detailed information on camera calibration are available in LUBIS. Within the first FME data preparation routine, these were exported into an XML file (see 2.3.3 and Figure 6).
- Run automatic fiducial detection
- Manipulate initial external orientation (EO) parameters ( $\kappa$ ) in function of scan orientation

These tasks are implemented as functions within the Python script. As an example, the function for running automatic fiducial detection is displayed:

#### 2.3.6.2 Automatic fiducial detection

```

import os, pci
from pci.autofid import *

def runAutoFID (oeproji,cal_id):
    autofid_db_dir =
r'\\v0t0020a.adr.admin.ch\topo\tbk\tbkb\frame\HAP\530_GN79_46\2_autofid_chip_DB'
    chipfile = os.path.join(autofid_db_dir, 'GN79_46_Chip_DB.cdb')
    chipsens = cal_id
    caledge = 'Left' # use the left edge of the images as the calibration edge
    autofid (oeproji, chipfile, chipsens, caledge, 'fid.prj')

```

This function requires for input the photogrammetric project file (*oeproji*) and information about the camera type (*cal\_id*). The *cal\_id* value is derived from the block name in the very beginning of the batch file and passed into the *runAutoFID* function. The script runs the *autofid* function from the OrthoEngine Python API. This function allows for identifying the fiducial marks on all images defined in the photogrammetric project file. The *autofid* function can be run on templates of the fiducial marks stored in a so-called *chip database*. In our case, the type of fiducials varies with the camera. Therefore, a set of fiducials for each camera was digitized and stored in the chip database. The block name allows for identifying the camera type and assigning the corresponding template.

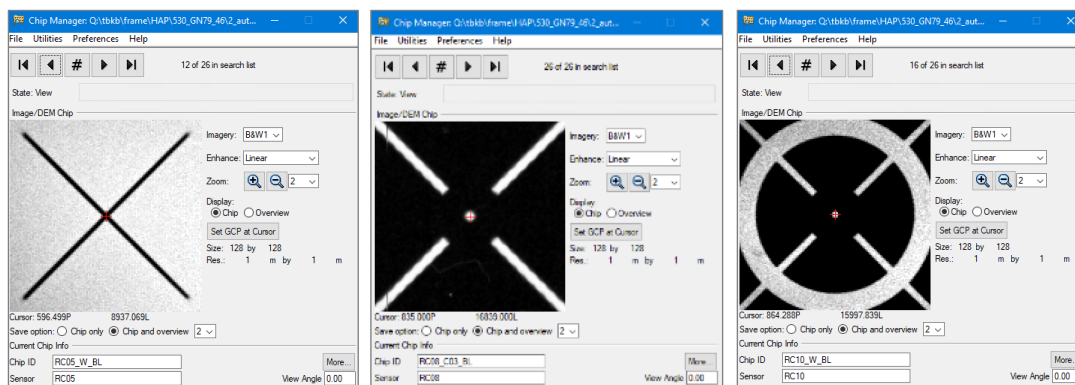


**Figure 10: Fiducial templates for the cameras Wild RC05 (left), RC08 (middle) and RC10 (right). The automatic fiducial detection proved to produce complete and reliable results throughout the whole production process.**

The pixel coordinates of the identified fiducial marks are written to the photogrammetric project file:

```

{
    PhotoId: 'E_000-218-486'
    FidType: Corner
    Fiducial: 0 1657.9742 836.5669
    Fiducial: 1 16828.1013 826.8510
    Fiducial: 2 16838.2770 15997.6089
    Fiducial: 3 1669.9141 16005.2497
    Principal: 9248.5666 8416.5691
    CalibrationEdge: Left
}

```

OrthoEngine uses a 2D affine transformation to derive the parameters of internal orientation. The 2D affine transformation is described by 6 parameters (2 translation parameters, 2 scale parameters, 2 angle parameters). With the eight measurements of fiducials (4 in X, 4 in Y) an over-determination is given. The over-determination allows for to estimate the agreement between the theoretical model (calibration) and the measures of fiducials. This agreement is expressed in residuals in [pixels]. The residuals of the fiducial detection can be exported from OrthoEngine as a list for validation purposes:

ImageId	NumFids	TL	TR	BR	BL
E_000-227-431	4	0.56	0.56	0.56	0.56
E_000-227-432	4	0.98	0.98	0.98	0.98
E_000-227-433	4	0.72	0.72	0.72	0.72
E_000-227-434	4	0.52	0.52	0.52	0.52
E_000-227-435	4	0.56	0.56	0.56	0.56
E_000-227-436	4	0.63	0.63	0.63	0.63
E_000-227-437	4	0.13	0.13	0.13	0.13

In practice, the list was exported and quickly analyzed for each AT block. The average residual for each image is around 0.5 pixels. In general, no outliers (residuals > 2 Pixels) did show up. The scan image file sizes is around 17'000 pixels by 17'000 pixels. The automatic measures of fiducials have shown to be adequately precise and reliable for the further orientation process.

### 2.3.6.3 *Modification of Kappa*

Another function from the Python script shall be presented here: the modification of initial external orientation parameter. During the *Ingest* process, the HAP process apparently “constructs” flight line geometries based on the image projection centers from the coarse georeferencing and the sequence of image naming.

For the alignment process, the initial parameters for omega and phi are internally set to zero, whereas the kappa value of each image corresponds to the azimuth of the constructed flight line that it belongs to. Assignment of the correct kappa value to the image scan file is dependent on the scan image orientation. In the world’s image archive there seem to dominate two widespread alternative approaches for orienting scan image files:

- North-up: North-oriented scan orientation. The images are scanned so that the most northern part of the image contents is always on the top edge.
- Head-up: Scan orientation is normalized with regard to the instrument panel. All scan image file in the archive carry, e.g., the instrument panel on the left edge.

The chosen “scan philosophy” has implications on any automated processing. The HAP *Ingest* process expects north-oriented scan orientation. In our case, however, our scan image archives are oriented according to the Head-Up approach. Therefore, we have to correct the flight line azimuth at this stage.

As mentioned in 2.3.3, the scan image files obtain, when copied from the image archives to the workspace, a prefix in function of the azimuth of the flight line they belong to. This prefix is now used in the function *writeAndRotateEOFFile* to correct for HAP’s invalid assumption of north-oriented image scan files:

```

def writeAndRotateEOFile(infile,outfile):
    with open(infile,'r') as inreadfile:
        with open(outfile,'w') as outwritefile:
            for line_read in inreadfile:
                if line_read.startswith('!'):
                    outwritefile.write(line_read)
                else:
                    new_line = str(line_read)[0:]
                    group_number =
re.findall('(\d+\.\d+)',line_read)
                    number_decimal =
int(len(re.findall('(\.\d+)',group_number[-1])[0]))-1
                    angle_deg = float(group_number[-1])
                    len_last_group = len(group_number[-1])
                    character_minus = new_line[-len_last_group-2:-
len_last_group-1]

                    if character_minus == '-':
                        angle_deg *= -1
                    if line_read.startswith('E_'):
                        angle_deg -= 90.0
                    if line_read.startswith('W_'):
                        angle_deg += 90.0
                    if line_read.startswith('S_'):
                        angle_deg += 180.0
                    while angle_deg >= 360.0:
                        angle_deg -= 360.0
                    while angle_deg < - 360:
                        angle_deg += 360.0
                    angle_deg_format =
'{{:.\{:d}f}}'.format(int(number_decimal)).format(angle_deg)
                    new_line = new_line[:-len_last_group-2] +
angle_deg_format + '\n'
                    outwritefile.write(new_line)

```

Table 1 shows how the initial Kappa is changed through the above function in order to account for the erroneous assumption of North-oriented image scans.

**Table 1: Initial external orientation elements and modification of initial kappa ( $Kap_{deg}$ ) value to corrected values ( $Kap_{deg\_new}$ ) for images from two different flight lines. At this stage, the coordinates of projection centers are still in UTM projection.**

!Scene_ID	Easting	Northing	Altitude	Ome_deg	Phi_deg	Kap_deg	Kap_deg_new
S_000-225-532	286660.132	5140699.88	4100	0	0	-42.033881	137.966119
S_000-225-533	287775.7	5141937.39	4100	0	0	-42.033881	137.966119
S_000-225-534	288891.274	5143174.89	4100	0	0	-42.033881	137.966119
W_000-225-544	277195.29	5124627.83	2700	0	0	42.548748	132.548748
W_000-225-545	277933.729	5125305.66	2700	0	0	42.548748	132.548748
W_000-225-546	278672.151	5125982.48	2700	0	0	42.548748	132.548748
W_000-225-547	279410.593	5126660.29	2700	0	0	42.548748	132.548748

### 2.3.7 HAP coarse alignment

The next line in the batch file calls and executes the HAP coarse alignment routine.



```

REM run first HAP coarse alignment
'C:\Program Files\PCI Geomatics\Geomatica
Banff\exe\python2.7\pci\hap\tecAlign.py' '%i_path%\%block_name%\4_alignment' -
strategy %coarseAlign%
'%i_path%\%block_name%\2_metadata_reference\%block_name%_SI_DOP25_LV03_3m.pix'
'%i_path%\%block_name%\2_metadata_reference\%block_name%_swissALTI_LV03_LN02_2m.
pix' '%i_path%\%block_name%\4_alignment'

```

The functionality of the HAP alignment run is described in the publication part of this Thesis. The call of the HAP coarse alignment routine requires specification of arguments that define the input folder, the reference files and a parameter file. The parameter file is defined as a Python script:

```

## to be used with 3m resolution reference op reference
## GCP
oStrat.mbDoGcp = True
oStrat.msGcpSampleSrc = 'GRID:256'
oStrat.msGcpAlgo = 'coarse8 0 1500 FFTP 0.75; coarse 0 15 FFTP 0.75'
oStrat.mbGcpRefnFlag = True
oStrat.mfGcpRefnParams = [5, 10, 10]

## TP
oStrat.mbDoTp = True
oStrat.msTpSampleSrc = 'GRID:64'
oStrat.msTpAlgo = 'coarse8 0 1000 FFTP 0.75; fine 0 30 FFTP 0.75'
oStrat.mbTpRefnFlag = True
oStrat.mfTpRefnParams = [5, 5, 5, -1]

```

The parameter file specifies that

- GCP detection (*oStrat.mbDoGcp*) and filtering (*oStrat.mbGcpRefnFlag*) are carried out (*=True*)
- The pattern of GCP search (*oStrat.msGcpSampleSrc*) departs on a regular grid of 256 points in the input image (*GRID:256*).
- GCP detection (*oStrat.msGcpAlgo*) starts on the *coarse8* level (8 \* 8 pyramids) of the input images with a search radius of 1500 pixels and a minimum correlation score of 0.75 (*coarse8 0 1500 FFTP 0.75*)  
GCP detection stops at the *coarse* level (4 \* 4 pyramids) of the input images. Candidates detected on the *coarse8* level need to be confirmed on the *coarse* level. The search radius is 15 pixel and the correlation threshold is 0.75 (*coarse 0 15 FFTP 0.75*)
- GCP filtering (*oStrat.mfGcpRefnParams*) stops at residuals of 10 pixels in X and Y.
- TP detection (*oStrat.mbDoTp*) and filtering (*oStrat.mbTpRefnFlag*) are carried out (*=True*)
- The pattern of TP search (*oStrat.msTpSampleSrc*) departs on a regular grid of 64 points in the input image (*GRID:64*).
- TP detection (*coarse8 0 1000 FFTP 0.75*) starts on the *coarse8* level (8 \* 8 pyramids) of the input images with a search radius of 1000 pixels and a minimum correlation score of 0.75 (*coarse8 0 1000 FFTP 0.75*)  
TP detection stops at the *fine* level (full resolution) of the input images. Candidates detected on the *coarse8* level need to be confirmed on the *fine* level. The search radius is 30 pixel and the correlation threshold is 0.75 (*coarse 0 30 FFTP 0.75*)
- TP filtering (*oStrat.mfTpRefnParams*) stops at residuals of 5 pixels in X and Y.

The DEM reference file passed for the coarse alignment run is the SWISSALTI3D with 2 m pixel size created in 2.3.4. The ortho mosaic reference file used for GCP detection is the panchromatic derivative of the SWISSIMAGE product with 3 m pixel size created in 2.3.4. The idea of using the low resolution reference file (instead of the 1 m resolution ortho reference) in the coarse alignment run relates to the fact that GCP detection stops at the coarse (4 by 4 pyramids) level of input imagery. The matching process

is expected to earn better matches if final image matching level and ortho reference resolution are of similar dimension. In practice, the approach of using 3 meter resolution ortho reference has led to a fast processing and satisfying results. It should be expected, though, that a more thorough determination of resulting image pixel size and corresponding ortho reference file may yield even better results and matches.

### 2.3.8 HAP fine alignment run

The execution of the HAP alignment run is designed to improve the EO parameters of the images in the photogrammetric project file. The second alignment run uses these improved EO parameters for input into the second alignment run. The actual measurements of TPs and GCPs from the coarse alignment run are disregarded in the fine alignment run, though. After successful execution of the coarse alignment run, the second (fine) alignment run is called from the batch file:

```
REM run first HAP fine alignment
'C:\Program Files\PCI Geomatics\Geomatica
Banff\exe\python2.7\pci\hap\tecAlign.py' '%i_path%\%block_name%\4_alignment' -
strategy %fineAlign%
'%i_path%\%block_name%\2_metadata_reference\%block_name%_SI_DOP25_LV03_1m.pix'
'%i_path%\%block_name%\2_metadata_reference\%block_name%_swissALTI_LV03_LN02_2m.
pix' '%i_path%\%block_name%\4_alignment'

Pause
```

Running the HAP fine alignment is the last step in the automatic processing. The fine alignment run calls the same routine as the coarse alignment does. The required parameters for the call are therefore the same: Specification of input and output folder, reference DEM and reference ortho mosaic and the parameter file. As discussed in 2.3.7, the GCP search in fine alignment is carried out on the 1 m resolution ortho reference. Height information, though, are provided through the same 2 m resolution DEM file as in coarse alignment. The parameter file in the fine alignment process is defined as follows:

```
## to be used with 1m resolution reference op
## GCP
oStrat.mbDoGcp = True
oStrat.msGcpSampleSrc = 'SUSAN:256'
oStrat.msGcpAlgo = 'coarse8 0 750 FFTP 0.75; fine 0 30 FFTP 0.75'
oStrat.mbGcpRefnFlag = True
oStrat.mfGcpRefnParams = [5, 10, 10]

## TP
oStrat.mbDoTp = True
oStrat.msTpSampleSrc = 'SUSAN:64'
oStrat.msTpAlgo = 'coarse8 0 500 FFTP 0.75; fine 0 30 FFTP 0.75'
oStrat.mbTpRefnFlag = True
oStrat.mfTpRefnParams = [5, 5, 5,-1]
```

The parametrization of the fine alignment run bases on the assumption that the orientation of the images has improved compared to their initial state. The meaning of the variables in the parameter file remains unchanged to those of the coarse alignment run. The most important changes of parameter values (compared to the parametrization of the coarse alignment process) are:

- Using the *SUSAN* algorithm instead of *GRID* in search for GCPs and TPs (parameters *oStrat.msGcpSampleSrc* and *oStrat.msTpSampleSrc*). The HAP online help<sup>5</sup> compares the two:

<sup>5</sup> <https://www.pcigeomatics.com/geomatica-help/>

- “With SUSAN, candidates are found by running a corner-detection algorithm on the image, which looks for corner-like features to use as candidates.”
- “With GRID, candidates are created in a grid-like pattern. This option does not preprocess the image; therefore, it tends to be faster. However, it also finds fewer matches, because the grid point may be on a featureless flat patch in the image that cannot be matched to anything in the overlapping images.”

The SUSAN algorithm is described to earn better results. Since the point matches yielded in this stage determine the final accuracy of orientations, the SUSAN algorithm is employed in this stage.

- GCP detection starts on the *coarse8* level and stops only on the full resolution *fine* level of input images.
- Reducing the search radius for TP and GCP search (*oStrat.msGcpAlgo*).

The HAP parametrization in both alignment runs is considered crucial for the efficiency of the orientation process. On one hand side, the detected points in this step determine the accuracy that can be obtained in the subsequent Quality Assurance (QA) work. On the other hand side, the completeness of detected TPs and GCPs on the AT block strongly influence the time that may need to be spent on complementing TP measurements manually. The presented parametrization earned satisfying results on both points. However, some regions gave more complete matches in function of, e.g., land cover or flight configuration. Supposedly, more systematic empirical investigation about the influence of each parameter on the results may lead to furtherly-optimized parametrization of the process.

## 2.4 Quality Assurance process

### 2.4.1 Check jpegs

The performance of the automatic processing routine highly depends on a good consistency of both, input data and metadata. A quick block-wise visual control of the image scan files has shown to be an economic but valuable means to enhance the input data consistency. Even though it showed that more than 99 % of the input images met the required specifications, the remaining share of inconsistent data can cause considerable problems in the later process. Typical problems to be detected with the image scan files in our case include:

- Wrong scan orientation
- Incomplete images
- Wrong file naming or wrong sequence of image scans

The visual control helps to identify and fix these problems. Detected problems are solved in the image archives as well.

This visual control is carried out in parallel to the automated block-wise processing. The data preparation routine copies the full resolution image scan files and corresponding quickviews (JPEG format) to the data input folder structure (see 3.3.3). For the quick visual control, the JPEG images are used since the alternative use of full resolution images takes considerable time for loading and visualizing. Figure 11 shows quick views of two image scans from a Wild RC10 camera. The scan files do not include the instrument panel. A counter in the lower right corner allows for to check the sequence of acquisitions and the image scan orientation on the image scan files.

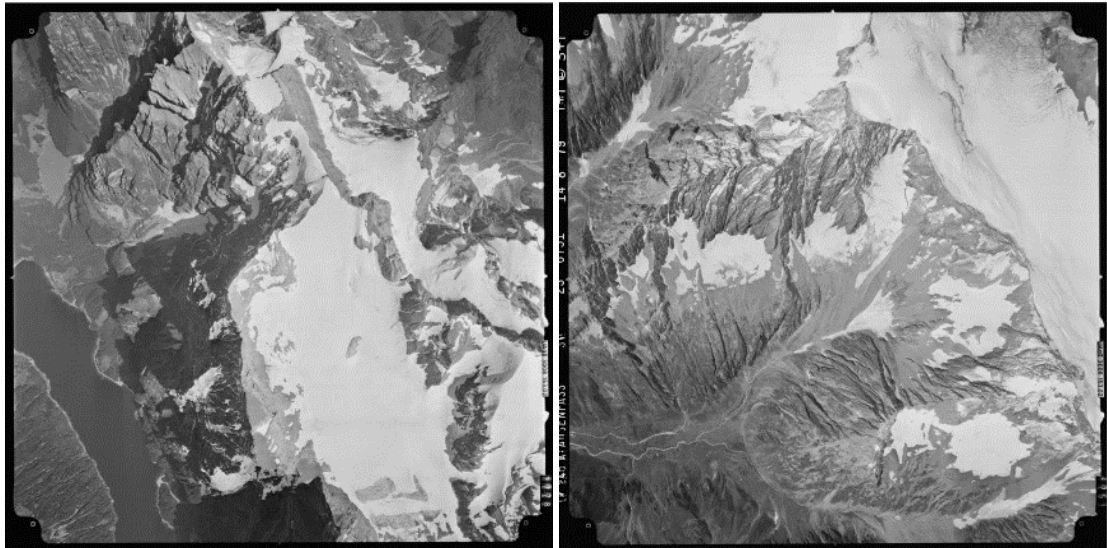


Figure 11: Quickviews from two image scan files.

## 2.4.2 OrthoEngine

With the fine alignment run (2.3.8) the last step of the automated processing has ended. The result of the automated processing routine is essentially a photogrammetric project file that ideally contains all elements required to run a final bundle block adjustment, i.e.

- Calibration information
- Fiducial marks measurements
- Abundant and reliable TP and GCP measurements

However, in practice a certain amount of manual work needs to be carried out in a so-called *Quality Assurance* (QA) Process in OrthoEngine. The Quality Assurance work requires human working time. It is evident that the data processing routine needs to be optimized as to reduce the required human working time as much as possible. This optimization should be considered as a permanent challenge resulting theoretically in a fully-automated high precision image orientation process capable of processing thousands of images.

*OrthoEngine* is the software module from PCI Geomatics for photogrammetric processing. The described HAP process largely is built on the OrthoEngine Python API. Compared to other commercial state-of-the-art photogrammetric software packages (INPHO Trimble, ERDAS Leica Photogrammetry Suite) OrthoEngine comes with a relatively simple but straight-forward GUI.

Available tools in the main window bar are displayed in function of the *processing step*. The first processing step is referred to as *Project*. The functions available in this step are tools to define the project itself, the camera calibration, the projection system and GCP/TP accuracy.

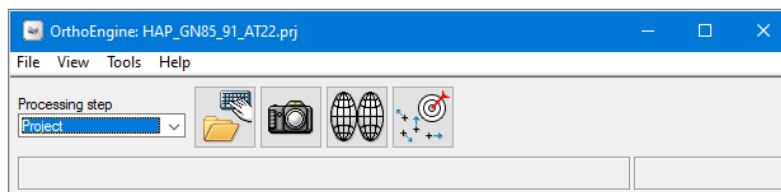


Figure 12: Tools in the "Project" processing step

In our case, these parameters were defined from within the automated processing chain as described. However, the possibility to check these parameters represents means to assure the integrity of the workflow.

The most important views on the project are the *Project Overview* and the *Raw Image Summary Table* (RIST).

The Project Overview allows for displaying the current state of projection centres, image footprints, TP and GCPs measurements and residuals. It allows for to, e.g., validate sufficient overlap between the images and an adequate geographic distribution of GCPs and TPs. The Project Overview offers a synoptic view of the project as it may enable an operator to identify a number of problematic configurations from a visual inspection only.

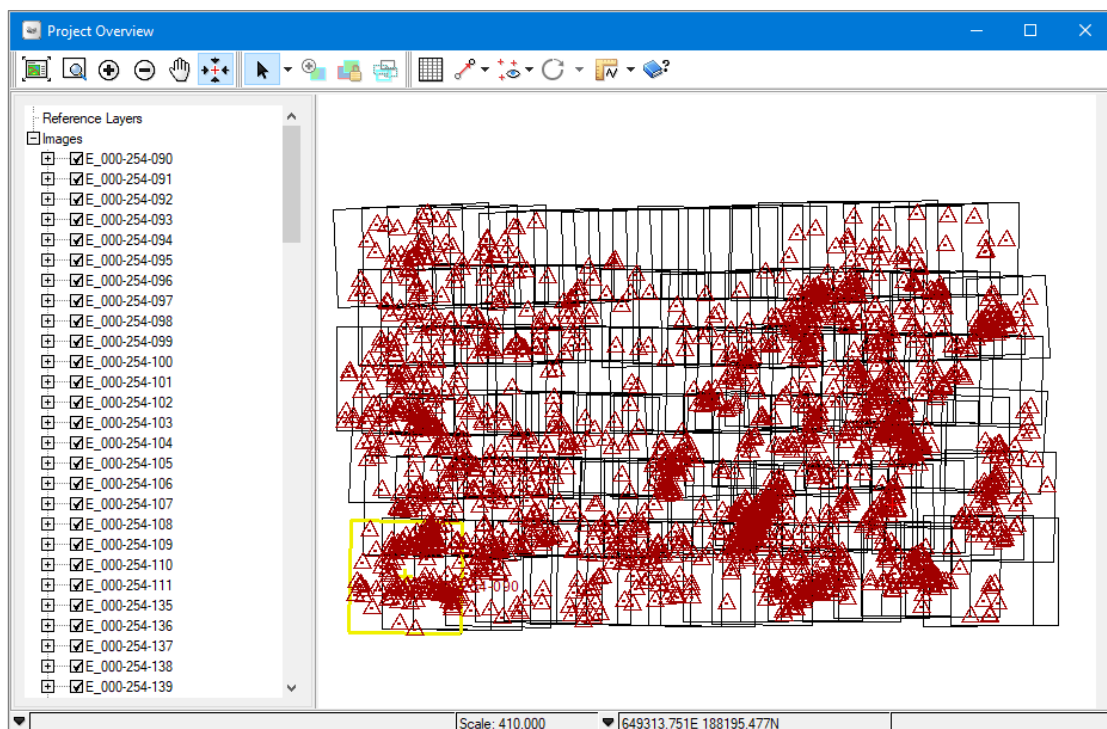


Figure 13: The Project Overview dialog allowing for synoptic display of project configuration.

The *Raw Image Summary Table* (RIST) summarizes statistical information for each image of the block into a table. The RIST complements the geographic information from the *Project Overview*. Most importantly, the RIST displays information about number of TPs and GCPs and summarized residuals from the last BBA run. From the RIST, the operator can identify images that do not contain a sufficient number of TPs or reveal high residuals on GCPs and/or TPs. A sufficient number of point measures with corresponding low residuals, does not assure a good orientation alone. The measures need as well to be geographically well distributed on the image. The distribution of measures on single images cannot be consulted through the RIST.

#	Image ID	Flightline ID	State	Active GCPs	Inactive GCPs	Active TPs	Inactive TPs	Check points	RMS	Active GCP RMS	Active TP RMS	Check point RMS	Total Overlap Pairs	Pairs with TPs	% Pairs with TPs
1	W_000-254-225	8_23		22	15	92	9	0	0.52	1.21	0.09	0.00	7	6	85.71
2	W_000-254-179	7_24		37	12	153	19	0	0.52	1.20	0.12	0.00	11	9	81.82
3	W_000-254-134	6_23		32	15	196	11	0	0.44	1.17	0.11	0.00	11	11	100.00
4	W_000-254-224	8_22		14	10	150	16	0	0.38	1.34	0.09	0.00	9	8	88.89
5	W_000-254-162	7_7		23	10	242	16	0	0.37	1.26	0.11	0.00	19	18	94.74
6	W_000-254-113	6_2		20	3	217	14	0	0.37	1.25	0.12	0.00	15	13	86.67
7	W_000-254-130	6_19		21	6	188	20	0	0.36	1.13	0.13	0.00	19	18	94.74
8	W_000-254-178	7_23		25	11	218	21	0	0.35	1.07	0.12	0.00	14	12	85.71
9	W_000-254-203	8_1		4	1	52	2	0	0.33	1.23	0.08	0.00	8	6	75.00
10	W_000-254-163	7_9		19	5	272	22	0	0.33	1.24	0.12	0.00	19	19	100.00
11	W_000-254-122	6_11		38	10	266	17	0	0.32	0.89	0.10	0.00	18	16	88.89
12	W_000-254-161	7_6		20	7	233	9	0	0.31	1.07	0.10	0.00	20	17	85.00
13	W_000-254-117	6_6		16	6	179	12	0	0.30	1.02	0.10	0.00	20	18	90.00
14	W_000-254-131	6_20		16	7	209	25	0	0.30	1.07	0.13	0.00	19	17	89.47
15	W_000-254-126	6_15		11	8	214	29	0	0.30	1.31	0.12	0.00	18	17	94.44
16	W_000-254-121	6_10		34	12	297	14	0	0.30	0.89	0.11	0.00	18	17	94.44
17	W_000-254-133	6_22		25	10	223	19	0	0.29	0.88	0.12	0.00	15	14	93.33
18	W_000-254-208	8_6		13	4	211	12	0	0.29	1.12	0.12	0.00	12	12	100.00
19	W_000-254-177	7_22		26	9	311	32	0	0.29	0.97	0.13	0.00	17	15	88.24
20	W_000-254-129	6_18		5	8	107	25	0	0.28	1.29	0.14	0.00	20	15	75.00
21	W_000-254-123	6_12		13	236	24	0	0.28	0.84	0.09	0.00	19	17	89.47	
22	W_000-254-112	6_1		14	3	189	7	0	0.28	1.00	0.11	0.00	12	10	83.33
23	W_000-254-116	6_5		12	6	137	6	0	0.28	0.95	0.09	0.00	20	17	85.00
24	W_000-254-128	6_17		10	7	194	27	0	0.28	1.17	0.13	0.00	20	17	85.00
25	W_000-254-207	8_5		18	9	208	15	0	0.27	0.91	0.11	0.00	12	10	83.33
26	W_000-254-132	6_21		4	17	242	30	0	0.27	1.00	0.12	0.00	17	16	94.12
27	W_000-254-127	6_16		11	3	242	22	0	0.27	1.19	0.12	0.00	18	16	88.89
28	W_000-254-222	8_20		10	7	201	21	0	0.26	1.17	0.10	0.00	13	12	92.31
29	W_000-254-166	7_11		13	5	291	22	0	0.26	1.14	0.13	0.00	18	18	100.00
30	W_000-254-165	7_10		8	10	288	13	0	0.25	1.32	0.14	0.00	21	17	80.95
31	W_000-254-114	6_3		5	5	175	9	0	0.25	1.39	0.12	0.00	18	16	88.89

Figure 14: Raw Image Summary Table

### 2.4.3 Digitize missing TPs

The process ‘GCP/TP Collection’ in the OrthoEngine main window contains most of the tools that are required to conduct the QA work within OrthoEngine.

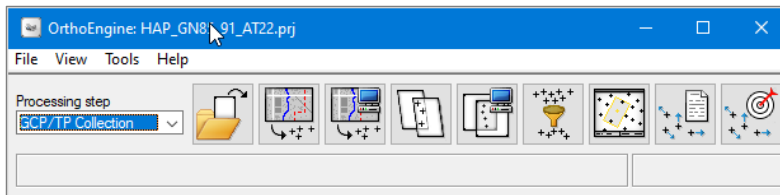


Figure 15: Tools in the “GCP/TP Collection” processing step

The most important tools in our workflow figured to be *Point Thinning and Refinement*, *GCP/TP accuracy*, *Manually collect Tie Points* and the *Residual report* tool.

#### 2.4.3.1 Point Thinning and Refinement

In our workflow, this tool is used only to thin redundant TP measures out. With the settings from the automated processing (see 2.3.8) we aim at assuring a minimum number of automatic point measures for all images. Depending on the land cover and flight configuration, these settings may lead to high numbers of reliable but highly redundant point measures in some regions. With the current parametrization, on some images up to 3000 TPs were extracted. A high number of image measures does not present a problem per se except for longer calculation times in the BBA. In order to reduce the number of TP measures for to reduce BBA run time, the *Point thinning and Refinement* tool is carried out:

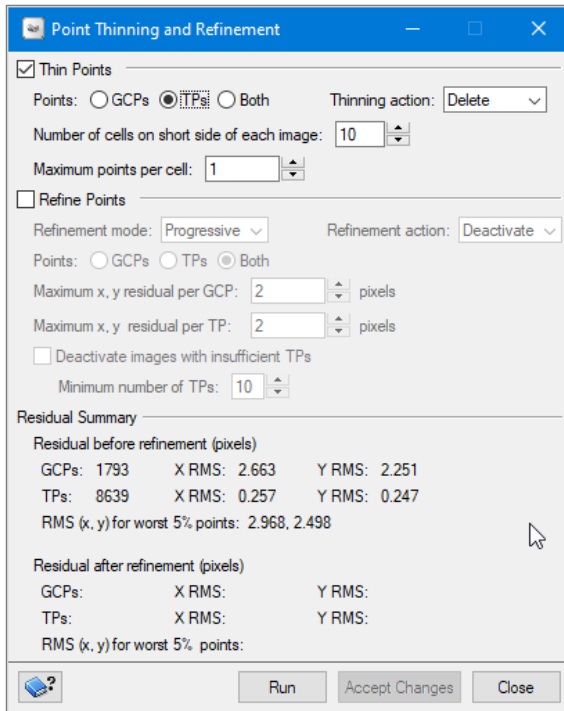


Figure 16: Point thinning and refinement tool

It is, in our case, configured to delete redundant TP measures only, using the tool's default parametrization. The removal of TPs leads to a more homogeneous distribution of remaining TP measures per image. The image is subdivided into a regular grid of cells and a maximum number of points is defined. This way, clusters of TPs are mitigated. The removal of GCPs is renounced here since it was not found that the number of GCPs showed a limiting influence on the time for running BBA.

### 2.4.3.2 Digitizing missing TPs

After the removal of redundant TP measures, TP measures are added to images that show non-sufficient number or distribution of TPs. In principal, adding TP measures can either be done manually or through an *Automatic Tie Point Collection* process. Where it appeals to be tempting, if not logical, to use the Automatic Tie Point Collection, the advantages of the manual Tie Point collection process where found to outweigh its disadvantages. The manual TP collection process gives full visual control to the user and cannot, if carefully executed, produce any new blunders. An automated TP collection process has already been carried out during the HAP processing. If the process failed once it is often for a good reason. The reason may, e.g., be based in the radiometry of the images (very low contrast, no texture etc.) or maybe due to data inconsistencies that were not detected. When compared to automatic TP detection, the manual TP detection process is, depending on the operator, sensitive in reflecting *why* an automated TP detection routine may have failed.

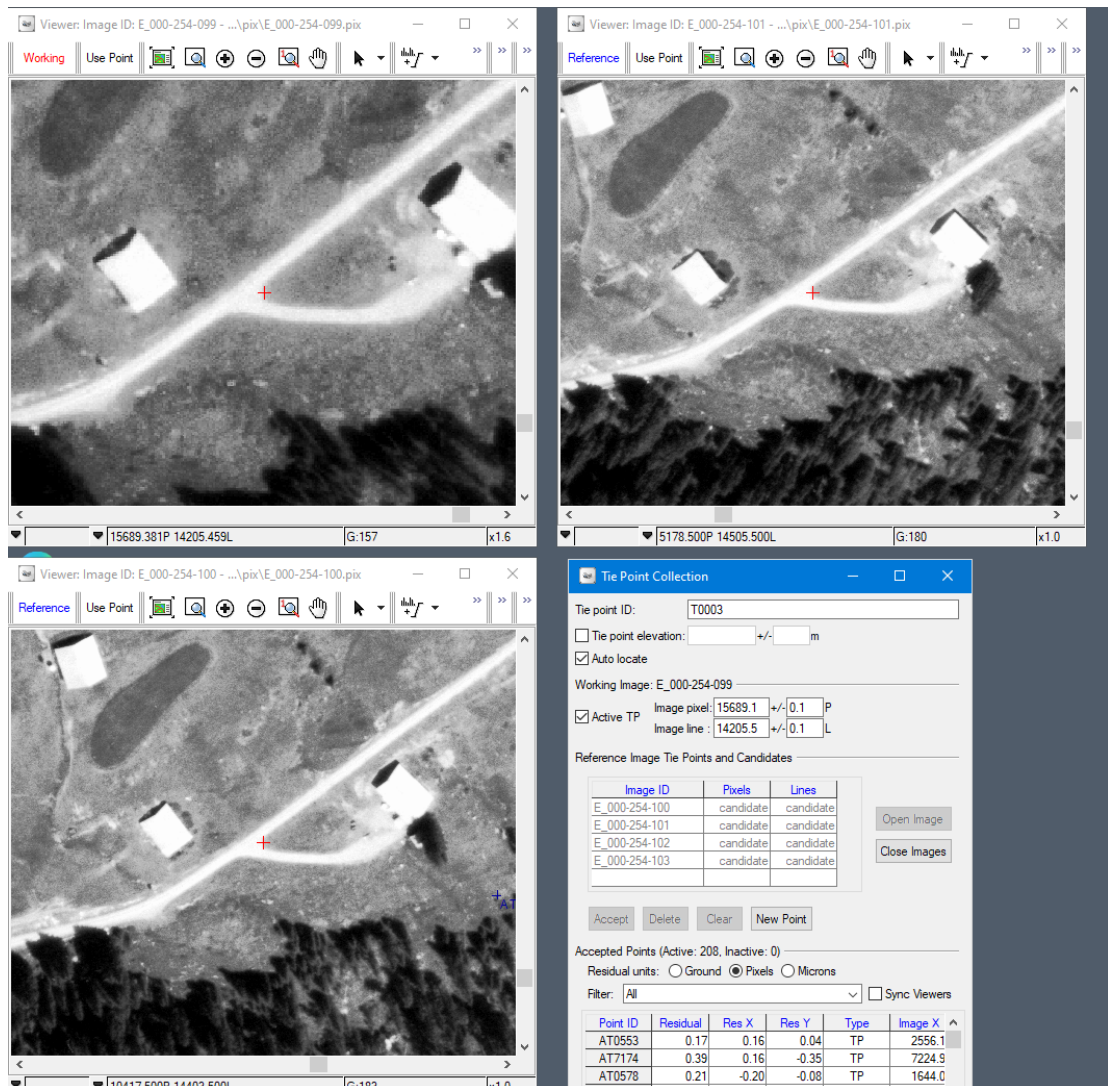


Figure 17: Digitization of manual TP with OrthoEngine

Manual TP identification is assisted through an *Auto locate* functionality. When a measurement of a TP is performed, OrthoEngine autolocates its position on overlapping images based on the current state of the orientations. The more realistic the orientations get throughout the QA process, the more precise will the auto-locate estimations of the position get.

In general, manual TPs were defined with a minimum of 3-4 measures for each TP. As pointed out, in the first part of this Thesis, the human work time spent on TP collection still represents a critical aspect of the processing chain. Whereas a number of blocks, even in Alpine regions, could be processed without the need of any additional TP measures, other blocks required to digitize a significant number of these.

## 2.4.4 Running bundle block adjustment

### 2.4.4.1 TPs only

Once that each image is assured to dispose of a sufficient number and adequate distribution of TPs, BBA is run in an iterative procedure. The principal objective at this stage lies in the identification and elimination of remaining TP blunders.

The *Residual Errors* pane is the principal interface for analysis of TP and GCP measures in OrthoEngine. Bundle block adjustment is as well executed from within the *Residual Errors* pane (command button



Compute Model, see Figure 18). The *Residual Errors* pane furthermore lists all measures with their corresponding residuals that result from the last bundle block adjustment run. Through the *Edit Point* command, GCP and TP measures can be visualized and edited on corresponding images. The *Automatic Point Selection* function allows for to select TPs and/or GCPs based on their residuals and further criteria from the most recent BBA run. Selected non-desired measures can either be viewed and edited, *de-activated* or deleted. The de-activation of point measures has the important advantage over deleting it, that the measures itself do not go loose. De-activated measures can be re-inserted into the model by activating them again in a later stage. De-activated GCP measures do, behave like independent Check Points (CPs).

For the detection of TP blunders, all GCP measures are first set to *inactive* through the *Residual Errors* pane. In the *Bundle Adjustment Settings* (see Figure 19) *Traditional block bundle* is specified for triangulation mode in the *GCP/TP Accuracy Settings* dialog (see Figure 19). When the BBA calculation has finished, the exterior orientation elements and all resulting residuals are updated. TP measures with outlying values should now be examined and then either be corrected for, de-activated or deleted. The BBA is then run again and the results will be re-examined. The existence of TP blunders may also become visual through examination of resulting footprints in the geographically oriented *Project Overview*. Highly deformed footprints often indicate the existence of blunder TPs. The operator at this stage needs to make best use of the complementary information provided through the *RIST*, the *Project Overview* and the *Residual Errors* pane in order to identify and eliminate problematic TP measures. This stage is completed when all images dispose of average residuals on TP measures (*Active TP RMS* in the *RIST*) not (much) higher than 1 pixel.

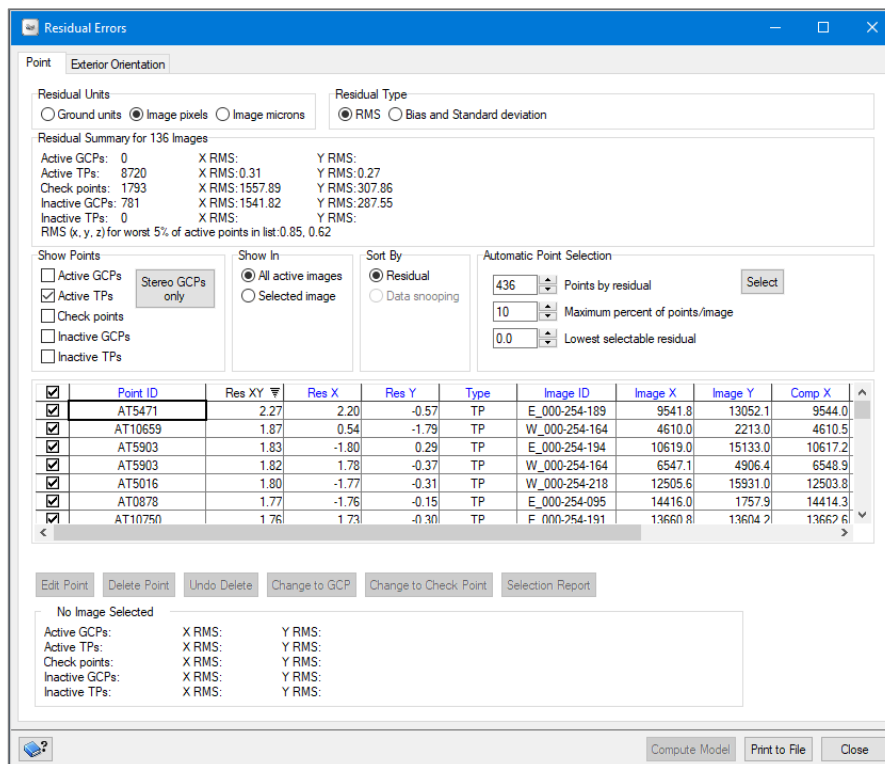


Figure 18: The *Residual Errors* pane

#### 2.4.4.2 TPs and GCPs combined

In this next step, the aim consists of establishing final external image orientations. While the status (active vs. inactive) of all TPs from the last BBA run is preserved, all formerly de-activated GCPs are set to *active*. A uniform geographical distribution (like, e.g. in Figure 13) of existing GCP measures over the

project extent is an important pre-requisite for obtaining a good exterior orientation. Next, the GCP accuracy settings (Figure 19) need to be set or validated.

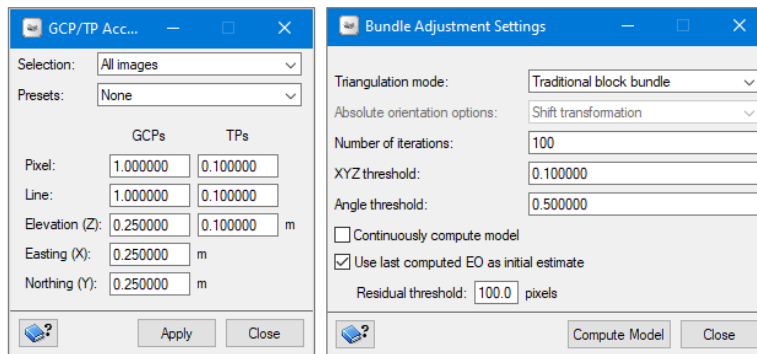


Figure 19: GCP/TP Accuracy Settings dialog (left) and Bundle Adjustment Settings dialog (right)

In our case, the accuracy for GCP measure where defined with 25 cm in X, Y and Z. The precision of GCP detection was defined with 1 pixel in X and Y. In reality, and in contrast to the traditional use of manually digitized and measured GCPs, the actual precision and accuracy of our automatically detected GCP measures is unknown. It can be assumed, though, that the defined values tend to be overly optimistic. This assumption was often confirmed through the visual inspection of single automated GCP measures.

However, a number of BBA test runs with different GCP and TP accuracy settings were carried out. The resulting residuals on both, GCPs and TPs, were examined. It was found that the above given values for GCP/TP accuracies resulted in more precise absolute image orientations than the use of less strict GCP/TP accuracy settings supposed to be more realistic. This finding was confirmed through validation of absolute accuracy on calculated orthorectified images. A possible explanation to this finding may lay in the fact that imprecise measures have a potential to compensate or partially level each other out in the determination of the external orientation elements using BBA. This will be the case only if the imprecision in the automatic measures is randomly distributed. Therefore, GCPs in the BBA do not necessarily need to be very precise *and* accurate to earn precise absolute image orientations. Usually, low precision combined with high accuracy (resulting in *randomly distributed errors*, compare Figure 20) in conjunction with a *high number* of GCP measures apparently suffice to yield precise external image orientations. The visual checking for random distribution of GCP residuals (see Figure 21) therefore is an integral part of the QA works.

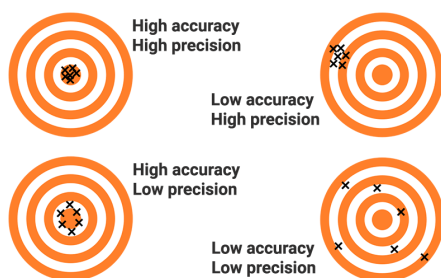
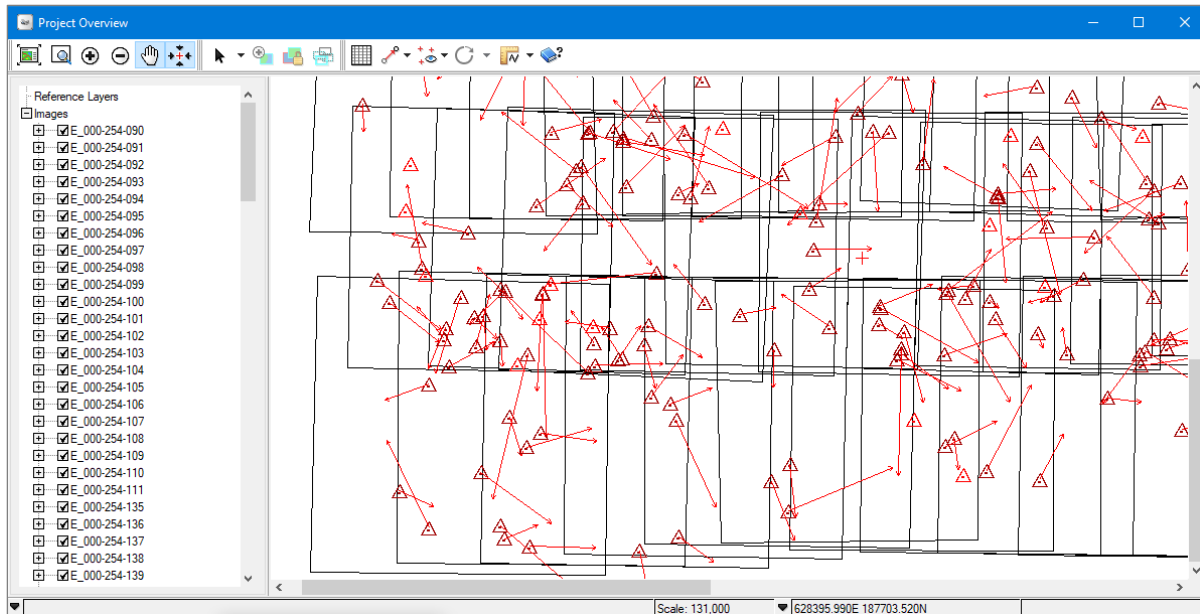


Figure 20: Accuracy and precision



**Figure 21: Visual checking for randomly distributed GPC residuals. Unfortunately, OrthoEngine does not display a legend for the magnitude of GPC residuals.**

When filtering and de-activating GCPs based on residuals, it is important to keep an eye on the distribution of remaining active GCPs. GCPs on the periphery of the block extent tend to show higher residuals than in the center of it. Losing adequate GCPs on the periphery results in losing accuracy for external orientation elements in the corresponding images. One measure to partially compensate for this effect is the definition and use of additional lines (see 2.2.3.).

#### 2.4.5 Check orthoimages

During the QA process and based on BBA statistics and TP and GCP distribution, doubts on the accuracy of resulting image orientations on some images in the block may arise. A useful approach to validate resulting image orientations consists in the calculation of selected orthoimages. Therefore, a number of between 1 – 10 images per block are orthorectified in this stage and their accuracy is assessed. The choice of which images to orthorectify is led by the above-mentioned criteria.



**Figure 22: The Ortho Generation process in OrthoEngine's main toolbar**

Calculations of orthoimagery in OrthoEngine is conducted by using the *Ortho Image Production* pane (see Figure 23). The *Ortho Image production pane* requires specification of the DEM file, the resulting orthoimage file, the output format etc.

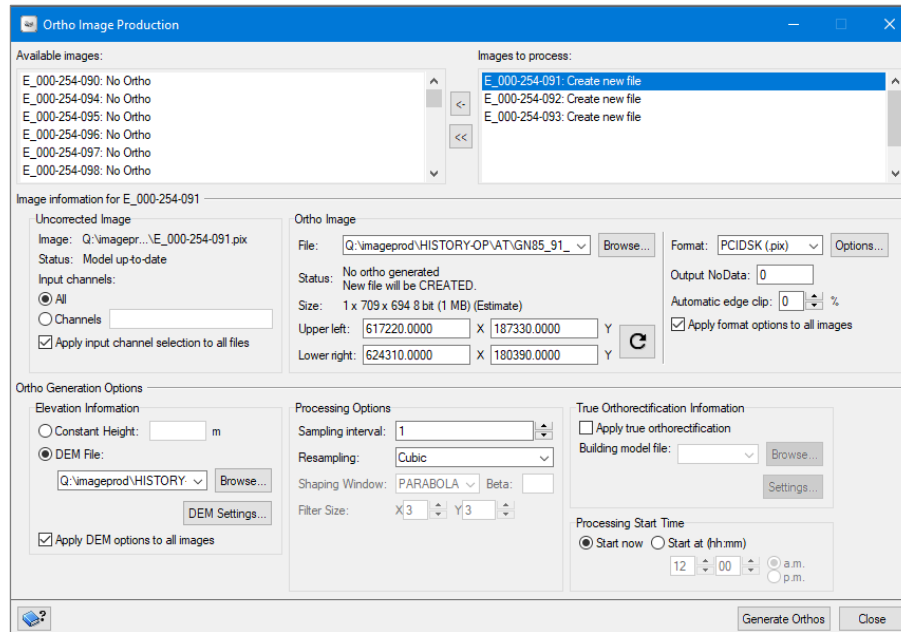


**Figure 23: The Ortho Image Production pane.**

In our workflow, the geometric accuracy of the resulting sample orthoimages is assessed in ArcMap based on comparison with different vector and raster reference data sets. A very efficient way showed to be to overlay the orthoimages with an up-to-date road network from the national landscape model. In alpine regions, however, road network data are typically too sparse for to judge the orthoimage accuracy. An existing internal data set on mountain ridges (see Figure 23, right) proved to be a useful substitute for this cause.

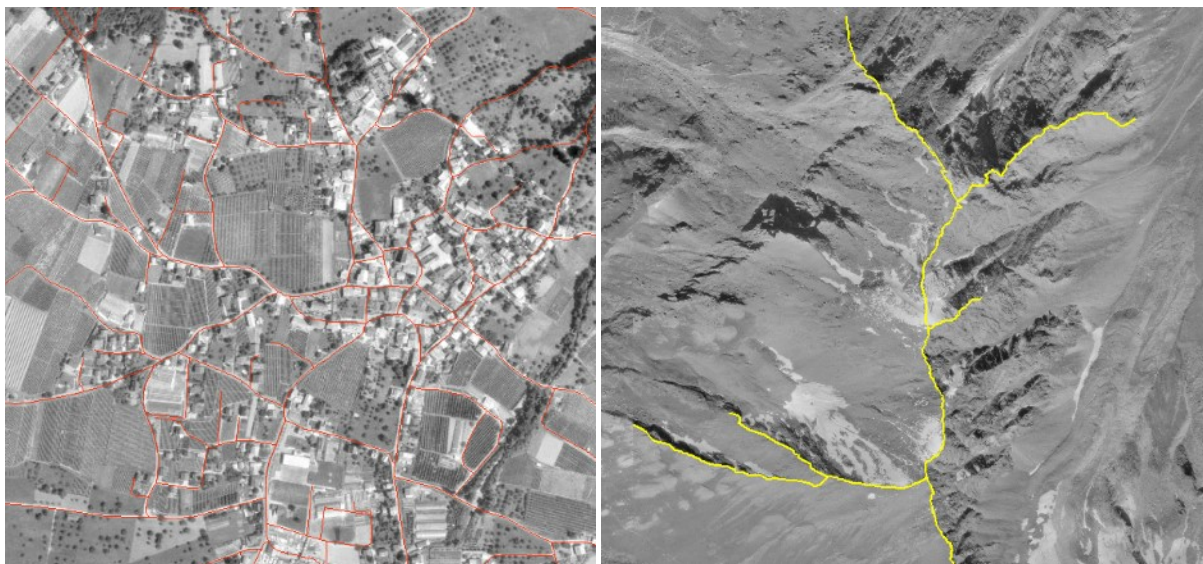


**Figure 24: Assessing orthoimage accuracy by overlaying vector layers. Left: overlay with road network vector data. Right: overlay with vector data on mountain ridges.**

If the sample orthoimage accuracy assessment unveiled problematic cases, the causes for these need to be identified and solved in further iterative steps of re-(de)fining point measurements and consecutive BBA runs. If no further problems were identified and general statistics are in comparable range to previously processed blocks, the QA work in OrthoEngine finishes here.

## 2.4.6 Report statistics

For the sake of documentation, the key statistical figures from the last BBA run are reported block-wise into a spreadsheet table. Reported statistics include maximum residuals and residual mean squared error (RMS) on TPs and GCPs. The statistics for the processing of the discussed data set of 8'507 images acquired between 1985 - 1991 is given in the journal publication part of this thesis. The relative homogeneity of these key statistical figures for the 36 blocks is striking. Whereas the maximum residual for GCPs is practically always between 3 and 4 meters, the RMSE on GCPs is practically always between 0.6 and 1.0 meters. This finding may indicate that the process is capable of achieving similar orientation accuracies independent of, e.g., land cover or block configuration. The variation of image photo scale between different blocks is of low magnitude.

The results of the independent control of geometric quality in the ortho mosaic confirm the impression of the overall homogeneous geometric quality obtained in the orientation process. The homogeneity found in the orientation is interpreted to largely rely on the homogeneity of the input data and metadata quality. All images have, e.g., been scanned with the same scanner following a well-defined procedure including QA in the scan process.

## 2.5 HAP\_PostAT

The next step consists in writing the obtained parameters for internal and external orientation for each image of the block, but excluding those of the additional lines, to the LUBIS metadata base through an application. The required *HAP\_PostAT* routine was internally developed by a professional developer. The author provided details on the required functionality and performed all necessary tests.

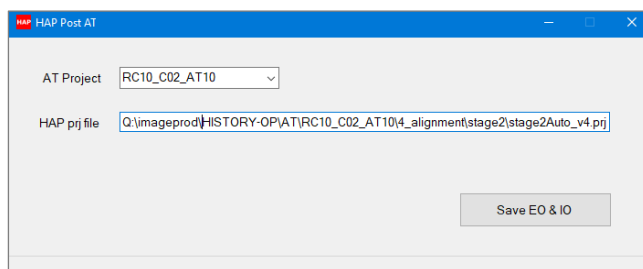


Figure 25: GUI of the HAP\_PostAT routine

The internal and external orientation parameters are read image-wise from the photogrammetric project file and converted into the LUBIS conform format. In the ASCII based project file, the EO parameters are given in the form:

```

ExtOrient:
{
  PhotoId: 'E_000-254-090'
  X: 6.1895971195025858E+05
  Y: 1.8369138589115982E+05
  Z: 5.3746916611405168E+03
  Omega: -2.2720127349571928E-01
  Phi: 7.4577027219182945E-01
  Kappa: -1.3710680859121236E+00
  GPSX: 6.1889998899999994E+05 1.0000000000000000E+03
  GPSY: 1.8399997700000001E+05 1.0000000000000000E+03
  GPSZ: 5.2400000000000000E+03 1.0000000000000000E+03
  GPSOmega: 0.0000000000000000E+00 5.0000000000000000E+00
  GPSPhi: 0.0000000000000000E+00 5.0000000000000000E+00
  GPSKappa: -1.1385000000000001E+00 5.0000000000000000E+00
}

```

In contrast, EO parameters in LUBIS follows a convention which expresses the EO angles in the form of the rotation matrix. The rotation matrix converts omega, phi and kappa into a 3 \* 3 matrix based on following equation:

$$R_{\omega\phi\kappa} = \begin{pmatrix} \cos\phi \cos\kappa & -\cos\phi \sin\kappa & \sin\phi \\ \cos\omega \sin\kappa + \sin\omega \sin\phi \cos\kappa & \cos\omega \cos\kappa - \sin\omega \sin\phi \sin\kappa & -\sin\omega \cos\phi \\ \sin\omega \sin\kappa - \cos\omega \sin\phi \cos\kappa & \sin\omega \cos\kappa + \cos\omega \sin\phi \sin\kappa & \cos\omega \cos\phi \end{pmatrix}$$

EX	EY	EZ	E11	E12	E13	E21	E22	E23	E31	E32	E33	Inventarnummer *
618870.368204	199970.994731	4784.276563	-0.999988	-0.001879	-0.004467	0.001849	-0.999976	0.006603	-0.00448	0.006595	0.999968	254180
618959.71195	183691.385891	5374.691661	-0.999629	-0.023925	0.013016	0.023979	-0.999705	0.003965	0.012917	0.004276	0.999907	254090
618732.016517	191909.281176	5182.981173	-0.999962	-0.008681	0.00047	0.008693	-0.998891	0.046279	0.000067	0.046281	0.998928	254135
631468.108203	203839.157854	4755.399005	-0.999707	0.024206	-0.000153	-0.024207	-0.999707	0.000652	-0.000138	0.000655	1	254217

Figure 26: Example of external orientation parameters in LUBIS

The IO parameters are derived from the calibration information imported into the project file (see Figure 6) and the measures of fiducial marks (see 2.3.6.2) stored in the project file through applying a 2D affine transformation. The field ISIGMA in LUBIS summarizes the residuals that result from the overdetermination and can therefore be used as a means to judge the quality of the internal orientation of the image file.

LUBIS_FRA_IMAGEFILE											
ung	Filename	Scanrotation	IA0	IA1	IA2	IB0	IB1	IB2	ISIGMA		
14	\\v0t0010a.adr.admin.ch\lubis\frame2\000-254\000-254-088.tif	90	0.295	-71.407	8456.5	71.435	0.286	8401.9	9.397686	5	
14	\\v0t0010a.adr.admin.ch\lubis\frame2\000-254\000-254-089.tif	90	-0.107	-71.408	8412.8	71.436	-0.114	8443.5	8.236752	A	
14	\\v0t0010a.adr.admin.ch\lubis\frame2\000-254\000-254-090.tif	270	0.352	-71.431	8465.7	71.451	0.35	8395.4	11.694429	9	
14	\\v0t0010a.adr.admin.ch\lubis\frame2\000-254\000-254-091.tif	270	0.45	-71.426	8474.2	71.446	0.438	8386.5	20.57069	9	

Figure 27: Example of internal orientation parameters in LUBIS

### 3 DSM generation process

Within the scope of the processing of the 8'507 images, DSM generation has been performed on representative subsets for validation purposes only. At current, no systematic DSM generation on all oriented images is performed. However, the archived orientation parameters contain all information to do so in a later time. For completeness' sake, the process of interactive DSM generation from within the

graphical OrthoEngine interface will be shortly described. In OrthoEngine, the available tools are available within the processing step *DEM From Stereo*.

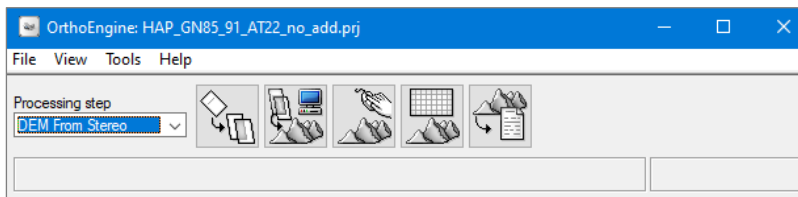


Figure 28

### 3.1 Epipolar pairs

First, epipolar image pairs are generated. Epipolar images are stereo pairs that are reprojected so that the left and right images have a common orientation, and matching features between the images appear along a common x axis. Using epipolar images increases the speed of the correlation process and reduces the possibility of incorrect matches<sup>6</sup>. The tool *Generate Epipolar Images* allows for to generate epipolar image pairs based on the overlap of their corresponding footprints reflecting the current state of the BBA model.

Image pairs may either be defined automatically (*Epipolar selection methods: Maximum overlapping pairs, All overlapping pairs or Optimum pairs*) or manually (*User select*). In our case, the manual definition option was used to have full control about epipolar image pair creation.

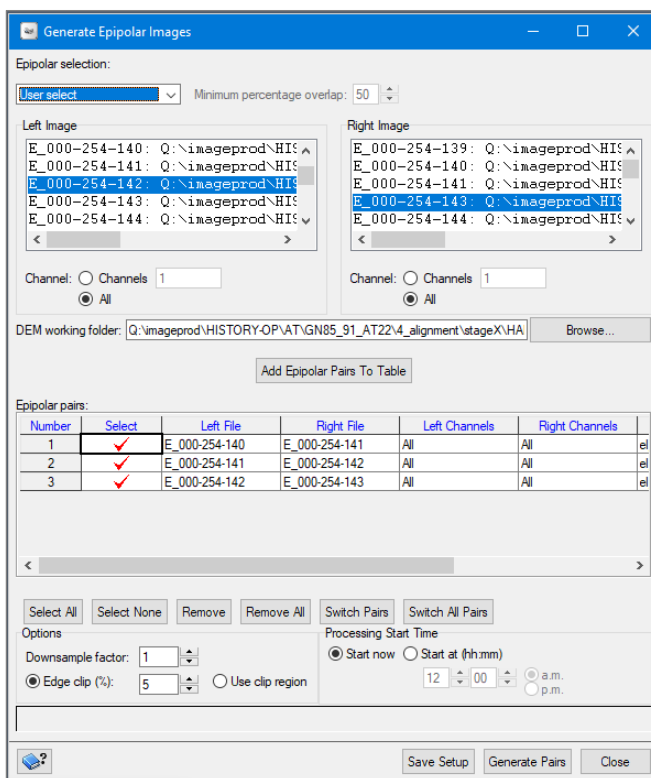


Figure 29: Graphical interface of the *Generate Epipolar Images* dialogue

<sup>6</sup> <https://www.pcigeomatix.com/geomatica-help/>

### 3.2 Generate DSMs

In the next step, DSMs are extracted for each epipolar image pair using the *Automatic DEM Extraction* tool. The tool requires for input the epipolar image pairs that have been created in the preceding step. The extraction method can either be set to SGM (*Semi-Global Matching*) or NCC (*Normalized cross-correlation*). The SGM algorithm is reported to produce higher-quality results with fewer errors and higher detail, but processing time is increased greatly<sup>7</sup>. In our case, the SGM algorithm was used.

The tool includes the option for creating a geocoded Digital Surface Model (DSM). If opted for, the extracted overlapping DSMs are merged into a single geocoded gridded output file in PCI's intrinsic PIX format. The tool produces a 3-band output. Band 1 contains the extracted height value in 32 bit float, band 2 contains a panchromatic true ortho image mosaic coded in 8 bit integer and band 3 contains a *score* information coded in 8 bit integer allowing to judge the quality of the correlation. The user needs to specify desired output resolution, the desired extent and the merging function. In our case, DSM extraction has been performed with 1 m output resolution and further processing options that correspond to those displayed in Figure 30.

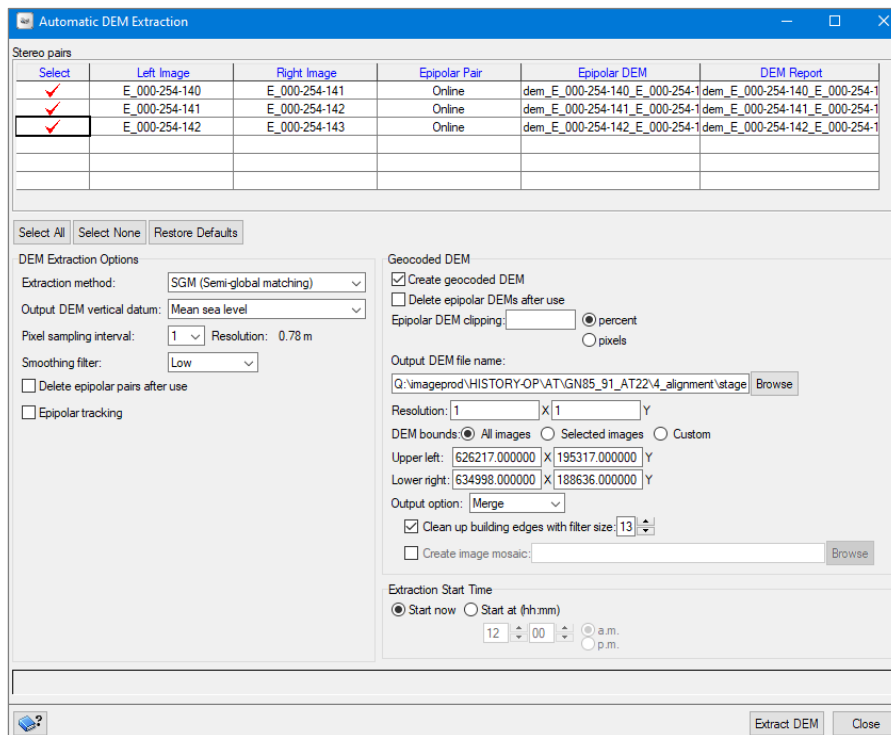


Figure 30: The Automatic DEM Extraction tool in OrthoEngine

### 3.3 Quality assessment: Hillshading and difference building

In order to judge the accuracy of the derived DSM, comparison is made with a reference height model of known accuracy. The reference height model used here was the same DTM used in the orientation process. In contrast to our derived DSM, the reference model is a Digital Terrain model (DTM) that does not contain elevated features like vegetation and buildings. The comparability of the two therefore remains limited to bare surfaces like paved zones or bare rock etc.

<sup>7</sup><https://www.pcigeomatics.com/geomatica-help/>



The comparison of the two elevation models is done by subtracting the correlated DSM from the reference DTM. First, the band 1 from the PIX file, containing the height information, is exported into TIFF/TFW format. This TIFF/TFW file is then subtracted from the reference file. Both files are in the same projection (EPSG:21781) referring to the same vertical datum. The subtraction was carried out using the ArcGIS tool *Minus* from the *Spatial Analyst* extension. The assessment of the resulting difference files was limited to visual inspection only. The assessment may easily be extended to derive quantitative measures of accordance to the reference height model by limiting the subtraction to pre-defined stable surfaces.

The *completeness* of the extracted DSMs was evaluated by visual inspection of hillshades that were calculated from the band 1 height values. The hillshades were calculated using the *Hillshade* tool from the ArcGIS *Spatial Analyst* extension. The analysis of the *score* band (band 3) from the extracted DSM exhibits further potential for assessing the completeness of the dense image matching process. This analysis, though, has not been systematically exploited since the DSM extraction does not form an integral part of the production process. Figure 31 displays the discussed outputs from the automatic DEM extraction.

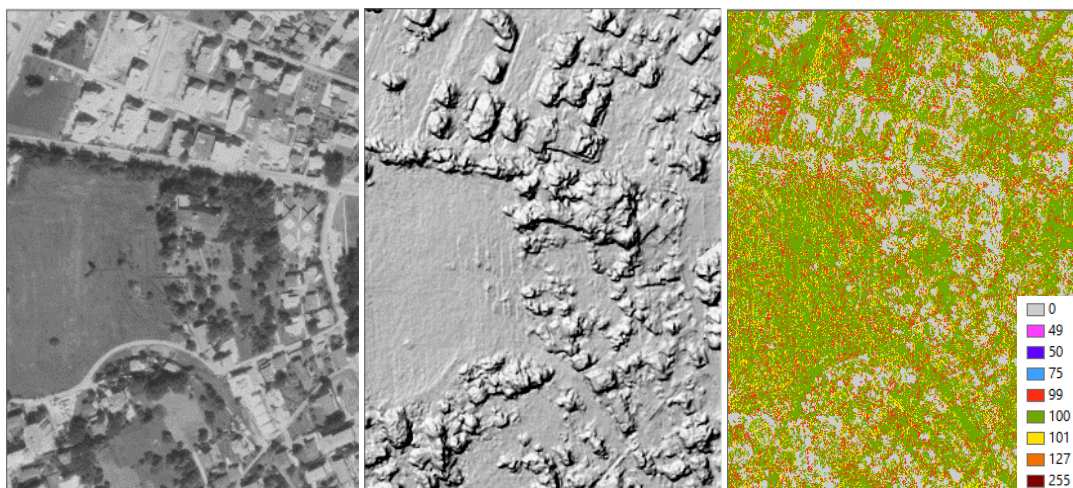


Figure 31: Orthoimage (left), hillshade (middle) and matching score (right). Matching score values mean: 0 - DSM elevation interpolated from surrounding elevation data. 99,100,101 - DSM elevations from matched imagery. The highest confidence is 100, with 99 and 101 less so. 200 -, 201 occluded pixel . 255 - background, no elevation.

## 4 Orthoimage generation process

The orthoimage generation process bases on existing workflows employed at the author's affiliation. It was adapted to the needs of the production workflow. The alternative of building a workflow based on OrthoEngine functionality was discarded due to resource constraints.

### 4.1 Create list

At the current state of the block-wise processing, obtained orientations have yet been written into the LUBIS metadata base (see 2.5). The next step is the batch calculation of orthoimages for all images of the block based on the information written to LUBIS metadata base. For to do so, first, a list of all images belonging to the block is created using the *FramelImageUtilities* tool. Another functionality of this pre-existing, in-house developed tool has been used for the definition of AT blocks in LUBIS in 2.2.2.

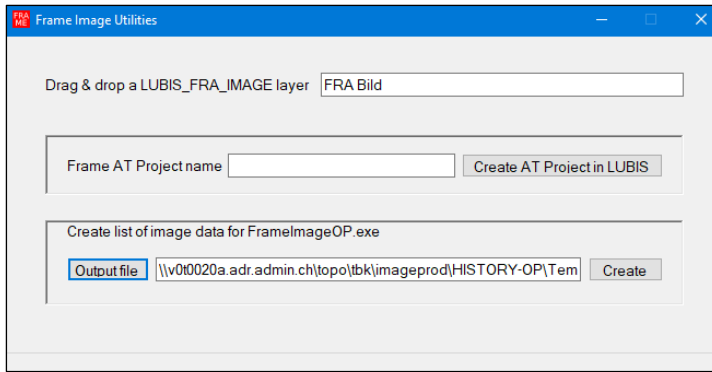


Figure 32: The *Frame Image Utilities* dialogue

The tool takes for input a LUBIS image layer with an interactive selection of the images to be processed, typically all images from one block, on it. When executed, the tool writes the UUIDs and the extent of its coarsely-geo-referenced footprints of all images to a user-specified text file in the form:

```
{9E59A2D5-6B38-4B35-971C-F1C319FF961D}, 719944, 180912, 724197, 185286
{CA9C7BE3-011F-4F61-9807-D4A9039AE6B7}, 721601, 157394, 726003, 161745
{40954D3E-5C14-44B8-A9BB-B47A0AE8EF1C}, 722424, 160578, 726716, 165007
```

## 4.2 Calculate Orthos

The calculation of the orthoimages is performed with the pre-existing in-house developed tool *Frame Image Orthophoto Production tool*. The *Frame Image Orthophoto Production tool* does, in fact, unite different batch processing functionalities in its GUI. The tool can be used for creating orthophotos to a given workspace, archiving orthophotos to the archives or retrieving orthophotos from the archives. For creating orthophotos, the image list created in 4.1 and the desired output directory are specified for input. Furthermore, the desired Ground Sampling Distance (GSD) and a DTM buffer need to be specified. Specification of the DTM buffer relates to the fact, that the coordinates of the bounding box of the image footprint in the image list still reflects the state of the initial geo-referencing in the LUBIS metadata base.

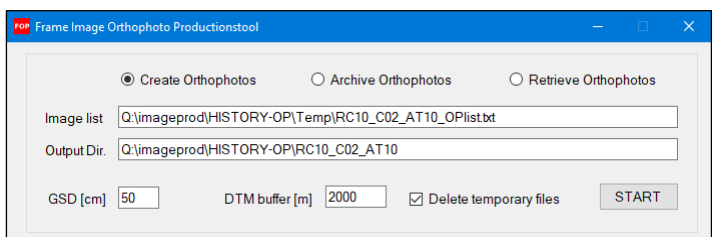


Figure 33: *Frame Image Orthophoto Production tool*

When executed, the *Frame Image Production tool* processes each line (image) of the input image list by (1) getting a DTM subset and (2) creating the corresponding orthoimage. The orthoimages have a radiometric resolution of 8 bit and are produced in the TIF/TFW format. The DTM subset (including the buffer) is clipped from a national coverage of the SWISSALTI3D model with 2 m resolution and copied to the working directory by employing the ESRI geoprocessing API (Geoprocessing tools).

The orthorectification process itself uses *OrthoMaster* from TRIMBLE/INPHO software. *The Frame Image Production tool* creates one INPHO PRJ file per image to be ortho-rectified. The PRJ file contains all information required by the OrthoMaster routine to execute the orthophoto calculation, i.e.

- General project information:

```

$PROJECT 9.2.0
# generated using Version 10.1.0-403ceff, build 10021 of 2020-07-22 14:10
$PROJECT_NAME : 000-238-123
$USER_ID : U80858223
$STARTING_DATE : 14:35:17 30/10/2020
$LAST_CHANGE : Fri Oct 30 14:37:03 2020
$IMAGE_TYPE : Aerial
$POINTFILE_TYPE : Text
$IMPORTED_DATA : autoproj
$REFRACT_CORR_DEFAULT : on
$CURV_CORR_DEFAULT : on
$INTERMEDIATE_COORD_SYSTEM : CH1903\ /\ LV03
$DELIVERABLES_COORD_SYSTEM : CH1903\ /\ LV03
$ANGULAR_UNITS : grad
$WARNING_LEVEL : 0
$END

```

- Information about the coordinate system
- Information about the image to be orthorectified: e.g. input scan file (read from the archive), IO and EO parameters (read from LUBIS):

```

$PHOTO
$PHOTO_NUM : 238123
$PHOTO_FILE : \\v0t0010a.adr.admin.ch\lubis\frame2\000-238\000-238-123.tif
$CAMERA_ID : 789F2115-AC03-47AA-9906-68209FC52F97
$TERRAIN_HEIGHT : 2888.191995
$PIXEL_SIZE : 0.013997
$SCAN_POS : 1
$IO_PARS : 2 2
$IO_STAT : manual
$ORI_STAT : Initial
$INT_ORI : 14:37:03 30/10/2020
    71.4360000000      0.0960000000      8418.6364834823
    0.1080000000     -71.4490000000      8421.7401899090
$EXT_ORI : 14:37:03 30/10/2020
    153.02000      789123.94336      168715.87928      5804.77614
    -0.023160290000      0.999672150000      -0.010917240000
    -0.999714220000      -0.023223190000      -0.005670620000
    -0.005922290000      0.010782790000      0.999924330000
$END

```

- Information about the camera calibration (read from the LUBIS metadata base):

```

$CAMERA_DEFINITION
$ID : 789F2115-AC03-47AA-9906-68209FC52F97
$MODEL : RC
$KIND : FilmFrame
$SERIAL : 789F2115-AC03-47AA-9906-68209FC52F97
$FIDUCIALS :
  1      106.00200      -105.99900  1
  2      -106.00500     -106.00300  2
  3      -106.00000      105.99700  3
  4       106.00100      105.99500  4
$END
$ACTIVE_CALIBRATION : 1
$CALIBRATION_SET :
  $ID : 1
  $MODE : manual
  $DATE : 00:00:00 28/02/1977
  $FOCAL_LENGTH : 153.020000
  $PRINCIPAL_POINT_PPA : 0.003000 0.003000
  $PRINCIPAL_POINT_PPS : 0.000000 -0.001000
$END
$END
$END

```

- Specification of the output orthoimage:

```

$ORTHO
$ORTHO_ID : TMP_000-238-123
$ORTHO_PATH : Q:\imageprod\HISTORY-OP\PAN\RC10_C02_AT12\temp\TMP_000-238-
123.tif
$END

```

- Specification of the DEM file to be used:

```

$DTM
$DTM_ID : DTM_238123
$DTM_FILE : Q:\imageprod\HISTORY-OP\PAN\RC10_C02_AT12\temp\DTM_000-238-123.tif
$FORMAT : geotiff
$XY_SCALE : 1.0000000000
$Z_SCALE : 1.0000000000
$END

```

The extent of the orthoimage file created by the *OrthoMaster* routine is the same as the extent of the DEM file. The extent of the DEM file contains a buffer that accounts for the inaccurate initial georeferencing of the image footprint. The orthoimage files produced by the above described *OrthoMaster* routine therefore needs to get clipped to the actual extent of the orthophoto. The extent of the orthoimages is the maximum rectangular area that contains Data values. The clipping is implemented into *Frame Image Orthophoto Production tool* using functionality provided by ESRI Geoprocessing tools.

In the orthorectification process, the SWISSALTI3D national digital *terrain* model with a reference year of 2013 is used. For maximum consistency, it would be preferable to use an elevation model that represents the topography at the time of image acquisition. A historic height model with sufficient geometric resolution is not available at the author's affiliation. It might be produced from the historic oriented images themselves following approaches described in chapter 3. The implications of using a DEM that does not correspond to the date of image acquisition need to be aware. In regions where the terrain height has undergone significant changes this will lead to geometric imprecisions in the planimetric accuracy of the orthoimage. The magnitude of these displacements is a function of the amount of the vertical change and the off-nadir angle of the pixel. The most dominant changes in terrain height over significant areas in Switzerland are the result of glacier shrinkage. Resulting displacements in the

orthophotos over glaciated surfaces need to be accepted with the choice of DEM that was made. Other changes in terrain height are of local extent only, like construction sites etc.

The other fundamental question about which DEM to use in the orthorectification process is whether to use a *Digital Surface Model* or a *Digital Terrain Model*. The use of Digital Surface Models leads to a so-called *True-orthophoto* where all elements on the terrain, like buildings and vegetation, are depicted in nadir-view. In contrast, the use of *Digital Terrain Model* leads to a leaning effect of such elements in the orthophotos. Where often users may tend to prefer the True-orthophoto for its principal advantage of representing building and vegetation geometry more correctly, True-orthophotos may contain artefacts like frayed building edges. These artefacts result from inaccuracies in the dense image matching. If artefacts in the orthorectification process shall be avoided, the production of a DSM typically requires substantial amount of manual editing. The production and editing of country-wide DSMs from historic images suitable for orthorectification lies clearly beyond the current scope of the outlined production line due to limited computational and human resources.

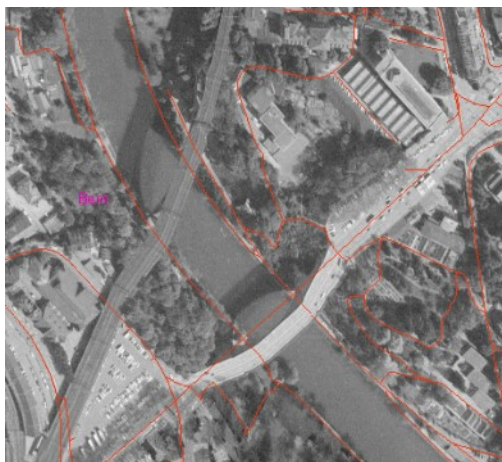


**Figure 34: Digital Terrain Models do not contain bridges. If not corrected for, the geometry of bridges in orthophotos calculated on DTMs may severely be distorted**

The orthoimages are, in the current workflow, all produced to a geometric resolution of 50 cm. Determining adequate geometric resolution for the orthorectification is done in function of photoimage scale and scan resolution. Although the chosen resolution undersamples images from flight lines acquired, e.g., at a lower altitude within the alpine valleys, a common resolution facilitates the mosaic production.

The orthorectification process may be carried out alternatively by the process lined out in 2.4.5 using functionality provided by OrthoEngine. There are, however, two good reasons to do the way described:

1. With the *Frame Image Production tool*, a productive batch processing routine existed already.
2. With the use of *Frame Image Production tool*, the orientation elements archived to the LUBIS system are read through a different software (OrthoMaster). The implementation of the conversion process of orientation elements (see 2.5) is, to a certain degree, error-prone. The calculation of orthoimages using a different software cross-ensures the consistency of derived orientation elements.

### **4.3 Post-treatment: Radiometric optimization**

The resulting orthoimages from the orthorectification process exhibit a potential for radiometric optimization and homogenization. A number of reasons in the acquisition process, the image

development, the deterioration over time and the scanning process contribute to this finding. Therefore, the orthoimages are, after calculation, submitted to a macro developed in *Adobe PhotoShop* that executes a number of enhancements on the orthophotos. Enhancement operations include overall histogram optimization, removal of vignetting effects and *smart-sharpening* of the orthoimages. The employed PhotoShop macro was developed by a colleague with professional expertise in macro development for PhotoShop. Figure 35 depicts an extract from the PhotoShop macro. Figure 36 and Figure 37 show its effect by comparing orthoimages before and after the treatment. Like the orthoimages input files, the PhotoShop macro generates output images with a radiometric resolution of 8 bit.



Figure 35: Extract from the PhotoShop Macro for radiometric harmonization of historic orthophotos

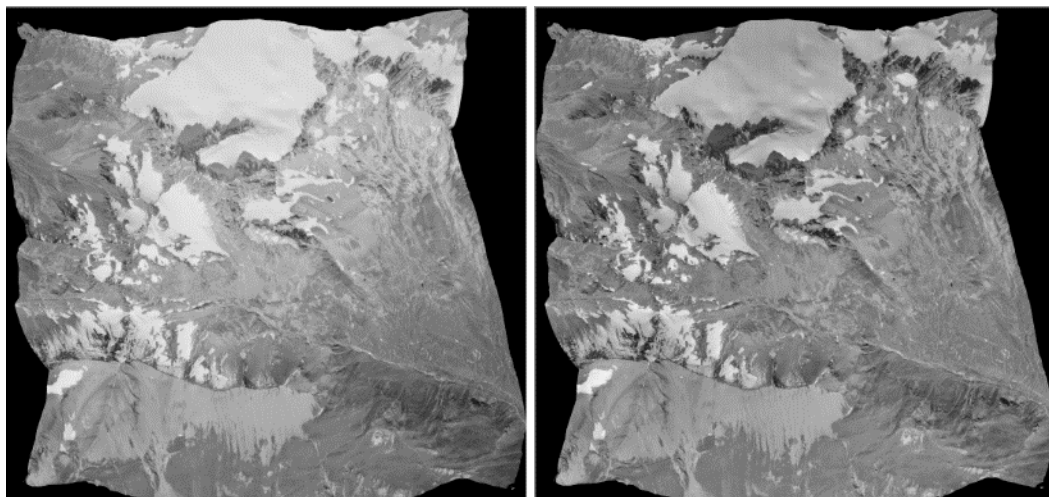


Figure 36: Orthophoto before (left) and after (right) running the PhotoShop macro. The vignetting effect is largely reduced and very light surfaces (snow and glacier) gain texture and detail.



Figure 37: Orthophoto subset before (left) and after (right) the PhotoShop macro. The contrast and the sharpness of the orthoimage is visibly enhanced.

#### 4.4 Identify incomplete orthoimages

In this step, a quick quality assurance is carried out on the radiometrically enhanced orthophotos. In *Adobe Bridge* overviews of all orthoimages are looked at in order to identify incomplete images. The two major reasons for incomplete images are (1) non-sufficient DTM buffer specified in 4.2 and (2) temporary license lost of OrthoMaster in the orthoimage calculation process. Whereas (1) results in an incomplete image cut, (2) may result in rectangular areas in the orthophotos with *NoData*. If such problems were identified, the corresponding orthophotos require re-calculation and re-submission to the radiometric harmonization process.

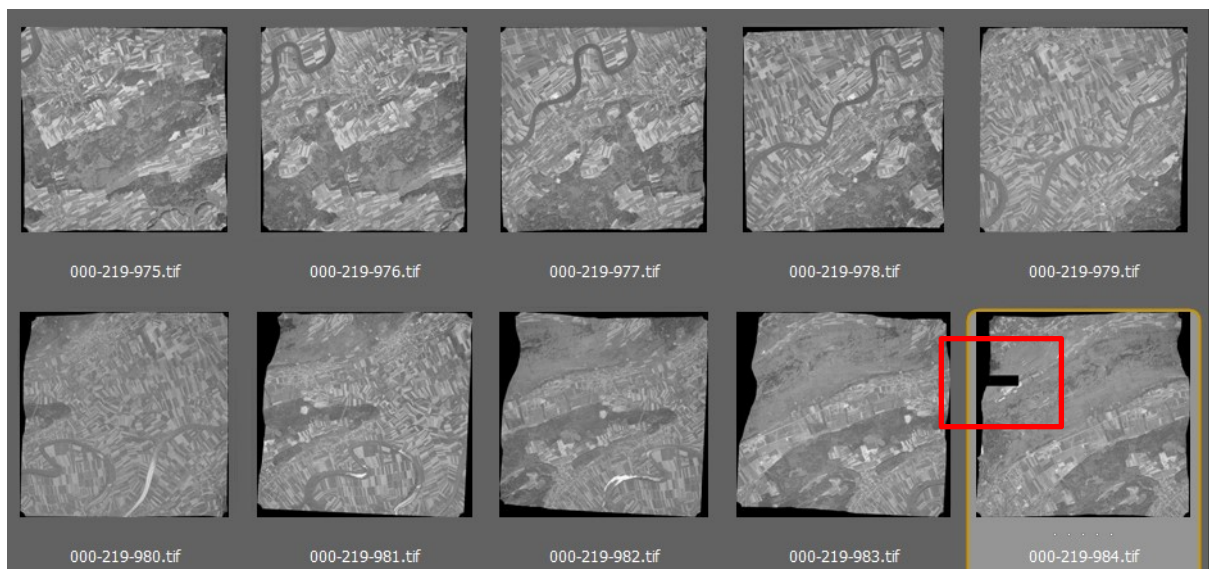


Figure 38: Quick quality assurance of orthoimages in Adobe Bridge. The image at the bottom right indicates a non-complete orthoimage calculation.

#### 4.5 Build Mosaic Dataset

The next step in the processing chain consists in preparing the radiometrically enhanced orthoimages for a quick control of their geometry in a GIS environment. A graphical model was created using the *ArcGIS ModelBuilder*, a visual framework for creating geoprocessing scripts. The model loads all orthoimages that belong to the block into a *Mosaic Dataset* upon which the geometry control is performed. The ESRI intrinsic mosaic dataset format allows to store, manage, view, and query collections of raster and image data<sup>8</sup>. It can be considered as a virtual mosaic and is created in an ESRI file geodatabase. It is especially useful in our case since it allows for integrating multiply overlapping images.

The created model takes for input the name of the block and the folder that contains the orthoimages of the AT block. The model creates a *Mosaic Dataset* in a pre-defined ESRI file geodatabase, defines its projection, loads all orthoimages of the AT block, builds footprints and overviews.

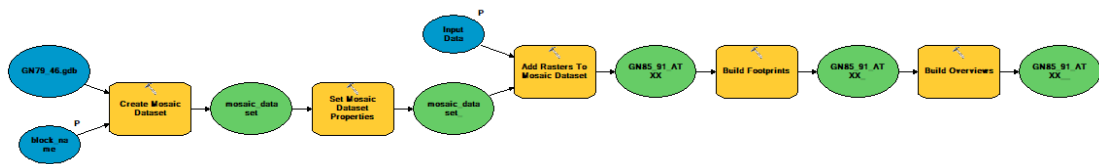


Figure 39: Model to create a *Mosaic Dataset* of orthoimages for inspection in ArcGIS

#### 4.6 Quality Assurance Mosaic Dataset

The control of the geometry of the orthoimages is performed by loading the created *Mosaic Dataset* into an ArcMap document and comparing it to vector and raster reference data. When comparing the *Mosaic Dataset* to reference datasets in Geographic Information Systems (GIS) software, one needs to be aware of the fact, that at any given point only one orthoimage can be displayed. In reality, and due to the lateral and in-flight overlap, each spot is covered by multiple orthoimages. Multiple overlap is especially enhanced in mountainous areas (see Figure 40). For this quick analysis we therefore need to take into account that the displayed orthoimage potentially covers or hides potential geometric problems of underlying orthoimages. This principal problem is mitigated by choosing a *dynamic* mosaicking method for the orthophotos in the *Mosaic Dataset*. In our case, it was chosen to display the orthoimage on-top to be the one that is closest to its image center. In consequence, by panning at an adequate scale over the complete *Mosaic Dataset*, practically all orthoimages get viewed at.

<sup>8</sup> <https://desktop.arcgis.com/en/arcmap/10.3/manage-data/raster-and-images/what-is-a-mosaic-dataset.htm>



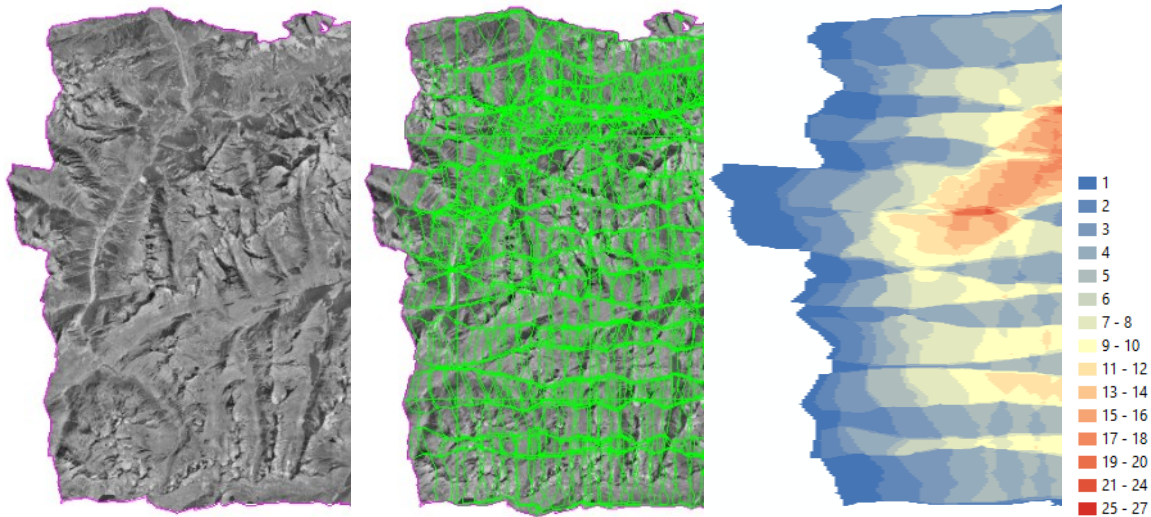


Figure 40: Mosaic Dataset consisting of 462 orthoimages belonging to the same aerial triangulation block. Display without (left) and with corresponding footprints (middle). The number of orthophotos covering one single spot may, especially in mountainous areas, be very high (right, with color legend displaying the number of orthoimages).

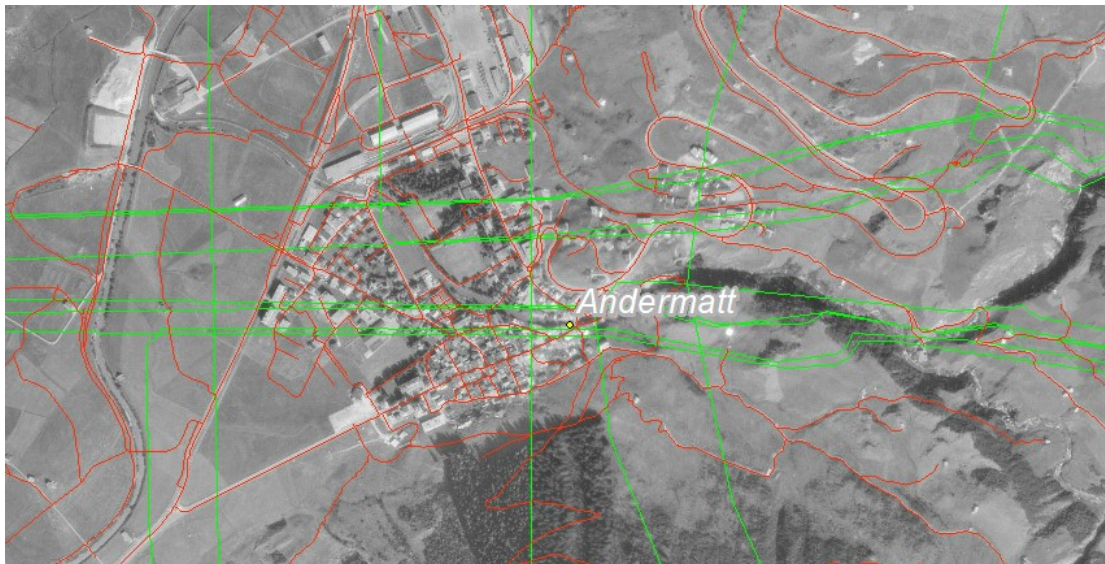


Figure 41: Geometric accuracy control on orthoimages. Green vectors correspond to image footprints, red vectors refer to roadnet reference data from the national landscape model TLM3D.

The geometric control of the block is done at a scale of 1 : 5'000 to 1 : 10'000. Problems in the orientation are identified where images deviate more than 3 – 5 m from the reference without other plausible explanation (change of road network, massive changes in terrain height etc.). If such problems are detected at this stage, the QA process of the orientation (see 2.4.3 to 2.4.5) has to be taken up again in order to enhance the corresponding images' orientations. The orientations for the corresponding images are re-archived (2.5) and orthophotos need to be re-calculated. Since these corrections are relatively tedious to perform, the motivation is increased to perform the image orientation with a very critical eye already in the first step.

As a general observation, the radiometric homogeneity of the orthophotos in the Mosaic Datasets is striking for practically all blocks (see Figure 40). Without the display of the footprints, it is hardly possible to visually make out the borders of an actual single orthophotos. This finding confirms the performance of the radiometric enhancement macro and lays a valuable base for achieving homogeneous physical

orthomosaic products. Furthermore, the normalization of radiometry potentially facilitates the use of automated image analysis and extraction routines that can be carried out on the orthophotos.

## 4.7 Archive orthoimages

Once the orthoimages of one block have passed radiometric and geometric quality controls, they can be written to the aerial image archive. From the archives they remain available to internal and external users through different applications. The *Archive Orthophotos* functionality of the *Frame Image Orthophoto Production tool* (see 4.2) is used to write the resulting orthophotos to the aerial image archive.

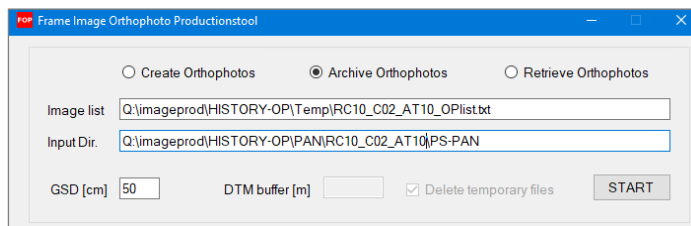


Figure 42: User interface of the Frame Image Orthophoto production tool for *archiving* orthophotos

The tool requires for input an image list and specification of the folder that hosts the orthophotos. The image list is typically re-used from the orthoimage calculation process (see 4.2). For to ensure maximum consistency of the image archive, the copy-process is controlled by the calculation of MD5 hash-codes. The MD5 message-digest algorithm is a widely used hash function producing a 128-bit hash value. The execution is done in the steps:

1. Calculate MD5 hash code of the orthoimage in the working folder
2. Copy the orthoimage to the archive
3. Calculate MD5 hash code of the archive image and compare to MD5 hash code in (1).

If the MD5 hash code calculated in (3) and (1) are equal, the copy process is validated and the next orthoimage is processed. If MD5 codes calculated in (3) and (1) differ, the steps (2) and (3) are repeated. Using hash codes in the way described ensures that the archived orthoimage is a complete identical copy of the calculated orthoimage.

The tool updates as well the footprint of the image in the corresponding LUBIS feature class. The footprint is derived from the actual active image region, i.e. where the orthoimage has non-*NoData* values. This functionality is implemented using ESRI geoprocessing tools.

## 5 Ortho mosaic generation process

### 5.1 General remarks

Apart from the orientation and calculation of single orthophotos, the production of an ortho mosaic is the third important production process of the workflow. Ortho mosaics are produced into year-wise contiguous mosaic blocks.

The ortho mosaic is produced into regular tiles with an extent of 4'375 by 3'000 m each. The maximum product extent (see Figure 43) contains 3432 tiles covering the complete Swiss territory including

Liechtenstein. Further product specifications<sup>9</sup> include the geometric resolution (50 cm) and the projection system (EPSG:21781).

The mosaic production workflow largely bases on existing workflows employed at the author's affiliation. The alternative of building a workflow based on OrthoEngine functionality was discarded.

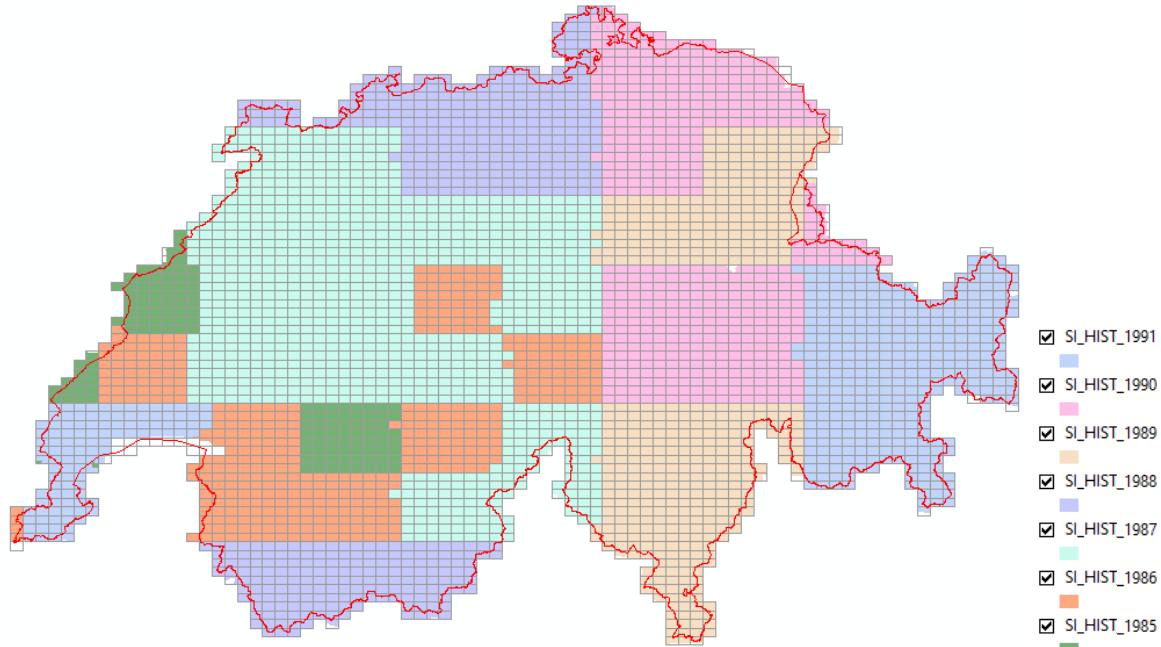


Figure 43: Maximum product extent of SI\_Hist and produced coverage from the acquisition years 1985 – 1991.

In average, mosaic tiles for around 1/6 of the country's surface for this period can be produced per acquisition year. The yearly coverage is separated into two or more zones. The repartition of images into the AT blocks (see 2.2) for the orientation process is not conform to the requirements of the mosaicking process. For the conduction of the mosaicking process, images are grouped into year-wise connected mosaic blocks. The progress of the production process is documented in a spreadsheet table (see Figure 44) which is constantly updated during the production process. The working unit in this process will be referred to as *mosaic block*.

MOS project name	STATUS	Operator	start time	Circle list FrameImage URLBase	nb Images	Retrieve Ops no redundant collapse Inset	Run OrthoVista	Circle pyramid OrthoVista	Prepare Seam Product	QA & Seam Edits	Run OrthoVista Seam Application	Nb of Tiles	Incomplete	gap	Clouds	Build MosaicDataset	QA MosaicDataset
GN1976_p1	finished	gae	15.09.2020		186							36	1251-44; 1291-13; 1291-31		1271-14; 1271-32; 1271-33		
GN1976_p2	finished	gae	15.09.2020		907							388	1012-31; 1012-33; 1047-24; 1049-24; 1050-13; 1050-34; 1050-23; 1051-13; 1052-31		1070-22		
GN1976_p3	finished	gae	18.09.2020		921							279	1192-31; 1209-24; 1228-24		1151-32; 1191-32; 1191-41 1129-13; 1129-14; 1129-31; 1129-33		
GN1976_p4	finished	gae	05.10.2020		148							31					
GN1977_p1	finished	gae	22.09.2020	RC10_C02_AT06	80							16					
GN1977_p2	finished	gae	28.09.2020	RC10_C02_AT16	501							93	1366-22		1326-12; 1326-14; 1326-21; 1326-23		
GN1977_p3	in progress	gae	02.11.2020	RC10_C02_AT15	570												
GN1977_p4	finished	gae	07.10.2020	RC10_C02_AT07	295							68	1271-11; 1290-31		1269-14; 1269-22; 1269-23; 1269-24; 1269-31; 1270-31		
GN1977_p5	in progress	gae	13.10.2020	RC10_C02_AT13/14	1189							273	1373-44; 1373-43; 1373-34; 1352-24; 1394-31; 1394-31; 1414-24; 1425-14; 1425-31; 1414-24; 1414-44; 1414-44		1272-21; 1272-23; 1272-14; 1272-12; 1273-14; 1213-21; 1333-33; 1332-11; 1294-42		
GN1978_C04_AT01	finished	heh	01.09.2020		97							39	1238-34; 1258-12; 1258-14; 1278-22; 1278-24; 1298-22; 1298-24; 1298-42; 1298-44		1238-33		
GN1978_p2	in progress	gae	09.10.2020		639												
GN1978_p3	in progress	gae	26.10.2020	AT02/03/04/05	847												
GN1978_p4	in progress	gae	26.10.2020	AT01/02/03	625							249	1033-13; 1033-32; 1034-31; 1051-22; 1054-24; 1076-32		115-14	1074-13; 1074-14; 1074-44; 1094-24	
GN1979_p1	finished	gae	29.10.2020	AT03/09/10	949												
GN1979_p2	in progress	gae	22.10.2020	AT04	303							64	1195-24; 1178-31; 1177-23				
GN1979_p3	finished	gae		AT11/12	589	240-273 to remove before next step											

Figure 44: Spreadsheet for documenting working progress in the mosaic process per mosaic block

<sup>9</sup> [https://shop.swisstopo.admin.ch/en/products/images/ortho\\_images/SWISSIMAGE\\_HIST](https://shop.swisstopo.admin.ch/en/products/images/ortho_images/SWISSIMAGE_HIST)

## 5.2 Build image list

The mosaic generation process starts by creating a list of images that conform to a mosaic block. The *FrameImageUtilities* tool (see 4.1) is used to create a list of images based on an interactive selection in ArcMap from the corresponding LUBIS feature class. Since the supplementary lines flown in valleys contain redundant information, they are typically ignored in the mosaic processing.

## 5.3 Retrieve orthoimages

Next, the orthoimages that were defined to form the input of a mosaic block are retrieved from the archive to a working folder. The *Retrieve Orthophotos* functionality of the *Frame Image Orthophoto Production tool* (see 4.2) is used for this operation. It requires specification of the image list (generated in 5.2) and the output working folder as arguments.

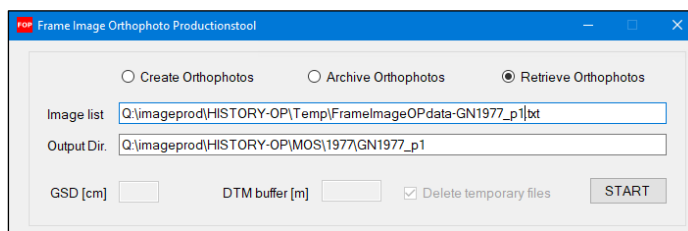


Figure 45: User interface of the Frame Image Orthophoto production tool for *retrieving* orthophotos

As with its *Archive Orthophotos* functionality (see 4.7), the tool generates and compares MD5-hash codes for the orthoimage files that are copied to the output folder. This way, maximum consistency of the copy process is ensured.

## 5.4 Run auto-mosaic

The software environment for the mosaic generation is *ApplicationsMaster* from INPHO/TRIMBLE. *ApplicationsMaster's* principle software modules for the mosaic generation are *OrthoVista* and *OrthoVista Seam Editor*.

*OrthoVista* is used to generate a first automatic mosaic output. First, a new *OrthoVista* project is created. Then the images belonging to the mosaic block and a tile definition file are loaded into the project file. Then the processing options are defined (see Figure 46). In the automated processing, two operations are performed:

1. Global Tilting Adjustment
2. Feature Detection

The *Global Tilting Adjustment* is intended to radiometrically homogenise the input orthoimages before the actual mosaicking operations. Since it has been shown, though, that the radiometric homogeneity of the orthoimages is already very good (see 4.6), the usefulness of the *Global Tilting Adjustment* at this stage may well be put into question.

The *Feature Detection* operation generates the actual seamlines and applies them to produce the output tiles. The output of the automatic processing consists in a TIF/TFW file for each mosaic output tile.

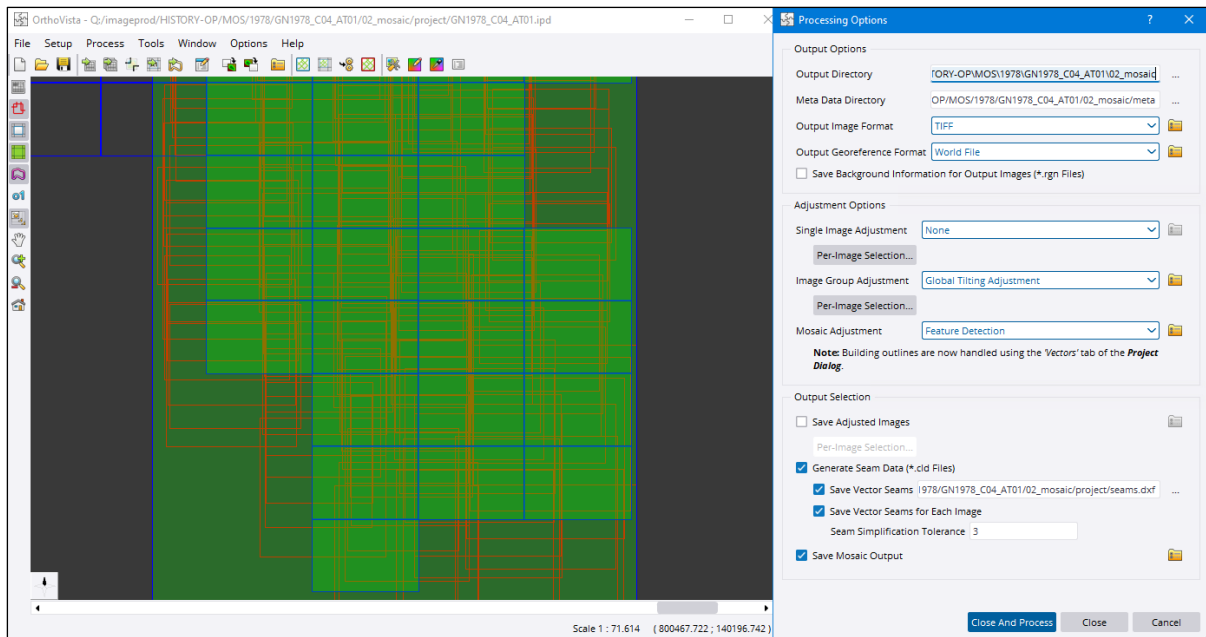


Figure 46: Definition of Processing Options in the OrthoVista GUI

## 5.5 Edit seam lines

In this step the results from the automatic mosaicking process are evaluated and, where feasible, enhanced through manual seamline editing.

A new *OrthoVista Seam Editor* project is created. Next, the automatically generated mosaic tiles are loaded as well as the original orthoimage files. The mosaic output is systematically assessed for problematic regions to be corrected. *Problematic* regions in the mosaic refer, in our case, mainly to

- regions that reveal cloud or cloud shadow cover
- regions that show significant share of stretched pixels in mountainous areas

For each problematic region, the operator evaluates the alternative orthoimages covering the same spot. If an alternative orthoimage can be identified, it is virtually inserted into the mosaic by replacing the problematic region through placing a new seam line. Geometric problems that relate to bridges (see Figure 34) are not corrected for. Neither corrected are problems that relate to regions that cover irrelevant surface types like, e.g., reflections on water surfaces.

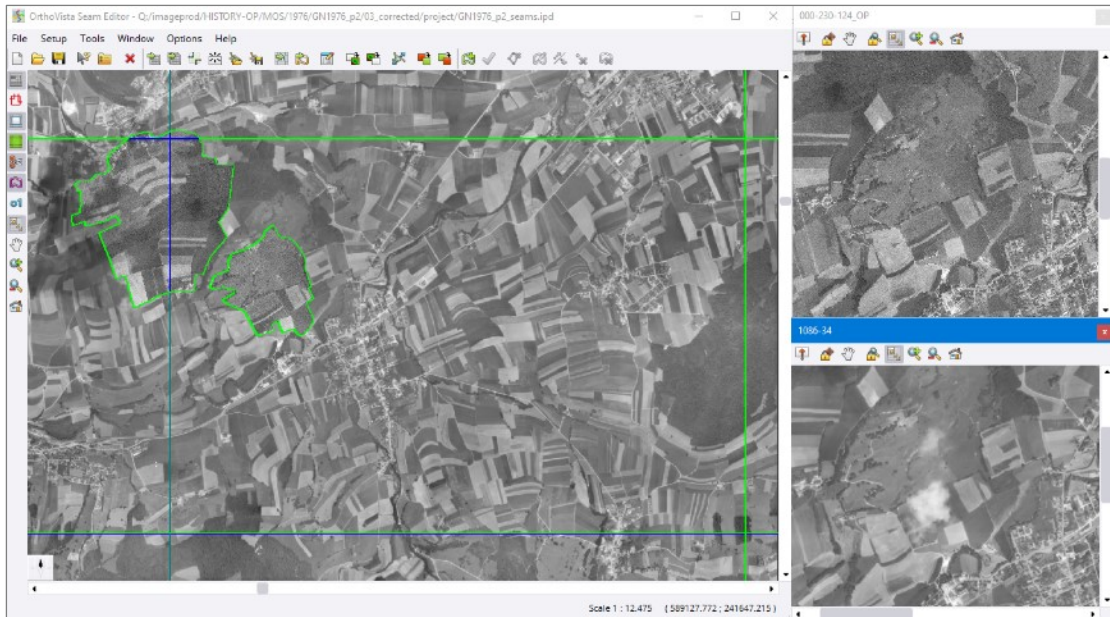


Figure 47: Correcting the automatic mosaic by manual seam line editing

Around 99% of the orthoimages are absolutely cloud-free. Since human labor is one of the most significant cost drivers of the whole process, the seam editing process is carried out with a good sense of pragmatism.

## 5.6 Seam applicator

In the next step, the generated manual seam line edits are used to generate corrected physical output mosaic tiles by employing the manual seam edits. This step is performed in *OrthoVista*. First, an OrthoVista project file is created. Then, the output mosaic tiles and the orthoimages are loaded together with the manual seam edits.

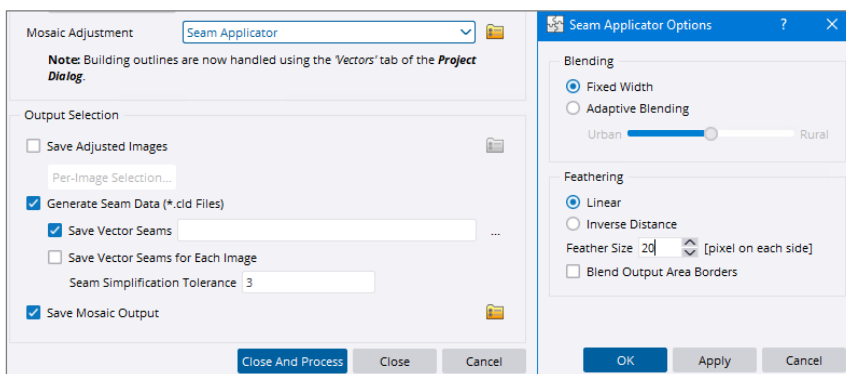


Figure 48: Processing options for the seam applicator process

In the OrthoVista processing options (Figure 48), *Mosaic Adjustment* is set to *Seam Applicator*. In the *Seam Applications Options*, the *Feather Size* is set to twenty pixels in order to get a smooth shift of the edited regions in the final mosaic output tiles. The process writes new mosaic output tiles to the specified output folder. On tiles where seam lines were not manually edited, the process simply copies the output tiles from the automatic mosaic generation (see 5.4). The output format is, again TIF/TFW with 8 bit radiometric resolution. The mosaic tile size is 8'750 pixels by 6'000 pixels.

## 5.7 Final quality assurance of produced mosaic tiles

The corrected mosaic tiles are subject to a final quality check in a GIS environment. For this purpose, a *Mosaic Dataset* of all mosaic tiles belonging to one mosaic block is created. The visual analysis of these non-overlapping image tiles is again conducted in ArcMap. Besides, the visual quality control is used for gathering required metadata of the produced mosaic tiles. These metadata contain, amongst other, binary information on remaining cloud cover (y/n) and existence of data gaps as caused by insufficient image overlap.

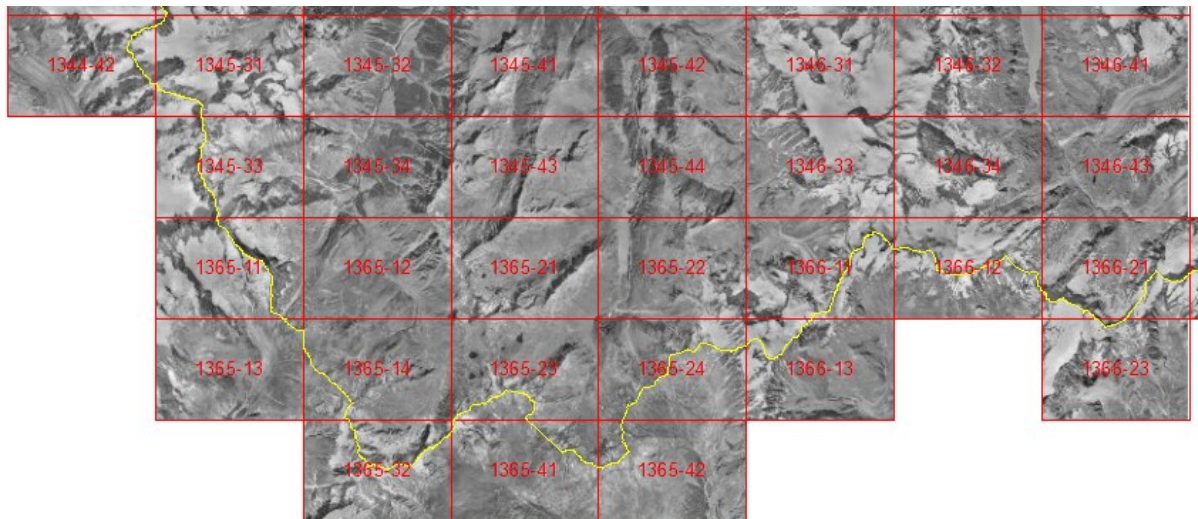


Figure 49: Subset of a Mosaic Dataset containing mosaic tile for final quality assurance

## 5.8 Metadata base

So far, the provenience of image pixel data in the mosaic tiles can only be traced back to the year of acquisition. If, e.g., the exact date of acquisition is looked for, this information can only be roughly estimated by manual comparison with metadata in LUBIS.

In this step, the footprints of the images in the mosaic tiles are extracted and written to a metadata base. This information allows to deduce the inventory number of the exact image that is represented in the mosaic. The inventory number can then be related to LUBIS which allows for to access complete metadata information like, e.g., the exact data of image acquisition, flying height, camera information etc.

Within the mosaicking process (see 5.4 to 5.6), resulting footprints are exported by OrthoVista into DXF format. A FME routine (see Figure 50) was built to read both, automatic and manual, seamlines from the mosaicking process. Since the manual seamlines process takes place after the automatic one, the former overwrite the latter ones in case of conflict. These seamlines are smoothed and written mosaic-block wise to an ESRI file geodatabase. The FME routine has been built under guidance of the author by an intern.

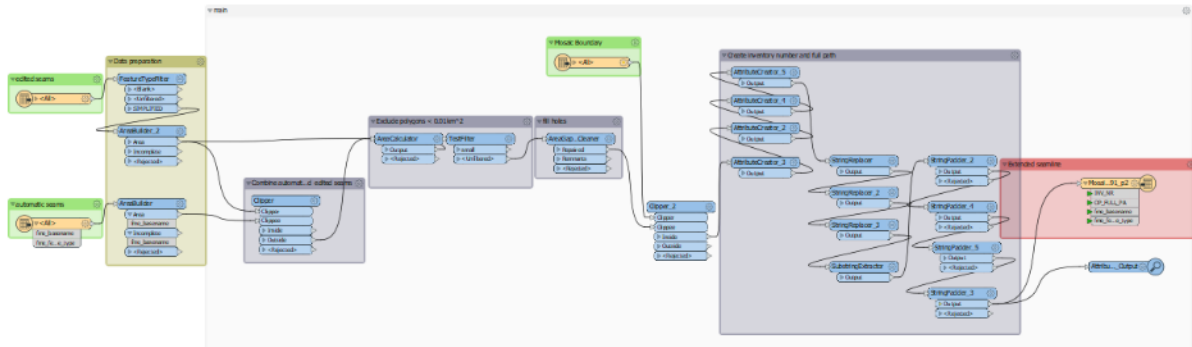


Figure 50: FME routine for calculation of image footprints in mosaic tiles

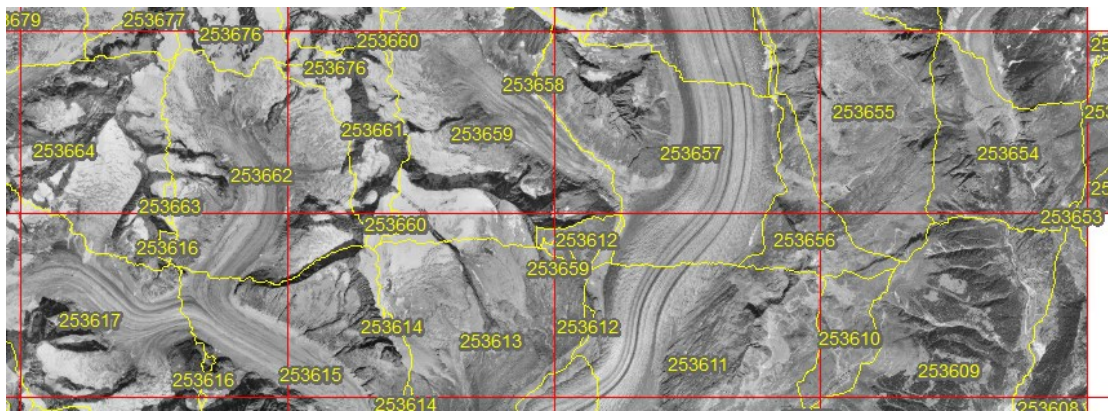


Figure 51: Display of image inventory numbers and bitmasks from images that built the mosaic

The produced seam lines are not part of the official mosaic product.

## 5.9 Integration of mosaic tiles for long-term storage

The produced mosaic tiles are integrated into a system for long-term data storage called *Geodata Warehouse for Rasters* (GDWH). The integration of the data, including collected metadata, is done through the internal *GDWH WebImport Tool*.